

Stevin Laboratory  
Faculty of Civil Engineering and Geosciences  
Delft University of Technology

Report 25.5-12.07

22 Oct 2012

# Shear Capacity of Concrete Beams without Shear Reinforcement under Sustained Loads

Experimental Tests

Ir. R. Sarkhosh  
Ir. J.A. den Uijl  
Dr.ir. C.R. Braam  
Prof.dr.ir. J.C. Walraven

Mailing address:  
Delft University of Technology (TU-Delft)  
Faculty of Civil Engineering and Geosciences  
Concrete Structures Section  
Stevin Laboratory II  
Stevinweg 1  
2628 CN Delft  
The Netherlands

## *Acknowledgment*

---

The experiments of this research were carried out in the Stevin laboratory of Delft University of Technology (*TU Delft*).

The assistance of Mr. Fred Schilperoort and Mr. Ton Blom during the execution of all the tests is very much appreciated. Furthermore, the authors are greatly indebted to the Ministry of Transport, Public Works and Water Management of the Netherlands (RWS) and the Netherlands Organisation for Applied Scientific Research (TNO) for their supervision and financial support.

## Table of Contents

---

<i>CONTENTS</i>	<i>page</i>
Acknowledgment .....	2
Table of Contents .....	3
Preface .....	4
1. Introduction .....	5
1.1. Problem definition .....	5
1.2. Goals of the test .....	7
2. Test Method .....	9
2.1. Design of the specimens .....	9
2.2. Theoretical failure loads .....	9
2.3. Variables .....	9
2.4. Geometry of the specimens .....	9
2.5. Material properties .....	10
2.5.1. Concrete Mix .....	10
2.5.2. Curing conditions .....	11
2.5.3. Reinforcing steel .....	11
3. Measuring programme .....	12
3.1. Standard compressive test on concrete .....	12
3.2. Test arrangement and setup .....	14
3.3. Deflections .....	15
3.4. Shear crack opening and propagation .....	15
3.5. Monitoring of individual cracks .....	15
4. Testing procedure .....	17
4.1. Short-term loading .....	17
4.2. Long-term loading .....	18
5. Results of tensile and compressive strength of cubes .....	20
5.1. Adjustment of shear capacity due to ageing of concrete .....	20
6. Results of short-term loading tests .....	22
6.1. Failure load .....	22
6.2. Types of failure .....	26
6.3. Midspan deflection .....	27
6.4. Crack opening displacement .....	29
6.5. Crack pattern .....	30
6.6. Summary of short-term loading tests .....	35
7. Results of long-term loading tests .....	36
7.1. Load level .....	36
7.1.1. Series II .....	36
7.1.2. Series III .....	37
7.1.3. Series IV .....	39
7.1.4. Series V .....	40
7.1.5. Series VI .....	41
7.1.6. Series VII .....	42
7.2. Observations within a couple of hours after applying the sustained load .....	43
7.3. Long-term test results .....	56
7.4. Crack patterns .....	64
7.5. Crack length in time .....	81
7.6. Crack opening in time .....	82
7.7. Appearance of new cracks .....	82
7.8. Summary of long-term sustained loading tests .....	83
Conclusions .....	85
References .....	86
Appendix I: Sieve analysis and concrete mix .....	87
Appendix II: Compressive and tensile tests .....	94
Appendix III: Analysis of specimens series I-V .....	97
Appendix IV: FE Modelling in ATENA .....	100
ATENA input data .....	100

## Preface

---

Concrete is a multiphase granular material consisting of aggregate particles of various sizes and irregular shape, embedded in hardened cement paste. The physicochemical processes during the hardening of the cement cause air voids, micro cracks and interfacial bond micro cracks. As a consequence of this heterogeneous structure, concrete displays a non-linear and time-dependent deformation response when subjected to long-term loading.

A challenging topic was and still is the failure behaviour of concrete beams without shear reinforcement. The behaviour of cracked reinforced concrete panels can now be satisfactorily predicted for monotonic short-term in-plane loading conditions. In spite of substantial experimental and theoretical efforts in the past, the shear transfer mechanism in concrete in case of sustained loading is not well known.

When a concrete beam is under high sustained loading, flexural crack pattern appears along the span. Here, various shear-carrying mechanisms may be developed by a beam, e.g. aggregate-interlock and dowel action. These mechanisms induce tensile stresses in the concrete near the crack tip and at the level of the reinforcement. Once the tensile strength of the concrete in these regions is reached, the existing flexural cracks propagate in a diagonal direction or new ones are created. The development of the critical shear crack, however, does not necessarily imply the collapse of the member but in case of high sustained loading, the crack length and therefore the crack width will increase.

The aim of this research is to predict the time-dependent mechanical behaviour of concrete beams subjected to sustained loads. The results should enable the designer to quantify the failure load (Ultimate load) and deformations and the propagation of the cracks of beams under sustained shear loads.

## 1. Introduction

Concrete is one of the oldest and most widely used construction materials in the world and possesses many unique qualities such as versatility, aesthetic appeal, eco-friendliness, cost-effectiveness and availability. Increasingly, architects and engineers are making concrete their material of choice. Its strength, durability and natural thermal mass result in structures that require low maintenance, offer high durability and have high operating energy efficiency. Well designed and well placed concrete offers exceptional durability and long life in any structure. Concrete structures built over 100 years ago, indeed as long ago as the Romans, are still in active service today. Infrastructures like underwater tunnels that are built in 1960's and 1970's are under sustained loading. At this point, the question is "are these structures as safe as the construction day or there is any reduction in the capacity (Shear or bending)?".

A very well-known phenomenon of viscoelastic materials under long-term loading is Creep or Relaxation, which is time-dependent strain under applied stress. When a beam is subjected to a high constant load, shear cracks as well as flexural cracks appear in the beam. If the loading continues for a while, an increasing deflection of the beam can be seen due to creep. This phenomenon leads to a further opening of current shear and flexural cracks as well as the increase of the length of the cracks. On the other hand, appearance of flexural and shear cracks causes the stress redistribution in the existing cracks.

### 1.1. Problem definition

Despite the fact that many researchers have been involved in study on shear capacity of concrete beams without shear reinforcement, a few of them, mostly discussing about the flexural capacity (e.g. Zhang et al., 1998 and Zhou, 1992), tried to investigate the sustained loading effect on concrete beams. According to Zhang et al. (1998), the ratio of sustained stress to Modulus of rupture decreases in time (Fig. 1), which means that under higher level of sustained loading, the beam fails in a shorter time. This type of test has, however, not been carried out for determination of shear capacity.

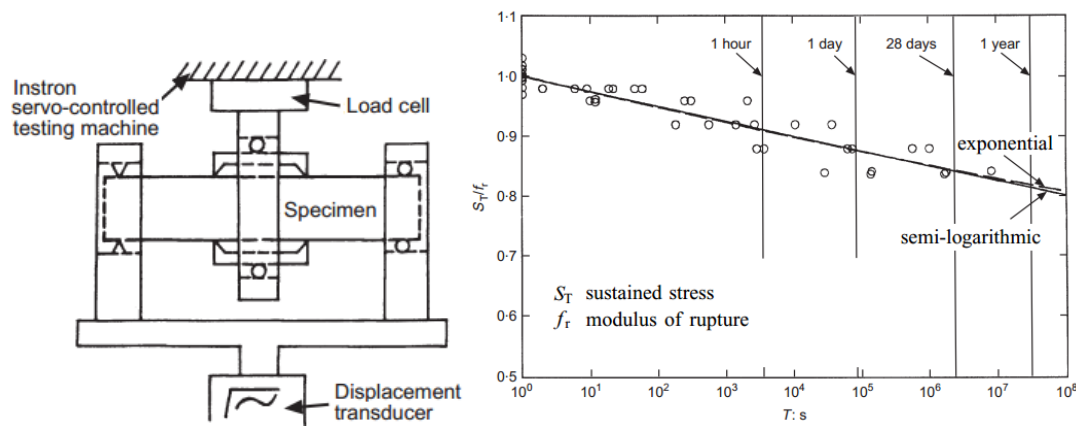


Fig. 1: Sustained loading test on plain concrete, by Zhang, Phillips and Green (1998)

The lack of experimental data has led to uncertainty of using a reduction factor for concrete strength in case of sustained loading. This factor should be used to account for the long-term versus the short-term concrete tensile strength and is evaluated based on the long-term behaviour of plain concrete loaded in tension. According to the Dutch Code, the concrete strength in long-term loading is 0,85 of short-term strength. In the Eurocode 2, in case of sustained loading, the values of the design compressive strength  $f_{cd}$  and design tensile strength  $f_{ctd}$  are defined as:

$$f_{cd} = \alpha_{cc} \cdot f_{ck} / \gamma_c \quad \text{for concrete in compression} \quad (1)$$

$$f_{ctd} = \alpha_{ct} \cdot f_{ctk 0,05} / \gamma_c \quad \text{for concrete in tension} \quad (2)$$

where,  $f_{ck}$  and  $f_{ctk,0.05}$  are characteristic compressive strength and characteristic axial tensile strength respectively,  $\alpha_{cc}$  is the coefficient taking account of long term effects on the compressive strength and of unfavourable effects resulting from the way the load is applied and  $\gamma_c$  is the partial safety factor for concrete, which is 1,50. The value of sustained loading factor ( $\alpha_{cc}$ ) may be assumed between 0,8 and 1. However, for normal density concrete the sustained loading factor is defined to be 1.

A well-known research program focussing on the effects of long-term loading was the one carried out by Rüschi (1960). He carried out tests on concrete prisms, which he loaded to a certain fraction of the short-term compressive strength: subsequently the load was kept constant for a long period. If the long-term loads were higher than about 80% of the short-term bearing capacity, failure occurred after a certain period. Fig. 2 reproduces Rüschi's diagrammatic representation of concrete strains as a function of the applied stresses for several loading times.

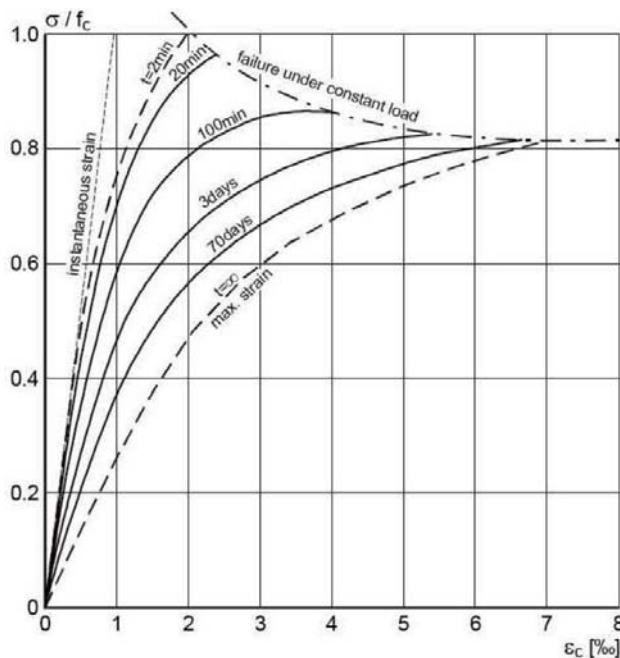


**Fig. 2: Stress-strain relations for several time durations of axial compressive loads (Rüschi, 1960)**

As can be seen, the longer the loading time, the more the ultimate strength approaches the long-term value 80%. The tests carried out by Rüschi were limited to concrete with maximum cube strength of about 60Mpa. Tests by Walraven and Han on concrete's with cube strength's up to 100 Mpa showed that the sustained loading behaviour for high strength concrete is similar to that of conventional concrete's [Han/Walraven, 1993].

However, Rüschi's tests were carried out on concrete, which had an age of 28 days at the time the load was applied. This condition will normally not hold for a structure in practice, which generally will be much older when subjected to a load. This means that the sustained loading effect is at least partially compensated by the increase in strength between 28 days and the age of loading. Fig. 3 shows the strength development in time according to the Eurocode 2 for concrete's made with rapid hardening high strength cements RS, normal and rapid hardening cements N and R, and slowly hardening cements SL.

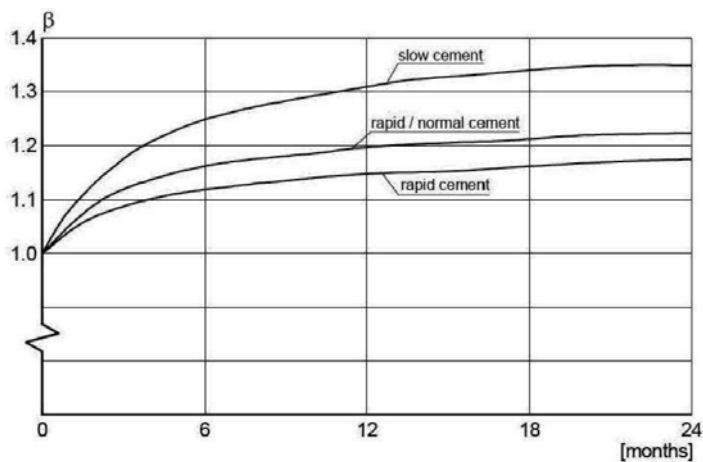


Fig. 3: Compressive strength development of concrete made with various types of cement acc. to Eurocode 2

Fig. 3 shows, that the gain in strength in 6 months ranges from 12% for rapid hardening cements to 25% for slowly hardening cements. So, a considerable part of the sustained loading effect is compensated for by the increase in strength.

Furthermore the bearing capacity as formulated in building codes is generally based on experiments in laboratories (shear, punching, torsion, capacity of columns). Normally those tests have a duration of at least 1,5 hours. In Fig. 2 it can be seen that in a test with a loading duration of 100 minutes, the reduction of strength with regard to 2 minutes is already about 15%. A certain sustained loading effect is therefore already included in the results of tests. It is therefore concluded that cases in which the sustained loading effect will really influence the bearing capacity of a structure in practice are seldom and do not justify a general reduction of the design strength with a sustained loading factor of 0,8. Such a case can for instance occur when the concrete strength is determined substantially after 28 days: in such a case, the gain in strength may be marginal so that a value  $\alpha_{cc}$  smaller than 1 is more appropriate (Eurocode 2).

In view of that, more tests need to be done to confirm the behaviour of concrete under sustained loading. In this research the influence of long-term loading on the shear capacity of concrete beams without web reinforcement is being investigated. The goal is to quantify the possible shear capacity loss due to long-term loading.

## 1.2. Goals of the test

This research has two main goals, which are;

- Investigation of the sustained loading effect in concrete beams without shear reinforcement.
- And presenting the formulation of the sustained loading effect, with special attention to the role of the short term reference strength.

In this part of the research that is experimental tests, the first goal is going to be accomplished. For that reason several test series has been carried out on concrete beams subjected to high shear loads close to the failure load. The beams have experienced this load for a minimum period of three months. Meanwhile, the deflection, crack growth and cracks width have been monitored. Finally a relation between loading duration, crack width and length, load level and concrete strength is established.

A total number of 42 concrete beams (divided in seven series, each group consisting of six beams) have been tested to investigate the behaviour of the beams under high sustained loads. The beams were designed to resist the bending and just to fail in shear. The first series, used as reference, was only tested in short-term loading, to obtain the ultimate shear capacity, crack opening displacement (COD), type of failure, and to gain insight into the scatter of the results. Series II-VII have been tested both in short-term and long-term loading in the following order; in each series, there are three beams those are tested in short-term loading to obtain the ultimate shear capacity and three other beams, which are tested in long-term loading with a load ratio of 87% to 97.5%.

The main objectives of the experimental research are:

- To study the influence of long-term loading on the shear capacity of beams without shear reinforcement.
- To evaluate the influence of the load level on crack propagation to find out if there is any relation between the level of loading and the shear capacity of a concrete beam.
- To evaluate the rate of crack growth (in width and length) in a concrete beam subjected to a sustained load. In case of sustained loads, the beam experiences the effects of creep, stress relaxation and ageing of the concrete. All these effects should be considered during the tests.
- To compare the behaviour of High Strength Concrete (HSC) beams with Normal Strength Concrete (NSC) beams regarding the crack pattern, crack width and load ratio.
- To propose a time-dependent relation for crack width and crack length in concrete beams subjected to sustained loads.

## 2. Test Method

### 2.1. Design of the specimens

In order to achieve the previously mentioned goals, a total number of 42 beams, casted with normal and high strength concrete, have been tested. The beams were designed to resist the bending and just to fail in shear. The details of the 3000 mm long  $\times$  200 mm wide  $\times$  450 mm deep beams those were tested under 3-point bending (2400 mm span length) will be explained in the section 2.3. The shear span is 1200 mm, this the  $a/d$  ratio is about 2,9.

The test program consists of seven series of beams. Series I-V were casted with normal strength concrete ( $f_{cm} = 35$  MPa) and high strength concrete ( $f_{cm} = 70$  MPa) is used for series VI-VII. For each series of casting, 36 cube tests are done to obtain the development of concrete compressive strength in time.

The longitudinal reinforcement in the beams was designed to resist in bending, yet the beams are weak in shear, the shear failure was expected during the tests. The FE-modelling was done in ATENA software with extra hand calculation using Rafla's empirical formula, see Appendix IV.

### 2.2. Theoretical failure loads

The calculation of the shear resistance of concrete beams based on the actual values of concrete strength is presented in section 4.2.

### 2.3. Variables

The experimental program comprised three variables:

- Concrete compressive strength ( $f_{cm}$ )  
Two types of concrete (Normal strength and high strength) were used, all with a maximum particle size of 16 mm. The concrete contained 330 kg (series I-V) and 425 kg (series VI-VII) cement per  $m^3$ . Details of the concrete are given in section 2.5. High strength concrete was chosen in view of the application of the test results to a wide range of structures.
- Reinforcement ratio ( $\rho$ )  
All beams were reinforced with three longitudinal steel bars at the bottom. A diameter of 20 mm was used for the beams with normal strength concrete (Series I-V) and for high strength concrete beams (series V-VII) steel bars with 25 mm diameter were used. The reinforcement ratios were 1,05% and 1,63%.
- Load ratio ( $V/V_u$ )  
The static shear resistance ( $V_u$ ) in each series of beams has been chosen as a calibration value. From three experiments in each series, the average shear capacity with a low coefficient of variation was considered as  $V_u$ . The shear load ratio of long term tests ( $V/V_u$ ) varies between 0,87 and 0,97.

### 2.4. Geometry of the specimens

The geometry of the specimens is presented in *Fig. 4*. The dimension of the specimens was 3000 $\times$ 450 $\times$ 200 mm<sup>3</sup>. Three longitudinal steel bars reinforce the concrete at the bottom. The span length is 2400 mm and the load applies in the middle. Reinforcing bars were welded to a steel plate at both ends of the beams to provide adequate anchorage. The dimension of steel plates was 100 $\times$ 200 $\times$ 10 mm<sup>3</sup> with three holes in order to weld the bars at both sides (*Fig. 2*).

**Table 1: Dimensions of casted beams**

Series No.	$h$ [mm]	$b$ [mm]	$d$ [mm]	$L_{\text{beam}}$ [mm]	$L_{\text{span}}$ [mm]	Main Reinforcement	Bar spacing [mm]	Reinforcement ratio $\rho$
I-V	450	200	410	3000	2400	3 $\varnothing$ 20mm	40	1,05%
VI-VII	450	200	407	3000	2400	3 $\varnothing$ 25mm	32	1,63%

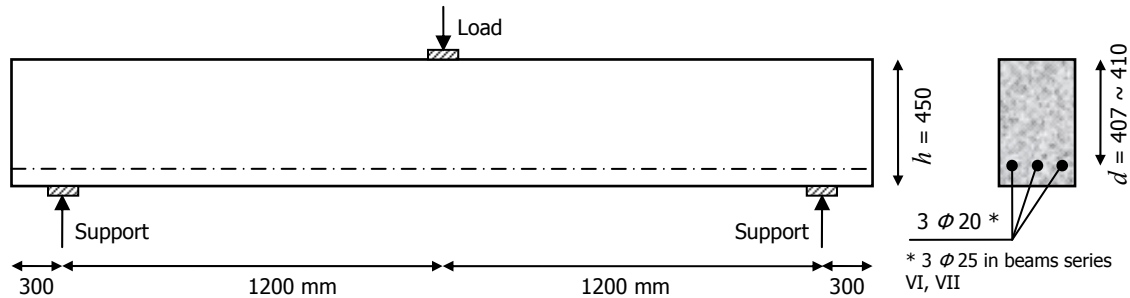


**Fig. 4: Dimensions and cross section of the beams**

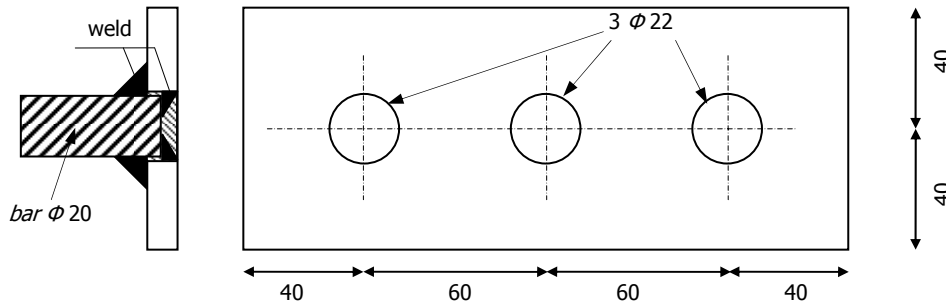


**Fig. 5: Layout of end plates for reinforcement in series I-V**

## 2.5. Material properties

### 2.5.1. Concrete Mix

Two concrete classes, C28/35 and C53/65, are chosen for normal concrete and high strength concrete respectively. The strength of concrete in each cast was different, (because the concrete was delivered by a commercial plant). In casts 1 and 2, the water of the aggregates was not accounted for in the water/cement ratio, thus the strength of the concrete is lower than the expected value for that concrete class. In cast 5, in order to have the same strength as casts 1 and 2, the concrete class is changed (Table 2). Due to the limited number of moulds, it was only possible to cast six beams at the same time.

**Table 2. General properties of concrete**

Series No.	Strength Class	Slump [mm]	W/C ratio	A/C ratio	Chloride M/M [%]	Temperature at casting place °C
I	C28/35	100-150	0,58	5,45	0,20	20
II	C28/35	100-150	0,59	5,47	0,20	15
III	C28/35	100-150	0,58	5,46	0,20	15
IV	C28/35	100-150	0,57	5,46	0,20	10
V	C20/25	100-150	0,61	5,47	0,21	15
VI	C53/65	100-150	0,402	3,94	0,16	20
VII	C53/65	100-150	0,388	3,98	0,16	23

The mix for cast 6 and 7 (high strength concrete) contains 280 kg/m<sup>3</sup> Portland Cement type I and 145 kg/m<sup>3</sup> cement type III/B whereas the mix for the normal concrete contained 330 kg/m<sup>3</sup> cement type III/B. The amount of cement in cast 5 is reduced to 320 kg/m<sup>3</sup> in the mix to have the same concrete strength

as casts I and II. Fine river aggregates are used in concrete mixtures. Sieve analysis and concrete mixtures are given in Appendix I.

The concrete was delivered by a truck mixer from the *Dyckerhoff Basal* plant in Delft. Each beam was cast in four layers and during casting poker vibrators were used to compact the concrete. For standard tests, 36 cubes (150 mm) are cast together with each series of casting. For compacting cubes from casts 1-4, small poker vibrators are used. This could be a reason for the large scatter in the results of compressive tests. Therefore, for compacting casts 5-7, a shaking table used with a compacting time of 30 seconds. The beams and cube samples are covered with plastic sheets after casting. For high strength concrete, one day after casting, the surface of the beams is made wet.

### **2.5.2. Curing conditions**

The concrete beams were casted in timber moulds with smooth surface. Synthetic moulds were used for the cubes. Immediately after casting, all specimens were covered with plastic sheets and were kept in the lab temperature (20°C). After 2 days the cubes were demoulded and the beams were demoulded after 10 days and stored in a fog room (20°C, 99% RH). Next, at an age of 28 days, after making the notch on the beam, they were placed in the laboratory (20°C, 50% RH) and kept for at least one week prior to the test to be dried.

### **2.5.3. Reinforcing steel**

Reinforcing bars of 20 mm diameter and 25 mm with namely grade of  $f_{sy} = 550 \text{ N/mm}^2$  were used. All bars were ribbed. Tensile tests performed on samples from reinforcing bars show a yield strength of 555 MPa and an ultimate strength of 680 MPa for bars with 20 mm diameter. For bars with 25 mm diameter, a yield strength of 572 MPa and an ultimate strength of 651 MPa is obtained.

### 3. Measuring programme

#### 3.1. Standard compressive test on concrete

Concrete strength increases with age as long as moisture and a favourable temperature are present for hydration of cement. To illustrate this, Fig. 6 contains the results of tests on concrete exposed to the ambient air (RH = 50%) the entire time; its strength being 55% of the strength of moist-cured concrete at 28 days. Exposed to the air, 3 and 7 days after casting, the strength reaches in 80% and 90%, respectively. Quality curing and a sealing compound allow the concrete to continue in strength gain beyond 28 days as shown in Fig. 6 for moist-cured concrete.

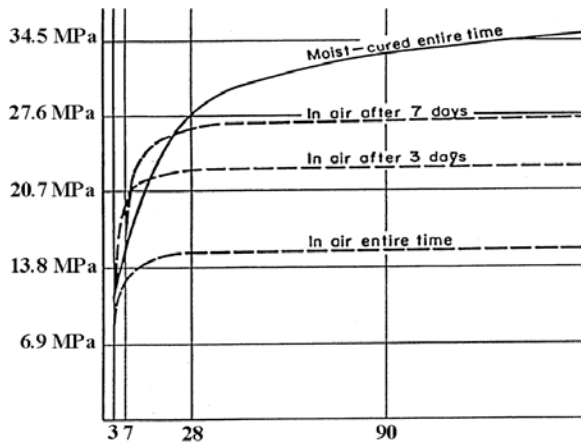


Fig. 6: Concrete compressive strength increases with age as long as moisture and a favourable temperature are present for hydration of cement, according to the Portland Cement Association [1]

Each casting batch consists of 36 cubes (150×150×150 mm<sup>3</sup>) tested at different ages of concrete to obtain the development of the compressive strength due to hydration. The results of compressive tests on cube samples are shown in

Fig. 8. The magnitudes of the compressive strength are presented in Appendix II, as well.

After performing the long-term tests on casts 2 and 3, the actual strength of the concrete is investigated. Cores are drilled with the axis normal to the side surface of the beams. The cores are drilled in the uncracked zone of the specimen (top-left or top-right of the beam), see

Fig. 7. The diameter of the drilled cores is 100 mm and the length is equal to the width of the beam (200 mm). Later on, they are cut into two pieces in the middle (2 × 100 mm). One core is drilled out of each beam; hence the total number of samples is six. The results of the compressive tests on drilled cores are characterized by a large scatter, out of the range of the compressive strength of the cubes. So the results of drilled cores are not taken into account. Besides, no more drilling is done for further tests.

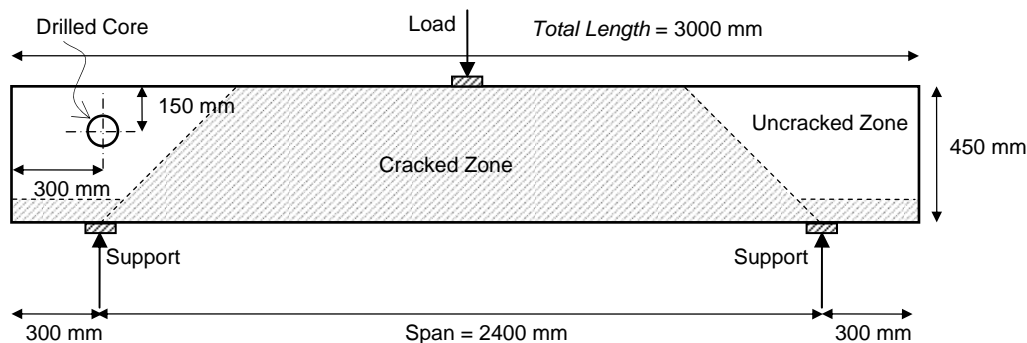


Fig. 7: Position of drilled cores on the side of the beam

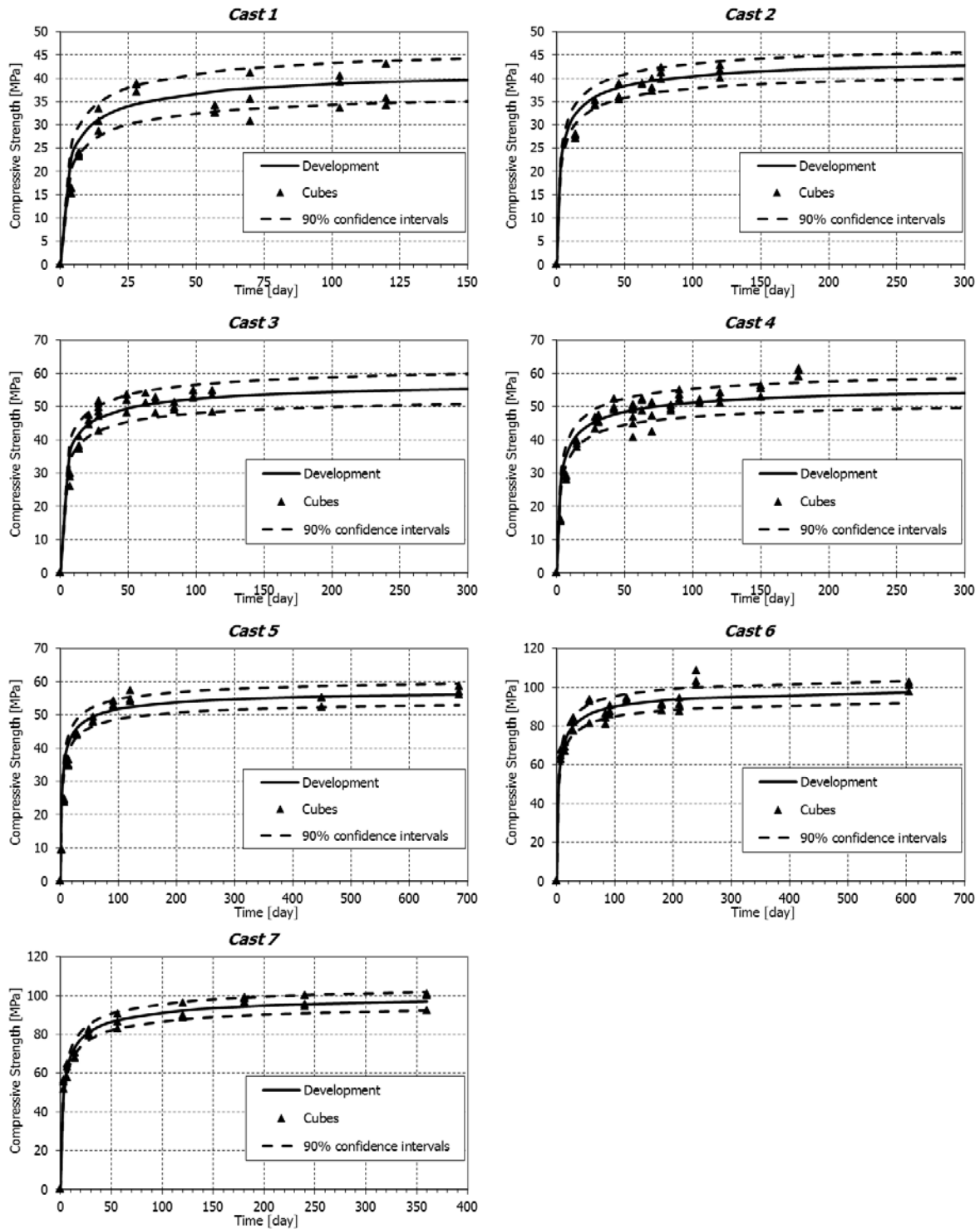


Fig. 8: Compressive strength of the cubes

The compressive strength of concrete at an age  $t$  depends on the type of cement, temperature and curing conditions. For a mean temperature of 20°C and curing in accordance with EN 12390 the compressive strength of concrete at various ages  $f_{cm}(t)$  may be estimated from (Eurocode 2);

$$f_{cm}(t) = \exp\{s [1 - (28/t)^{0.5}]\} f_{cm} \quad (3)$$

where  $f_{cm}$  is the mean compressive strength at 28 days,  $t$  is the age of concrete in days and  $s$  is a coefficient which depends on the type of cement, see *Table 3*.

**Table 3. Values of coefficient  $s$**

Cement Strength Classes	$s$
CEM 42,5 R, CEM 52,5 N, CEM 52,5 R (Class R)	0,2
CEM 32,5 R, CEM 42,5 N (Class N)	0,25
CEM 32,5 N (Class S)	0,38

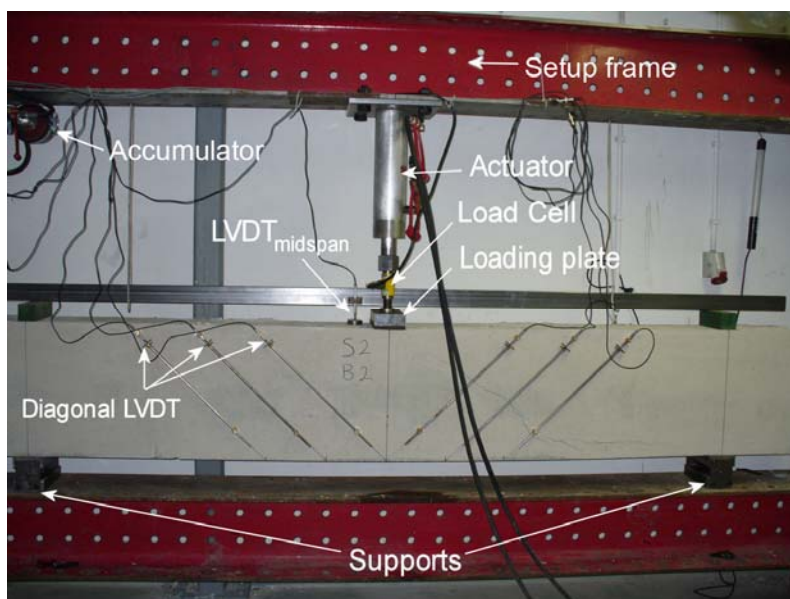
The development of the compressive strength in

Fig. 8 in each series is presented based on the all results of compressive tests in different time intervals and is according to Eq. (1).

### 3.2. Test arrangement and setup

Six parallel setups with capacities up to 400 kN were prepared in a climate room ( $RH=50\%$  and  $T=20^{\circ}\text{C}$ ) to perform the tests at the same time. Each setup as shown in *Fig. 9* consists of a steel frame which holds the concrete beam and loading system inside:

- A hydraulic oil actuator with 600 Bar capacity that applies the load,
- An oil accumulator to keep the oil pressure inside the actuator constant,
- A load cell with accuracy of 1,3 kN installed under the actuator and above the loading plate,
- A loading plate placed at the middle of the beam with a dimension of 50×100×200 mm (Height, length, width) which is placed laterally to cover the width of the beam,
- Two roller supports, each one with a contact area of 100×200 mm,
- A LVDT with 20 mm measuring range (linear variable displacement transducers) at the middle next to the loading plate,
- A pair of LVDT's with 10 mm measuring range, diagonally installed at both sides of the beam symmetrically.
- Additional measuring equipment with a manually operated LVDT (Measuring range = 20 mm) is applied on beams with high strength concrete.



**Fig. 9: The setup with capacity up to 200 kN**

In each test, the beam was placed centrally in the setup, see Fig. 9. The zero measurements are taken when the beams are only loaded by their dead weight. Thus, the influence of the concrete self-weight is not incorporated in the measuring results of the LVDT's.

The 3,0 m long beams are loaded in 3-point-bending with a span of 2,40 m. All tests were carried out in a load-controlled mode, as the application of the load was manual.

### 3.3. Deflections

The deflection in the middle was measured relative to the supports with a LVDT next to the loading plate. To measure the bending deflection relative to the supports, a steel profile with rectangular cross section (800×600 mm) which holds the LVDT was placed on top of the beam, see Fig. 9. It should be noticed that because of the position of loading plate at mid-span, the LVDT is installed at 100 mm distance from the mid-span (to the left in Fig. 10).

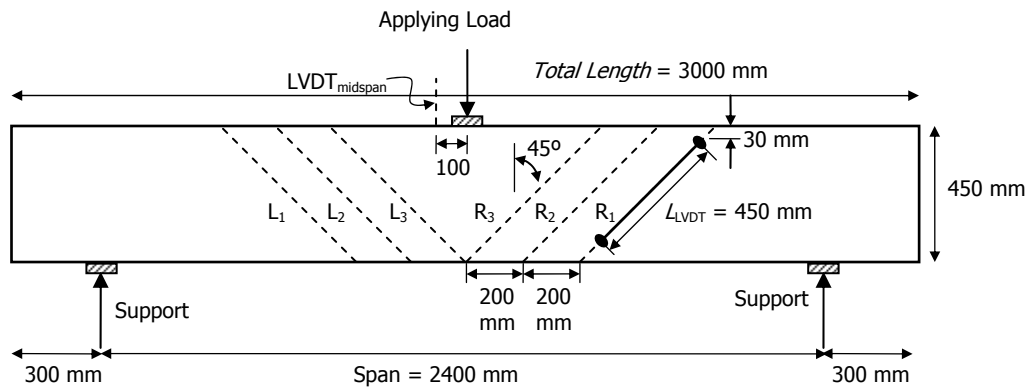


Fig. 10: Position of diagonal LVDT's (dashed-lines) and mid-span LVDT on the beams

### 3.4. Shear crack opening and propagation

In order to measure the opening of shear cracks, a pair of diagonal LVDT's was used. The locations of the LVDT's on the right/left side of the beam were optimized after analysing the results of tests with six LVDT's (Series II), see Fig. 10. The results of series II show that some main shear cracks are out of the measuring range of units L1 and R1. The positions of units L3 and R3 are too close to the middle and may not measure the initiation of the shear crack, which usually appears at a distance of 600-800 mm from the support. Therefore, for further tests, only two LVDT's (L2 and R2) were used. The LVDT's were installed only on one side of the beams is.

### 3.5. Monitoring of individual cracks

With the aim of measuring the surface strains and monitoring the crack width in detail, a measuring grid consists of 241 elements was placed on the front side of the beam (Fig. 11). The grid counts of 96 nodes with 100 mm distance, placed along 5 rows. At each node a measuring point (outer diameter  $\phi=8$  mm) was placed (Fig. 12). The bottom row was placed at the height of the longitudinal reinforcing steel. Later, a manually operated LVTD was used to measure the distance between individual measuring points, see Fig. 13. The manual LVDT device was connected to a laptop through a wire. The measuring data were displayed simultaneously on the screen and were stored in an Excel file. This measuring method was only applied in series V-VII.

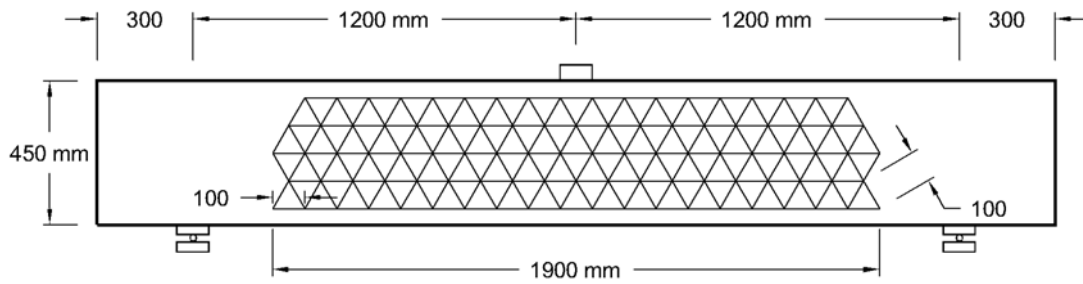


**Fig. 11:** The scheme of measuring grid to monitor the displacements on the surface of the specimen

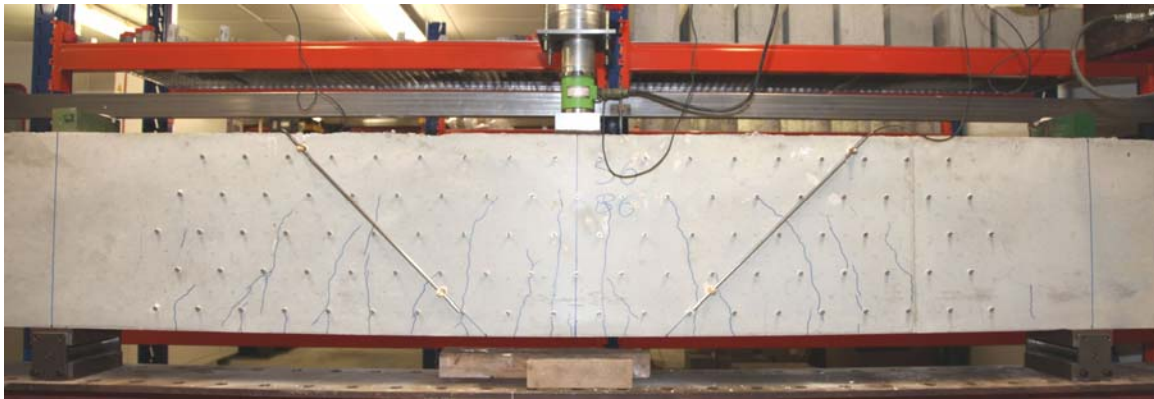


**Fig. 12:** Measuring points installed on beams series 5-7 to measure the strains and crack width on the surface of the beam



**Fig. 13:** Measuring of the distance between the points by means of a hand-operated LVDT

## 4. Testing procedure

The primary objective of the testing procedure is to investigate the time-dependency of shear behaviour of the beam and the shear crack growth in the unreinforced webs. The experiments involve determining the material properties, time dependency of flexural deformation, shear crack width and growth.

In summary, the chronological order of the experiments is as follows:

- Casting six beams together with 36 cubes in each series
- Preparation of the test

The specimens were stored in the fog room ( $RH=99\%$  and  $T=20^{\circ}\text{C}$ ) until 28 days age, then moved to the climate room ( $RH=50\%$  and  $T=20^{\circ}\text{C}$ ) and stored about two months.

- Testing three beams in each series in short-term loading

Arrangement of the test setup in the climate room in order to keep the environmental conditions constant during the tests, centring of the specimen in the testing frame, installation of LVDT's and measuring points, zero measurement of the LVDT's, zero measurement of gridlines, application of 3 kN force to the beam, removing the safety bolts from the roller supports and finally application of load until failure by a hydraulic pump within 10 minutes.

- *Application of long-term loading on three other beams*

A load ratio of 0,87 to 0,97 was chosen for the sustained loading, and was applied in a few minutes. Of course, as the load ratio increases, so does the chance of failure of the beam, because in most of the cases, the load ratio is already in the 95% interval of the short-term ultimate shear capacity.

- *Measurements under sustained loading*

Immediately after application of the sustained loading the displacements (flexural and diagonal deflections) as well as the loading were recorded periodically by the computer. In different time intervals (3 hours, 1 day, 3 days, 7 days, one month, three months,...) the gridlines were also measured by a hand-held measuring device. Any decrease of the sustained load was corrected by means of a manual hydraulic pump. During the tests, a maximum loss of 4 kN was observed, being less than 2,5% of the minimum sustained load.

- Removal of sustained loading

In series II and IV, the sustained loading was applied only for 3 or 6 months and later the beams were loaded to failure to obtain the influence of sustained loading on ultimate capacity. The rest of the beams were left in the setup under sustained loading for a very long time (more than 2 years).

More details on the short-term and long-term tests will be given in the following sections.

### 4.1. Short-term loading

In order to gain insight into the shear resistance of the beams, three short-term tests were carried out on each series of casting. The beams are loaded in short-term 3-point-bending until failure. During loading, flexural deflection and diagonal strains were measured by three LVDT's as shown in *Fig. 10*. The maximum load was reached within 10 minutes (except for specimen S3B2 that took 28 minutes to fail). Since the load was applied by a hand-operated hydraulic jack, the mean rate of loading in each test varies between 0,6 and 1,9 kN/s. The low-rate in some beams is due to a pause in loading after a wide crack appeared on the beam. In these cases, the idea was to see if the beam fails under the current applied load.

The results of the short-term tests were used as reference values to obtain the mean value of the shear resistance of the beam. The crack pattern for each beam is also presented in Chapter 6.

**Table 4: The status of the casted beams (test dates and type of test)**

Series No.	Label	Cast date	Test date	Type of Concrete	Type of test	Description
I	S1B1	8 Oct 09	5 Nov 09	NSC	Short-term	Tested, completed
	S1B2	8 Oct 09	5 Nov 09	NSC	Short-term	Tested, completed
	S1B3	8 Oct 09	5 Nov 09	NSC	Short-term	Tested, completed
	S1B4	8 Oct 09	5 Nov 09	NSC	Short-term	Tested, completed
	S1B5	8 Oct 09	9 Nov 09	NSC	Short-term	Tested, completed
	S1B6	8 Oct 09	9 Nov 09	NSC	Short-term	Tested, completed
II	S2B1	2 Nov 09	11 Jan 10	NSC	Short-term	Tested, completed
	S2B2	2 Nov 09	12 Jan 10	NSC	Short-term	Tested, completed
	S2B3	2 Nov 09	12 Jan 10	NSC	Short-term	Tested, completed
	S2B4	2 Nov 09	13 Jan 10	NSC	Long-term	Tested 98 days, completed
	S2B5	2 Nov 09	13 Jan 10	NSC	Long-term	Tested 98 days, completed
	S2B6	2 Nov 09	13 Jan 10	NSC	Long-term	Tested 98 days, completed
III	S3B1	20 Nov 09	11 Feb 10	NSC	Short-term	Tested, completed
	S3B2	20 Nov 09	11 Feb 10	NSC	Short-term	Tested, completed
	S3B3	20 Nov 09	11 Feb 10	NSC	Short-term	Tested, completed
	S3B4	20 Nov 09	15 Feb 10	NSC	x	Failed before the desired load
	S3B5	20 Nov 09	15 Feb 10	NSC	Long-term	Under sustained loading, still in the setup
	S3B6	20 Nov 09	15 Feb 10	NSC	Long-term	Tested 127 days, Failed while reloading
IV	S4B1	2 Feb 10	8 Apr 10	NSC	Short-term	Tested, completed
	S4B2	2 Feb 10	8 Apr 10	NSC	Short-term	Tested, completed
	S4B3	2 Feb 10	8 Apr 10	NSC	Short-term	Tested, completed
	S4B4	2 Feb 10	14 Apr 10	NSC	Long-term	Tested 330 days, completed
	S4B5	2 Feb 10	14 Apr 10	NSC	Long-term	Tested 330 days, completed
	S4B6	2 Feb 10	14 Apr 10	NSC	Long-term	Tested 2,5 hours, Failed
V	S5B1	7 Apr 10	25 Aug 11	NSC	Short-term	Tested, completed
	S5B2	7 Apr 10	25 Aug 11	NSC	Short-term	Tested, completed
	S5B3	7 Apr 10	25 Aug 11	NSC	Short-term	Tested, completed
	S5B4	7 Apr 10	1 Sep 11	NSC	Long-term	Under sustained loading, still in the setup
	S5B5	7 Apr 10	1 Sep 11	NSC	x	Failed before the desired load
	S5B6	7 Apr 10	1 Mar 12	NSC	Long-term	Under sustained loading, still in the setup
VI	S6B1	17 Jun 10	14 Sep 10	HSC	Short-term	Tested, completed
	S6B2	17 Jun 10	14 Sep 10	HSC	Short-term	Tested, completed
	S6B3	17 Jun 10	14 Sep 10	HSC	Short-term	Tested, completed
	S6B4	17 Jun 10	5 Oct 10	HSC	Long-term	Under sustained loading, still in the setup
	S6B5	17 Jun 10	5 Oct 10	HSC	x	Failed before the desired load
	S6B6	17 Jun 10	5 Oct 10	HSC	Long-term	Under sustained loading, still in the setup
VII	S7B1	10 Aug 10	8 Mar 11	HSC	Short-term	Tested, completed
	S7B2	10 Aug 10	8 Mar 11	HSC	Short-term	Tested, completed
	S7B3	10 Aug 10	8 Mar 11	HSC	Short-term	Tested, completed
	S7B4	10 Aug 10	17 Mar 11	HSC	x	Failed before the desired load
	S7B5	10 Aug 10	17 Mar 11	HSC	Long-term	Under sustained loading, still in the setup
	S7B6	10 Aug 10	17 Mar 11	HSC	Long-term	Tested 44 hours, Failed

## 4.2. Long-term loading

The time-dependency of the shear resistance can be investigated by studying the effect of loading time on crack width and crack length; since the crack development may indicate a degrading process that results in a reduced shear capacity. However, unless the failure is reached, it is not possible to make a relationship between shear capacity and time. During loading, the width of the cracks is measured by means of two diagonal LVDT's and a hand-operated detachable displacement transducer.

A series of tests has been carried out with different load ratios ( $V/V_u$ ) ranging from 87% to 97% of the static shear resistance ( $V_u$ , obtained from short-term tests). The corresponding time to reach failure (if it happens) will be used to find a relation between crack width, crack length and other material parameters like concrete strength.

In order to determine the overall rate of crack growth and to find a relation for crack propagation and failure of the beam, it was necessary to monitoring the individual cracks during sustained loading. In addition to the manual measurement system, the automatic equipment and software have been undergoing continuous enhancements, and the system could monitor the midspan deflection and diagonal strain and automatically record data while the beam was loaded. The software was sensitive to both alteration of load and displacement, so any increase or decrease in input data has been recorded.

## 5. Results of tensile and compressive strength of cubes

### 5.1. Adjustment of shear capacity due to ageing of concrete

Based on the compressive strength of the concrete, which was presented in Fig. 8, the shear resistance of the beams is recalculated using Rafla's formula (Appendix III) and ATENA Software, see Table 5 to Table 10. It should be mentioned that in the three-point bending tests with the same shear spans, the ultimate shear resistance  $V_{ur}$  is equal to  $V_u = P_{max}/2$  where  $P_{max}$  is the ultimate (maximum) load.

**Table 5. Actual shear capacity of the beam based on compressive strength of the cubes, Series I**

Age [days]	$f_{cm,cube}$ [MPa] from curve (trend line)	Ultimate Load $P_{max,mean}$ [kN] (Experimental test)	Ultimate Load $P_{max}$ based on FEM in ATENA [kN]	Ultimate Load $P_{max}$ based on Rafla's formula [kN]
3	20,6	-	-	-
7	26,9	-	-	-
28	34,5	184,7	166,8	154,0
90	38,5	-	176,2	162,6

**Table 6. Actual shear capacity of the beam based on compressive strength of the cubes, Series II**

Age [days]	$f_{cc}$ [MPa] from curve (trend line)	Ultimate Load $P_{max,mean}$ [kN] (Experimental test)	Ultimate Load $P_{max}$ based on FEM in ATENA [kN]	Ultimate Load $P_{max}$ based on Rafla's formula [kN]
3	21,5	-	-	-
7	28,0	-	-	-
28	36,0	-	170,4	157,3
70	39,5	186,7	179,2	165,7
90	40,2	-	180,6	166,2

**Table 7. Actual shear capacity of the beam based on compressive strength of the cubes, Series III**

Age [days]	$f_{cm,cube}$ [MPa] from curve (trend line)	Ultimate Load $P_{max,mean}$ [kN] (Experimental test)	Ultimate Load $P_{max}$ based on FEM in ATENA [kN]	Ultimate Load $P_{max}$ based on Rafla's formula [kN]
3	27,8	-	-	-
7	36,2	-	-	-
28	46,5	-	193,8	178,7
70	51,0	204,9	202,8	187,2
90	51,9	-	204,6	188,8
365	60,6	-	212,0	204,1

**Table 8. Actual shear capacity of the beam based on compressive strength of the cubes, Series IV**

Age [days]	$f_{cm,cube}$ [MPa] from curve (trend line)	Ultimate Load $P_{max,mean}$ [kN] (Experimental test)	Ultimate Load $P_{max}$ based on FEM in ATENA [kN]	Ultimate Load $P_{max}$ based on Rafla's formula [kN]
3	27,2	-	-	-
7	35,4	-	-	-
28	45,5	-	191,2	176,8
70	49,9	194,7	200,6	185,2
90	50,8	-	202,0	186,8
365	54,5	-	209,8	193,5

**Table 9. Actual shear capacity of the beam based on compressive strength of the cubes, Series V**

Age [days]	$f_{cm,cube}$ [MPa] from curve (trend line)	Ultimate Load $P_{max,mean}$ [kN] (Experimental test)	Ultimate Load $P_{max}$ based on FEM in ATENA [kN]	Ultimate Load $P_{max}$ based on Rafla's formula [kN]
28	46,0	-	192,6	177,8
90	51,4	-	203,6	187,9
365	55,1	-	210,8	194,6
449	55,5	203,2	211,6	195,3
685	56,2	-	212,8	196,5

**Table 10. Actual shear capacity of the beam based on compressive strength of the cubes, Series VI**

Age [days]	$f_{cm,cube}$ [MPa] from curve (trend line)	Ultimate Load $P_{max,mean}$ [kN] (Experimental test)	Ultimate Load $P_{max}$ based on FEM in ATENA [kN]
3	47,8	-	-
7	62,3	-	-
28	80,0	-	248,2
84	88,9	250,1	261,6
240	95,3	-	277,2

**Table 11. Actual shear capacity of the beam based on compressive strength of the cubes, Series 7**

Age [days]	$f_{cm,cube}$ [MPa] from curve (trend line)	Ultimate Load $P_{max,mean}$ [kN] (Experimental test)	Ultimate Load $P_{max}$ based on FEM in ATENA [kN]
3	48,5	-	-
7	63,1	-	-
28	81,0	-	249,8
90	90,5	-	264,0
240	94,2	229,9	271,2

When using the *3D Nonlinear Cementitious 2* material properties for concrete, the tensile strength and fracture energy are calculated by the software based on the given compressive strength. In this element type, the fracture is modelled by an orthotropic smeared crack model based on Rankine tensile criterion and the hardening–softening plasticity model is based on the Menétrey-William three-parameter failure surface to model concrete crushing (Menétrey & William 1995), see Appendix IV. Therefore the crack pattern changes if the strength changes.

## 6. Results of short-term loading tests

### 6.1. Failure load

In short-term tests, upon the growth of the crack to the compression zone, the beam fails by crushing of the concrete compressive-zone. This occurs before the tension zone reinforcement yields, which does not provide any warning as the fracture is instantaneous. The ultimate load  $P_{max}$  is considered to be the highest peak in the  $P-\delta$  curve. The value of  $P_{max}$  for each specimen is presented in Table 12 together with the mean values and coefficient of variations.

**Table 12. The failure load of the specimen tested in short-term loading**

Series	Cast date	Label	Age at loading [days]	Time of loading [sec]	Failure load, $P_{max}$ [kN]	Mean [kN]	COV %
I	8 Oct 2009	S1B1	28	226	192,0	184,7	4,59
		S1B2	28	92	176,1		
		S1B3	28	194	195,0		
		S1B4	28	258	174,1		
		S1B5	32	176	188,0		
		S1B6	32	162	182,9		
II	2 Nov 2009	S2B1	71	201	181,8	188,8	3,24
		S2B2	72	444	192,7		
		S2B3	72	191	192,1		
III	20 Nov 2009	S3B1	83	773	202,1	204,9	1,44
		S3B2	83	1697	208,0		
		S3B3	83	393	204,6		
IV	2 Feb 2010	S4B1	65	683	187,4	194,7	4,87
		S4B2	65	199	191,2		
		S4B3	65	346	205,4		
V	7 Apr 2010	S5B1	449	309	199,6	203,2	3,10
		S5B2	449	354	199,6		
		S5B3	449	404	210,5		
VI	17 Jun 2010	S6B1	89	212	250,3	250,1	2,74
		S6B2	89	239	256,8		
		S6B3	89	194	243,1		
VII	17 Aug 2010	S7B1	203	495	243,8	230,0	6,73
		S7B2	203	256	213,2		
		S7B3	203	325	232,7		

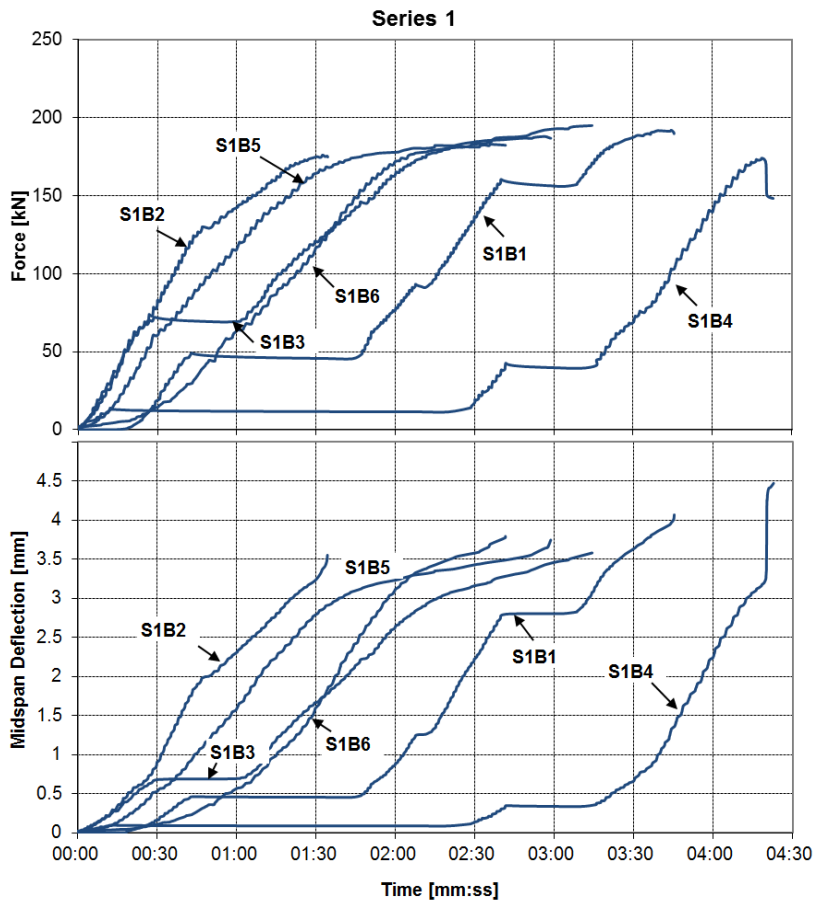


Fig. 14: Loading and midspan deflection of the beam in time, Series I

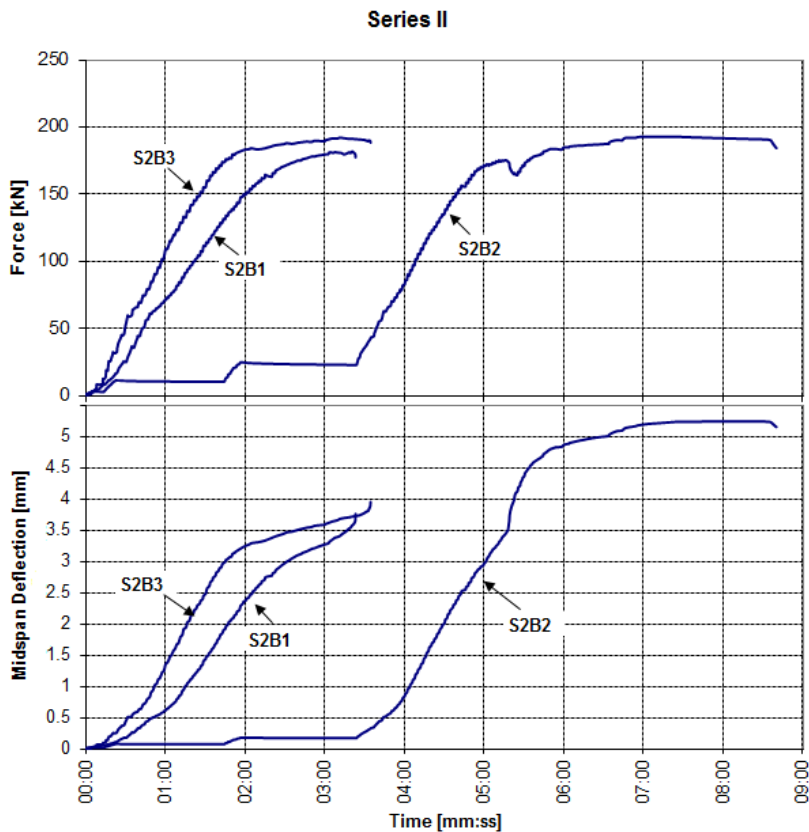


Fig. 15: Loading and midspan deflection of the beam in time, Series II

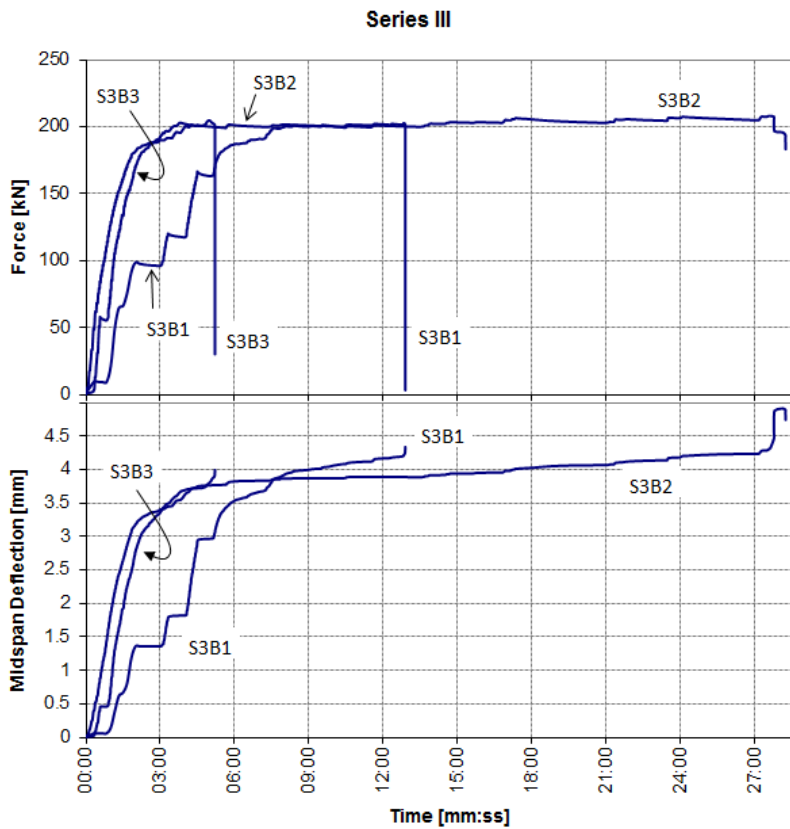


Fig. 16: Loading and midspan deflection of the beam in time, Series III

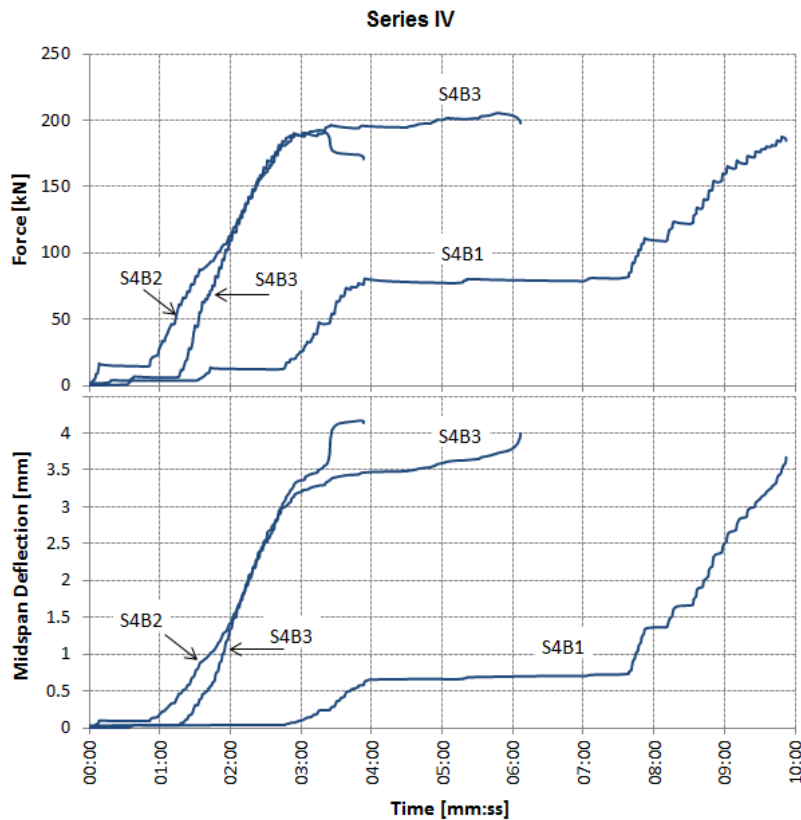


Fig. 17: Loading and midspan deflection of the beam in time, Series IV

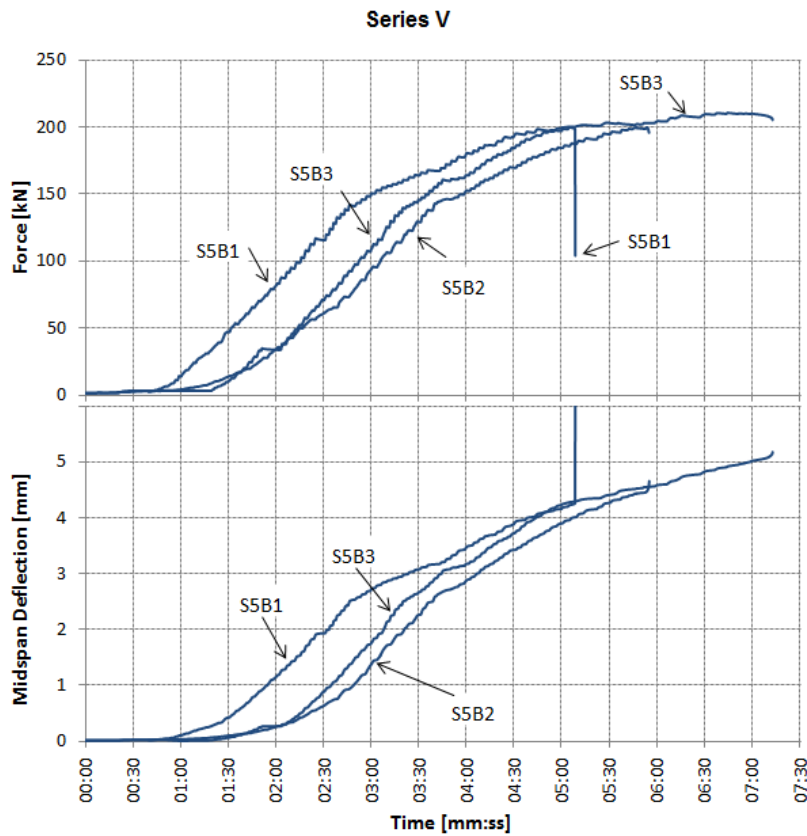


Fig. 18: Loading and midspan deflection of the beam in time, Series V

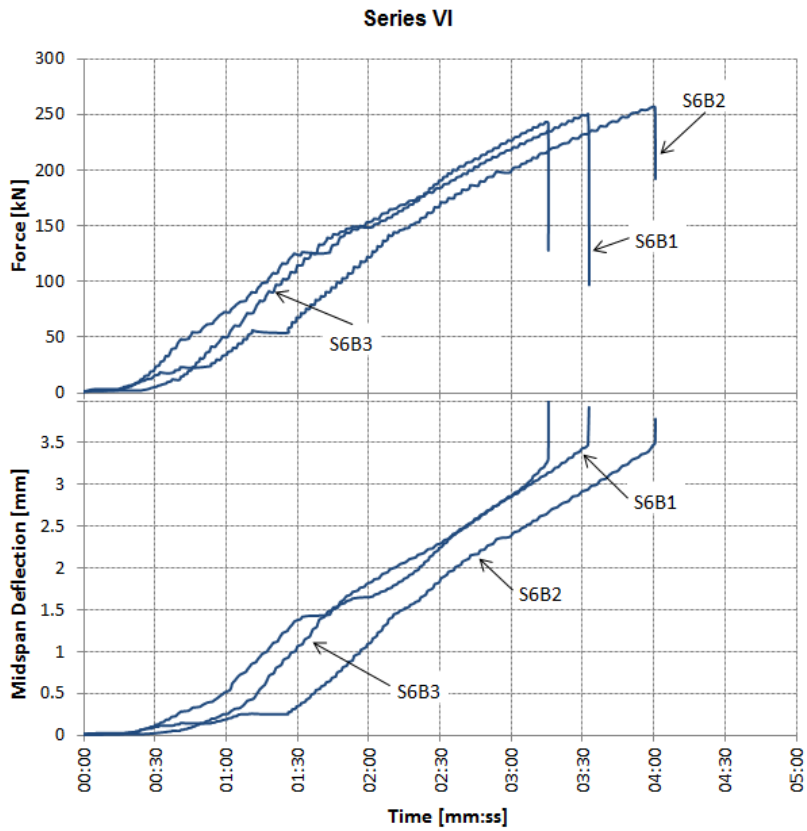


Fig. 19: Loading and midspan deflection of the beam in time, Series VI

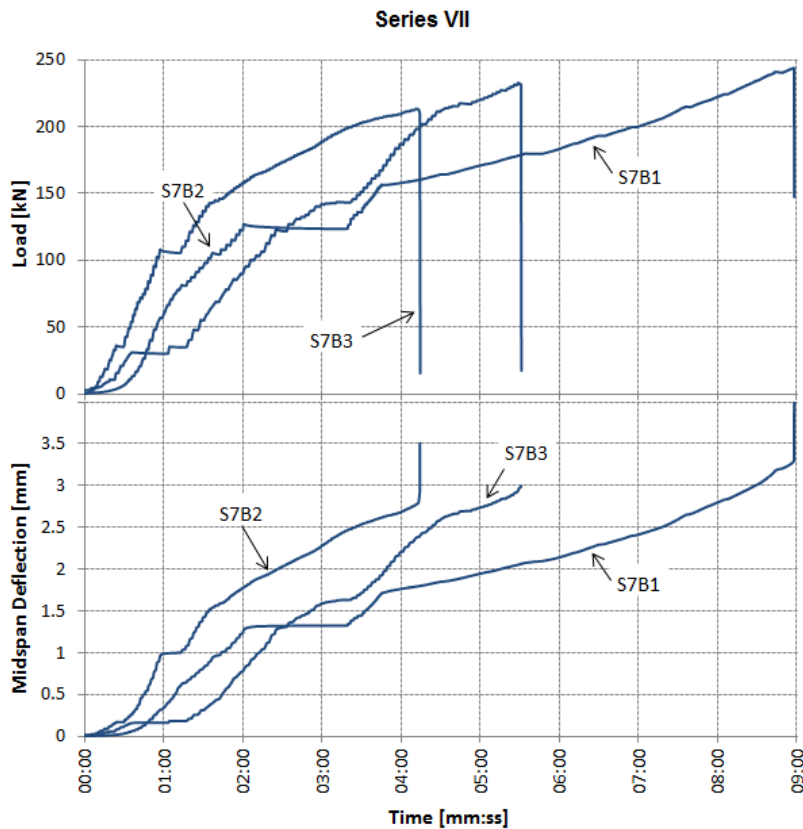


Fig. 20: Loading and midspan deflection of the beam in time, Series VII

## 6.2. Types of failure

Two types of failure are observed in the short-term tests. Both are flexural shear failure, but Type I is characterized by a shear crack crossing the potential compression strut and Type II is failure due to a crack not crossing the potential compression strut which is mostly associated with a relatively higher ultimate load, see Fig. 4. Specimens S1B4, S2B2, S3B2, S4B1 and S4B2 show Type II failure, which has a large midspan deflection and a large crack opening displacement. The reason to have a larger deflection and a larger crack opening than with the first failure type is that the crack tip ends under the loading plate and the confining action by the loading plate prevents the crack tip to open. However, more deflection leads to larger crack opening at the middle of the crack. The rest of the beams fail according to Type I, which involves instantaneous fracture of the beam.

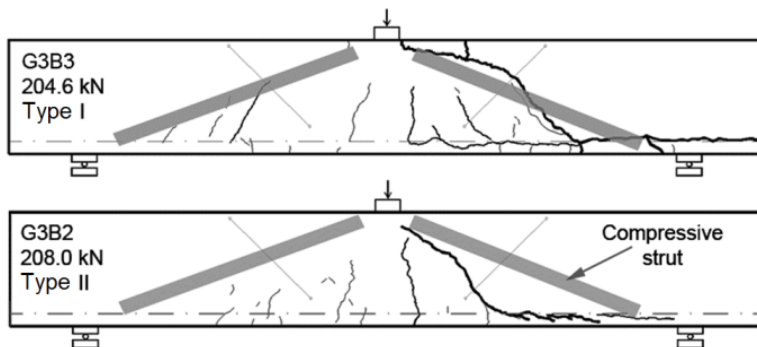
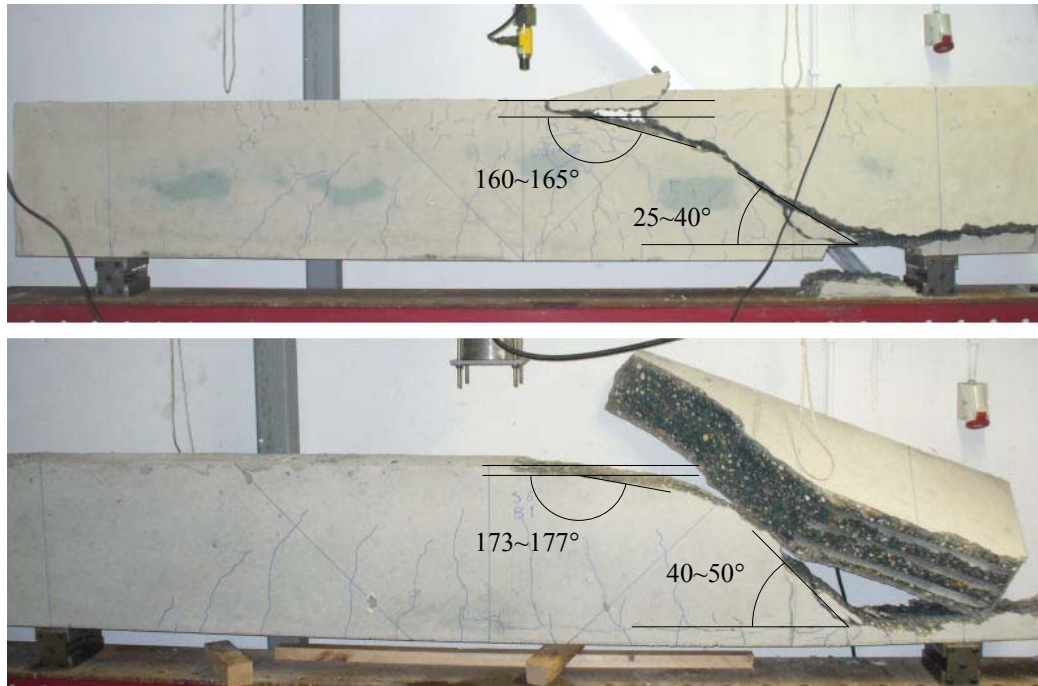


Fig. 21: Two types of failure; beam S3B3 failing in Type I and beam S3B2 failing in Type II.

The failure of the beams with Normal Strength Concrete is compared to the failure of the beams with High Strength Concrete in Fig. 22. The height of the compression zone in the HSC beams is smaller than in the NSC beams, whereas the angle at the base of the crack relative to the longitudinal axis is greater. The crack initiates

at the bottom of the beam as flexural crack and grows diagonally towards to the loading plate, while reaching the concrete compression zone, the crack angle reduces and it becomes flat. In HSC beams, the angle of the crack in the middle is greater than its angle in NSC beams. At the moment of failure, one of these cracks follow a 3<sup>rd</sup> order polynomial-shape curve and becomes inclined at top (close to loading point) and at bottom (along the reinforcement to the end of the beam).



**Fig. 22: Comparison of crack pattern in NSC (Top) and HSC beam (Bottom)**

In Fig. 23, the surface of the crack in a NSC beam and a HSC beam is presented. Noticeably, in HSC beams the shear crack crosses through the aggregates and while in NSC beams the crack follows a path between the aggregates. As a result, the roughness of the crack surface in NSC beams is more than HSC.



**Fig. 23: Surface of crack in NSC (Left) and HSC beam (Right)**

### 6.3. Midspan deflection

Fig. 24-28 plot the load-deflection response of specimens, which have been tested in short-term loading. These graphs show a very low scatter of the results.

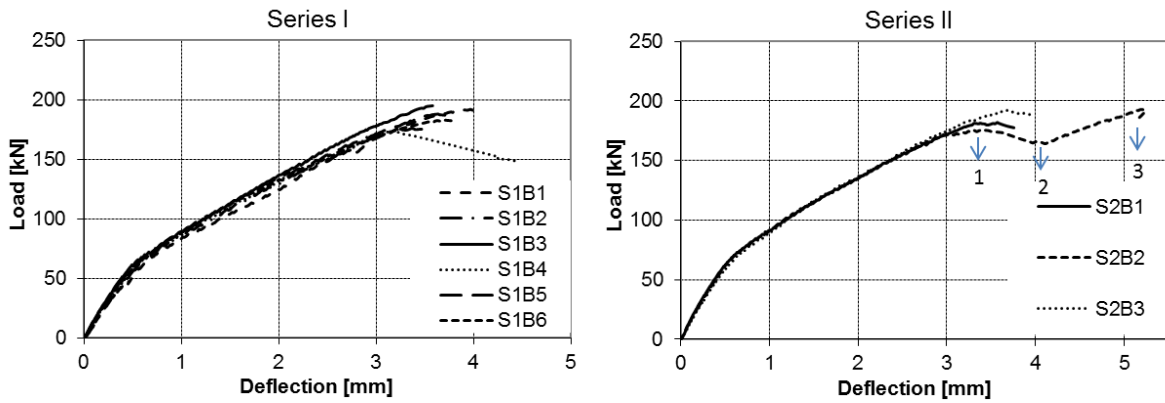


Fig. 24: Load-deflection curve, specimens series I and II, Numbers correspond to the cracks in Fig. 31

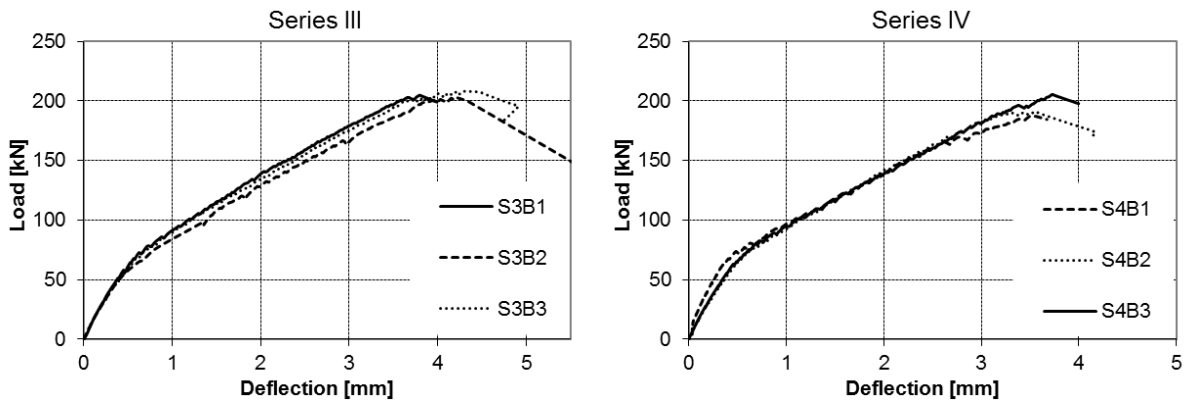


Fig. 25: Load-deflection curve, specimens series III and IV

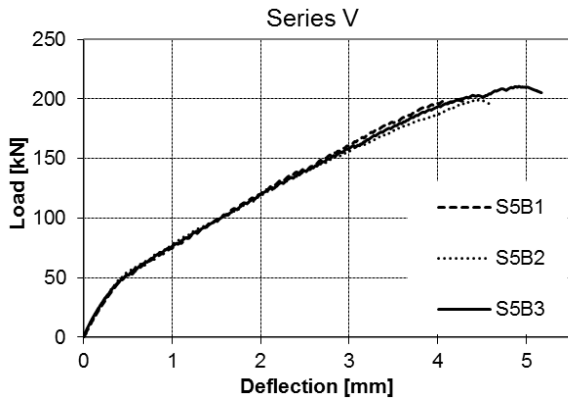


Fig. 26: Load-deflection curve, specimens series V

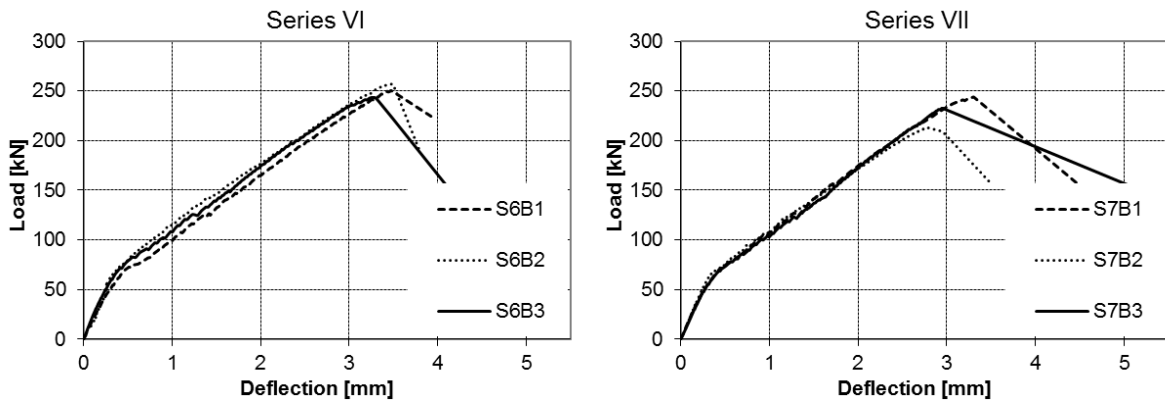


Fig. 27: Load-deflection curve, specimens series VI and VII (High strength concrete)

### 6.4. Crack opening displacement

Diagonal deflections of the beams versus the applied force are obtained for the reference beams. The deflections in Fig. 28, 29 are measured along two diagonal LVDT's that are installed on the surface of the beam (Fig. 12). The diagonal LVDT's have a measuring length of 40 cm and may cover several cracks.

As it is explained in Section 6.5, The crack pattern on the surface of the beam consists of shear cracks on both shear spans as well as flexural cracks in the middle of the beam. Due to symmetry of shear spans in three-point bending tests, two main shear cracks appear on the beam, which are wider and longer than other cracks and can be easily distinguished. In this report, they are called right and left shear cracks (i.e. the shear crack on the right/left side of the loading plate). However, the symmetry of the beam does not guaranty the similar length or similar width of the two main shear cracks. Usually, one of the cracks (left or right) is wider than the other is and propagates faster too. Upon the growth of the crack to the compression zone, the beam fails by crushing of the compressive-zone concrete and before the tension zone reinforcement yields, which does not provide any warning before failure as the fracture is instantaneous.

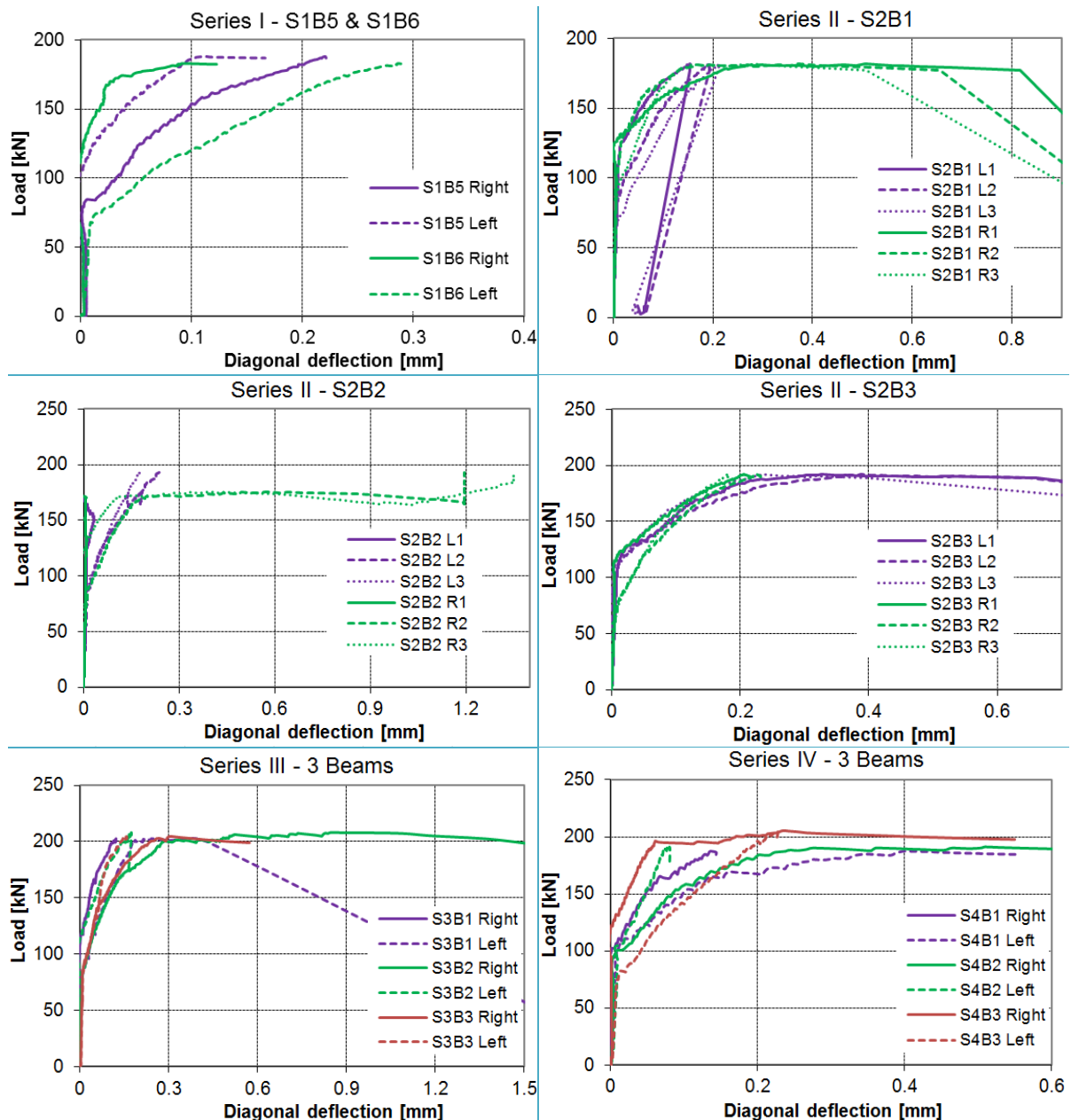


Fig. 28: Diagonal deflection of beams in series I-IV, recorded by the diagonal LVDT's

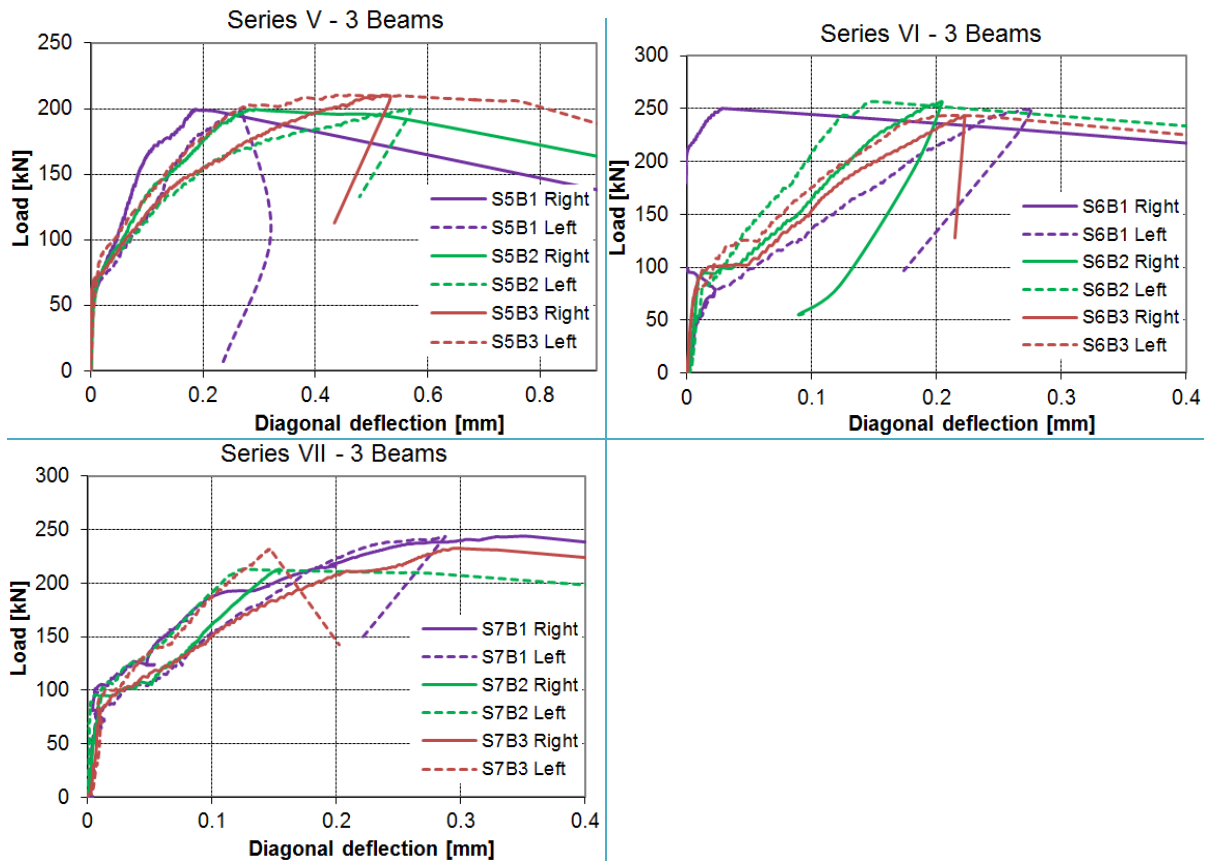


Fig. 29: Diagonal deflection of beams in series V-VII, recorded by the diagonal LVDT's

### 6.5. Crack pattern

After fracture of the beams in short-term loading, the crack pattern is highlighted on the surface of beam and later is schemed into an Autocad file. In this section, the crack pattern for each specimen is presented. The crack patterns, which are shown in **Error! Reference source not found.**-50 are obtained after the failure of the beam. Hence, due to the secondary effect of the instantaneous failure and the subsequent large deflection, some of the flexural cracks as well as longitudinal crack along the reinforcing bars, increase in both length and width. Thus in some crack pattern presentation, some flexural cracks as well as longitudinal crack along the reinforcing bar are presented as a wide open crack.

There are three types of cracks shown in the figures; a thick line represents the shear failure crack, semi-thick lines represent clearly visible wide cracks, which could cause the failure or contribute to failure, and thin lines to indicate cracks, which are barely visible. It is attempted to mark the shrinkage cracks before the test so that these cracks are not drawn in the crack pattern, however some thin cracks appeared during the test due to both shrinkage and loading stresses and it is hard to separate them from bending and shear cracks. Thus, these cracks are also shown in the figures. Blue lines and green lines represent the position of the longitudinal reinforcement and the position of diagonal LVDT's, respectively.

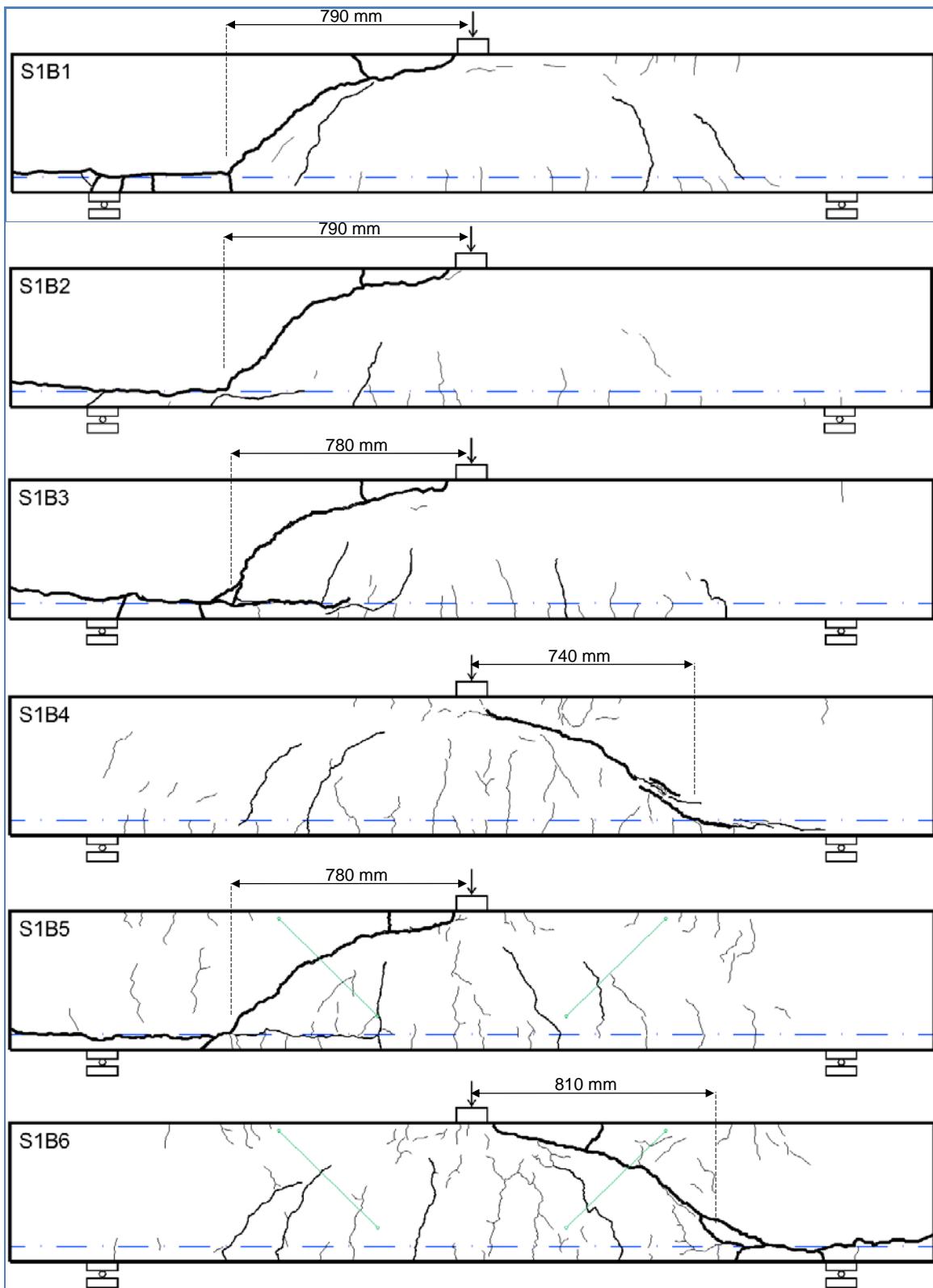


Fig. 30: Crack patterns of specimens series I

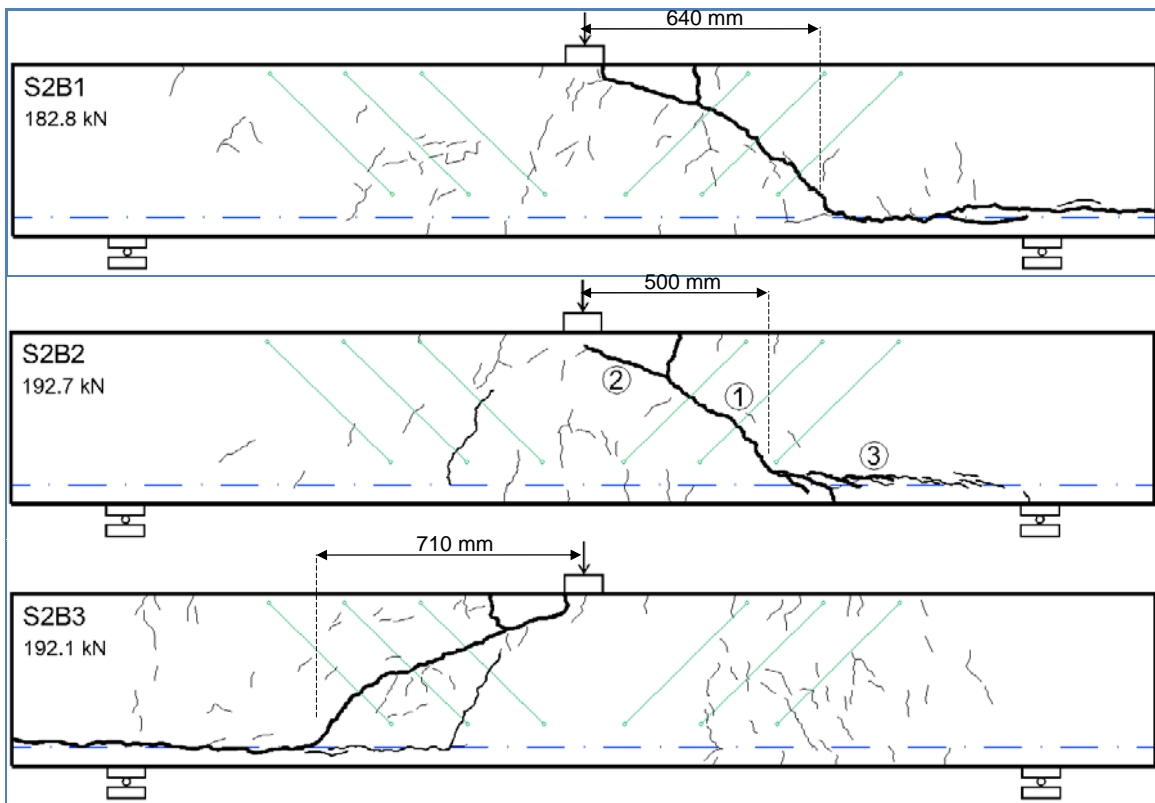


Fig. 31: Crack patterns of specimens series II

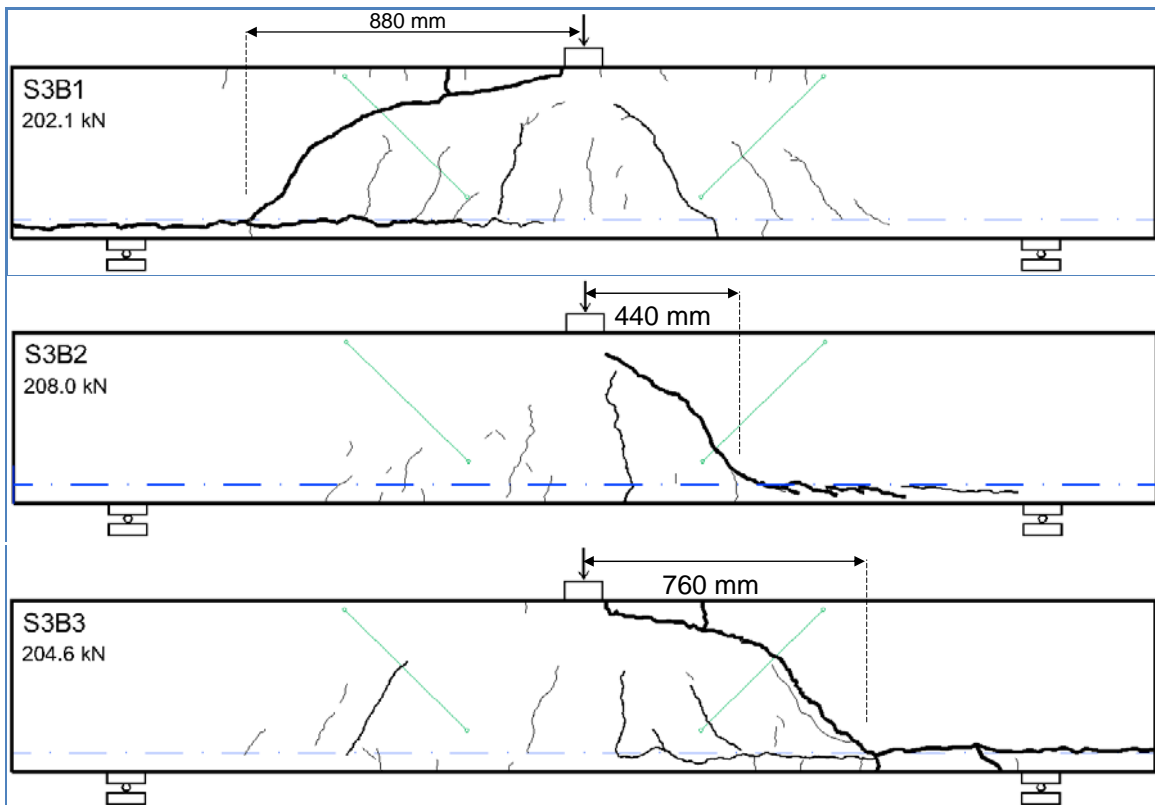


Fig. 32: Crack patterns in specimens series III

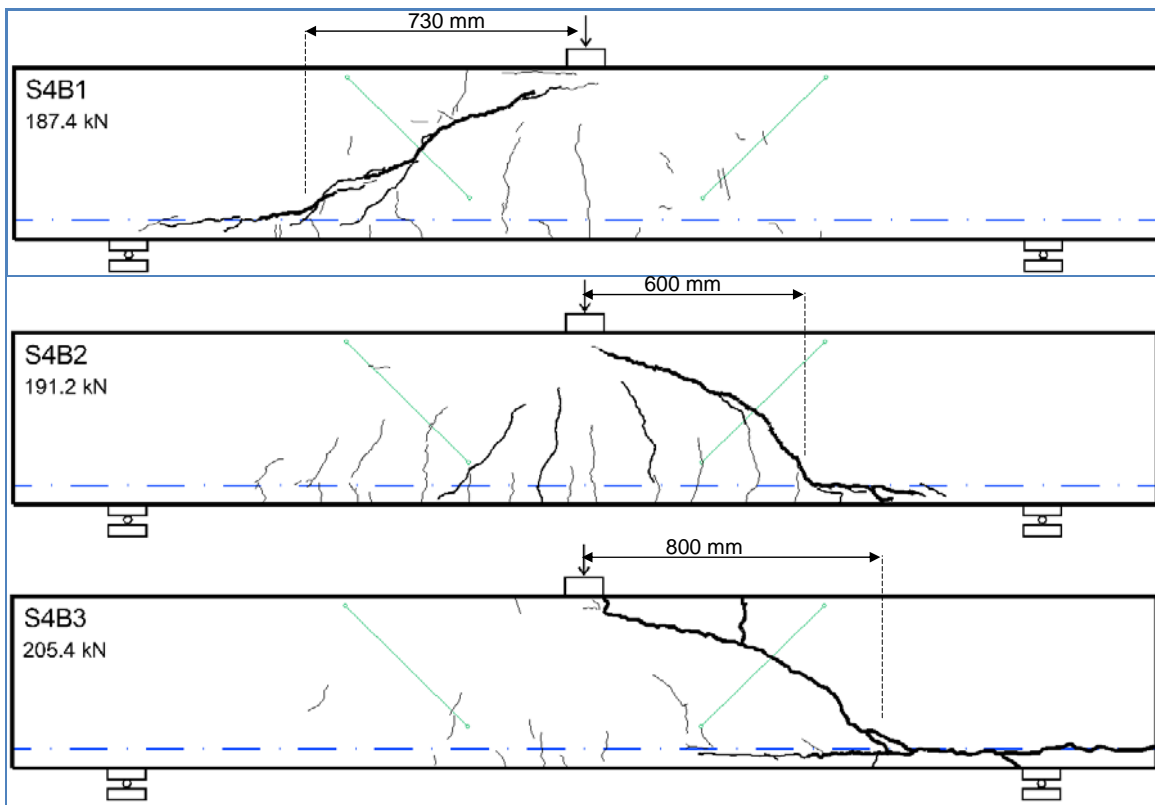


Fig. 33: Crack patterns of specimens series IV

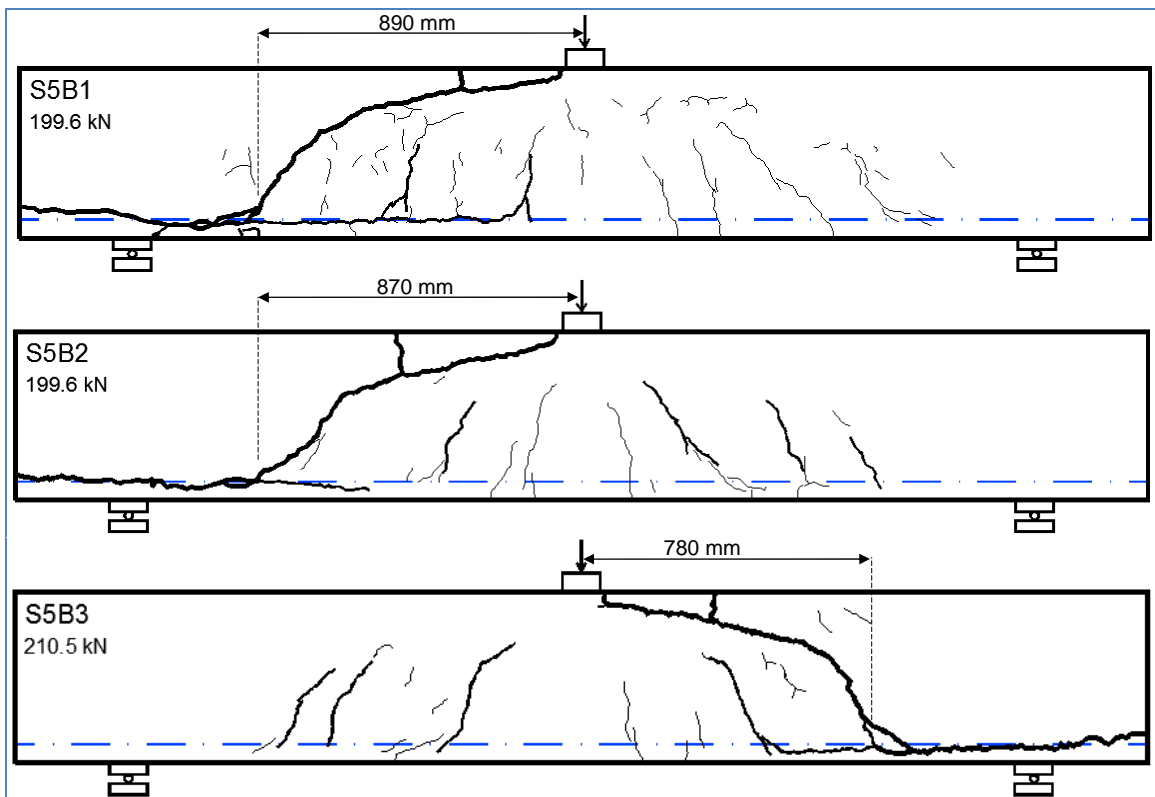


Fig. 34: Crack patterns of specimens series V

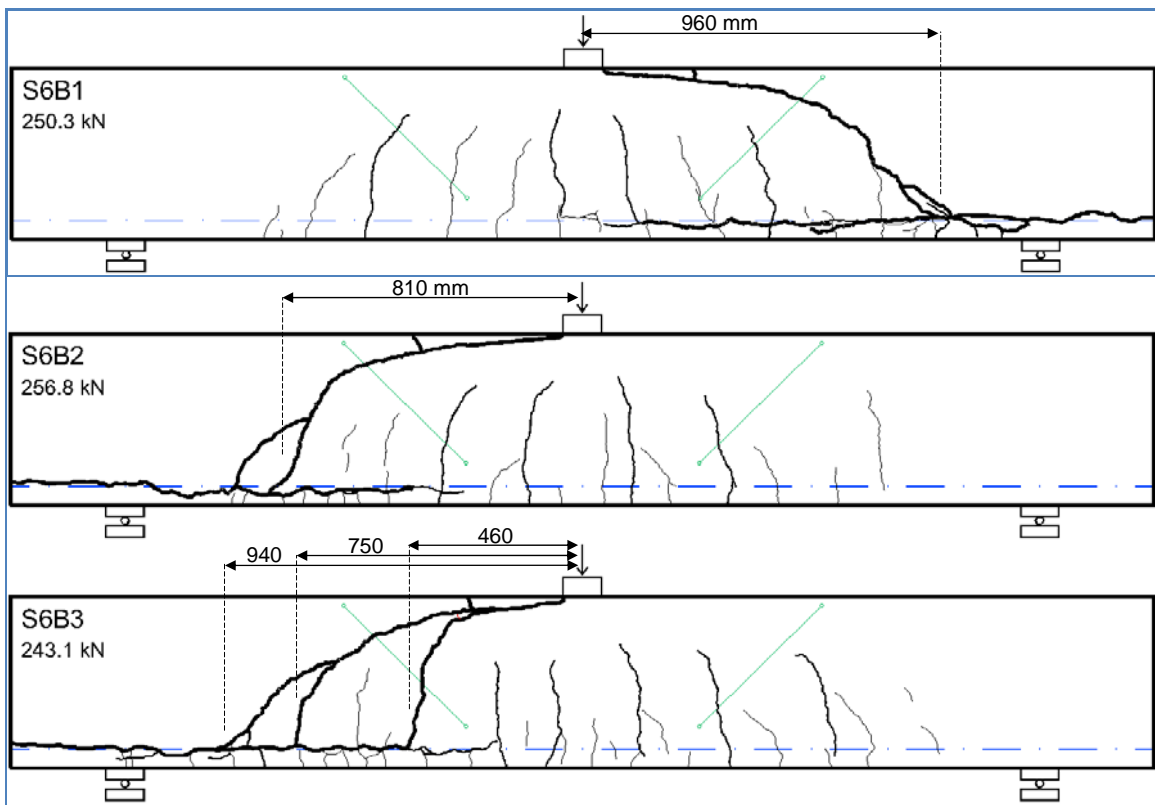


Fig. 35: Crack patterns of specimens series VI S6B3

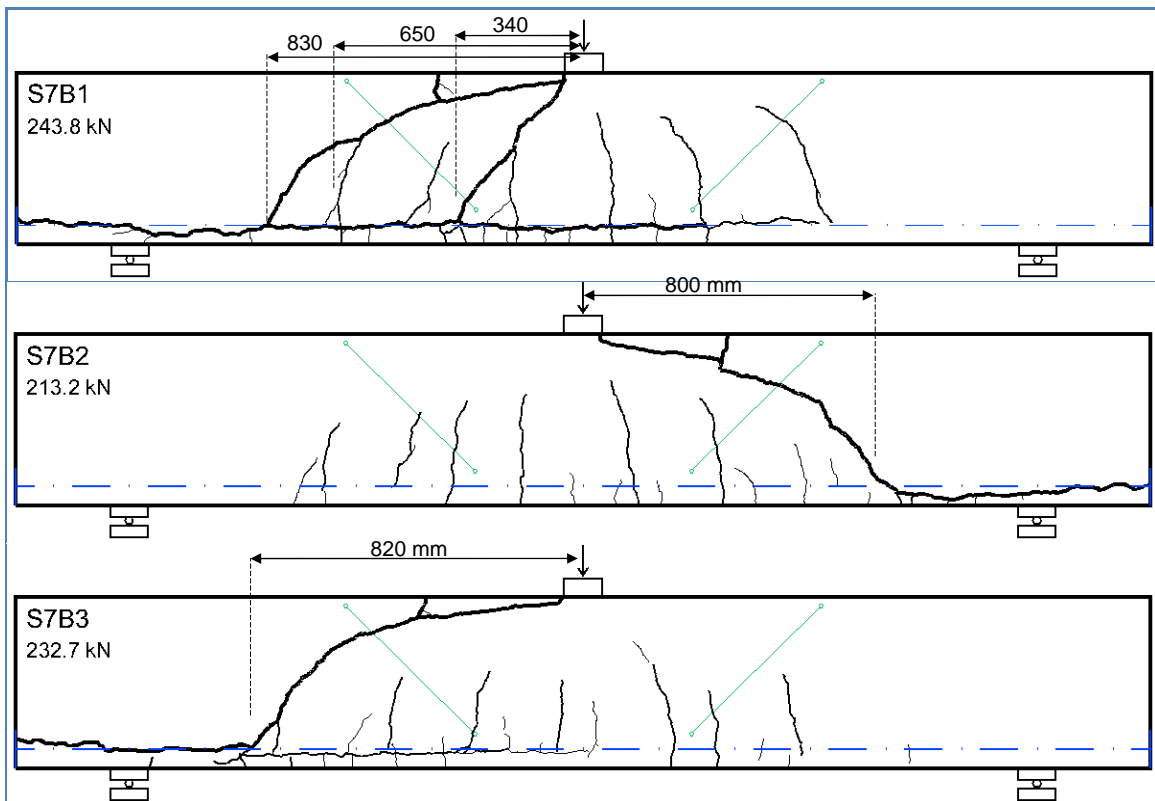


Fig. 36: Crack patterns of specimens series VII

## 6.6. Summary of short-term loading tests

A brief summary of testing concrete beams without shear reinforcement under short-term loading can be drawn as following:

- The test results on full-scale concrete beams show a relatively small scatter of  $P_{max}$  (in the same series) with a coefficient of variation from 1,44% to 6,73% as shown in Table 12.
- The mean value of the failure load  $P_{max}$  in each series will be used as a reference value for the further tests in long-term loading. Moreover, the load-deflection curves will be used to predict the failure of the beams subjected to long-term loading in early ages.
- The crack pattern and formation of the cracks in short-term loading enables a comparison to the crack pattern (angle, inclination and length) in short-term and in long-term loading and short-term loading.
- While testing specimen S2B2, the load reached the ultimate capacity of the testing setup, but the beam did not. At that point, the load was kept at the highest possible level and after a few minutes, the shear failure occurred. The effect of creep, shrinkage and stress relaxation were neglected in short-term loading.

## 7. Results of long-term loading tests

As discussed earlier, the concrete beams are subjected to long term loading for a period between 3 months and 3 years. The goal is to study the behaviour of wide and long shear cracks under high sustained loading, which is at a load close to the ultimate shear capacity. Three beams out of each series (except series I, which are all tested in short-term loading) are tested in long-term loading. Long-term sustained loading tests performed directly after performing the short-term static tests. Of course, a few days are required to install and prepare the specimens in the setup.

A load ratio between 87% and 95% of the  $P_{max}$  is applied to the beams, as explained in Table 1. Undeniably, due to the high load ratio (when the load is within the 95% interval of  $P_{max}$ ), the risk of failure during application of the load increases as the load ratio increases. In some cases (specimens S3B4, S5B5, S6B6 and S7B4) beam fails before reaching the desired load level. During the long-term loading tests, the crack opening development, the crack length development and the appearance of new cracks are monitored.

### 7.1. Load level

#### 7.1.1. Series II

Specimens S2B4, S2B5 and S2B6 in series II were the first specimens, which were tested in long-term loading. The long-term tests started at age of the concrete of 73 days (1 day after performance of the short-term tests). In order to prevent failure of the beams during loading, the first series of long-term loading was carried out with a load ratio of 87% of the mean short-term ultimate capacity  $P_{max, mean}$ . The mean value of the failure load under short term testing was  $P_{max, mean} = 188,8$  kN which is considered to be the primary ultimate load. Thus the sustained load for the first step of loading was;

$$P_{sustained,II} = 0,87 P_{max, mean} = 0,87 \cdot 188,8 = 165 \text{ kN} \quad (4)$$

where  $P_{sustained,II}$  is the sustained load applied to series II.

In order to calculate a confidence interval of the long-term loading, the mean value of short-term tests  $P_{max, mean}$  should be computed. The normal distribution function of ultimate capacities in short-term is shown in Fig. 37. The Upper and Lower Confidence limit can be computed by adding and subtracting 1,96 standard deviations to/from the mean value. The value of 1,96 is based on the fact that 95% of the area of a normal distribution is within 1,96 standard deviations of the mean; the standard error of the mean is 12,0 kN.

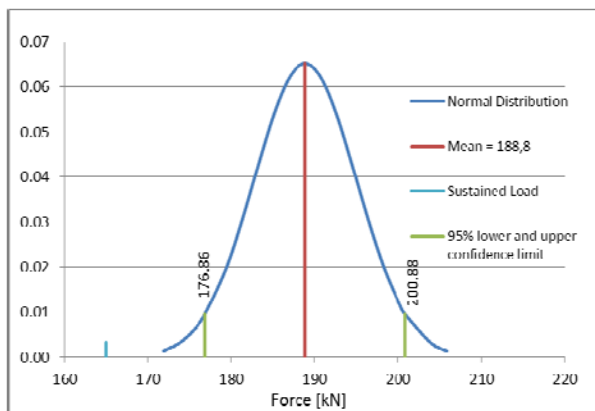


Fig. 37: Normal distribution function of test data, Series II. The sustained load (165 kN) is lower than lower confidence limit.

The 95% lower and upper confidence limits of series II are 176,8 kN and 200,8 kN, respectively, which means that the probability of failure of the beam under 176,8 kN is 2,5% and under 200,8 kN is 97,5 kN. If the beam is loaded at 165 kN, the chance of failure of the beam would be definitely lower than 2,5%.

The long-term load on the beams S2B4, S2B5 and S2B6 under 87% of the mean value of ultimate capacity was applied for 74 days. Cube compressive strength tests were also measured in time together with the beam tests to get insight into the concrete strength development. After 75 days of sustained loading (concrete age = 145 days), the loading ratio is adjusted to 90% of the actual shear strength, which was calculated using Raffla’s formula according to the actual cube compressive strength, see Table 6. The load ratio is kept at 90% for 5 days, and then it is increased to 92,5%. This procedure continues until failure of the beam. In Fig. 38 the results of these tests are presented.

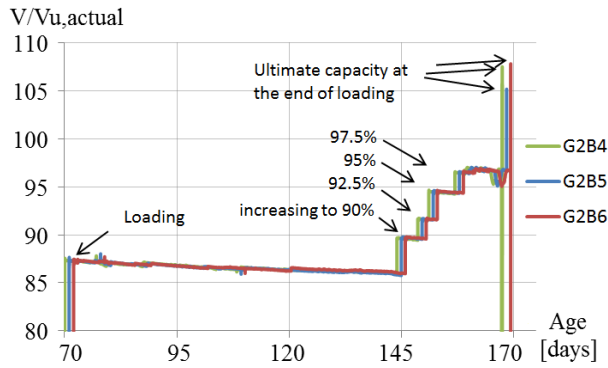


Fig. 38: Relative load in time and ultimate capacity after ending sustained loading.

The actual capacity of the beam at concrete age = 145 days according to Table 6 is:

$$P_{u,actual} (145 \text{ days}) = \sigma \cdot P_{max, mean} = 193,3 \text{ kN} \quad (5)$$

where,  $P_{u,actual}$  is the actual ultimate capacity of the beam and  $\sigma$  is the factor of the shear strength increase due to hydration of the cement in time, and can be calculated from:

$$\sigma = V_{u,Raffla} (147 \text{ days}) / V_{u,Raffla} (70 \text{ days}) = 1,024 \quad (6)$$

The loading steps with the duration of each step are shown in Table 13. Finally, after 97 days testing under sustained loading, the beams were loaded up to failure. As shown in Table 13, the shear capacities of the beams were 6-8% higher than the actual calculated value.

Table 13. Load steps and duration of long-term loading, specimen series II, concrete age at  $t=0$  was 70 d

Load step	S2B4	S2B5	S2B6
87% $P_{max}$	165 kN 74 days	165 kN 74 days	165 kN 74 days
90% $P_{u,actual} (145 \text{ days})$	172 kN 4 days	172 kN 4 days	172 kN 4 days
92% $P_{u,actual} (148 \text{ days})$	176 kN 3 days	176 kN 3 days	176 kN 3 days
95% $P_{u,actual} (154 \text{ days})$	181,5 kN 6 days	181,5 kN 6 days	181,5 kN 6 days
97,5% $P_{u,actual} (164 \text{ days})$	186 kN 10 days	186 kN 10 days	186 kN 10 days
Failure	206,9 kN	202,4 kN	207,4 kN

### 7.1.2. Series III

The long-term testing of series III started at a concrete age of 87 days. This series of long-term loading is carried out at a load level of 95% of the ultimate capacity. The mean value of the failure load under the short term tests was 205,1 kN. Thus the sustained load for the first step of sustained loading is;

$$P_{sustained,III} = 0,95 P_{max,mean} = 0,95 \cdot 205,1 = 194,8 \text{ kN} \quad (7)$$

where  $P_{sustained,III}$  is the sustained load level that is applied to series III.

The normal distribution function of the short-term ultimate capacities (S3B1, S3B2 and S3B3) is shown in Fig. 39. The Confidence Limits of series III are 199,1 kN and 210,7 kN, which means that if the beam is loaded at 194,8 kN, the chance of failure the beam would be lower than 2,5%.

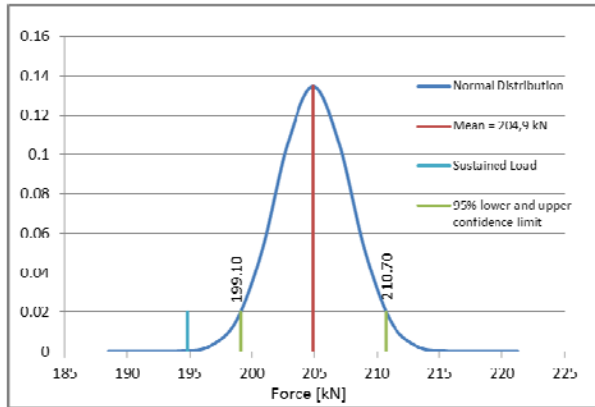


Fig. 39: Normal distribution function of test data, Series III. The sustained load (194,8 kN) is lower than lower confidence limit

Table 14. Load steps and duration of long-term loading, specimen series III, concrete age at t=0 was 87d

Load level	S3B4	S3B5	S3B6
95% $P_{max}$	Failed at 194,8 kN	195 kN	195 kN
	–	67 days	67 days
95,8% $P_{u,actual}$ (145 days)	–	200 kN	200 kN
	–	70 days loading	70 days loading
Unloaded	–	–	–
	–	55 days	55 days
94,5% $P_{u,actual}$ (279 days)	–	200 kN	Failed at 196 kN
	–	Since 16 Aug 10	–

Specimen S3B3 failed during the load application and just before sustained loading begins, at a load level of 194,8 kN. The long-term loading on beams S3B5 and S3B6 under 95% of the mean value of the ultimate capacity lasted 67 days. Similar to series I, the cube strength of the concrete was measured in time in order to evaluate the strength increase due to further hydration. According to the compressive strength development in Table 7, the ratio between the ultimate capacity at the 67<sup>th</sup> day of loading (concrete age = 154 days) and the ultimate capacity at the first day of loading (concrete age = 87 days) and is:

$$V_{u,Rafta (154 \text{ days})} / V_{u,Rafta (87 \text{ days})} = 1,018 \quad (8)$$

Likewise, the ratio of ultimate capacities at the time of reloading (concrete age = 279 days) and the first day of loading is:

$$V_{u,Rafta (279 \text{ days})} / V_{u,Rafta (87 \text{ days})} = 1,031 \quad (9)$$

Thus, the actual ultimate capacities can be expressed as:

$$P_{u,actual (154 \text{ days})} = 1,018 P_{max, mean} = 1,018 \cdot 205,1 = 208,8 \text{ kN} \quad (10)$$

$$P_{u,actual (279 \text{ days})} = 1,031 P_{max, mean} = 1,032 \cdot 205,1 = 211,7 \text{ kN} \quad (11)$$

where,  $P_{u,actual}$  is the actual ultimate capacity of the beams.

After 67 days of sustained loading (concrete age = 154 d), the load was increased to 200 kN. The loading steps with the duration of each step are shown in Table 14. The load level of 200 kN was maintained for 70 days. Because the capacity of the setup was already reached (200 kN) the actuators and load cells

were replaced by new ones, in order to apply higher loads up to 400 kN. Substituting of the new setup, took 55 days and during this time, all the specimens were unloaded.

After reloading the beams, specimen S3B6 failed at a load level of 196 kN. The last beam (S3B5) is still under long-term loading.

### 7.1.3. Series IV

The long-term testing of series IV started at a concrete age of 71 days. This series of long-term loading is carried out at a load level of 95% of the ultimate capacity. According to Table 12, The mean value of the failure load under the short term tests was  $P_{max,mean} = 194,7$  kN. Thus the sustained load for the first step of sustained loading is;

$$P_{sustained,IV} = 0,95 P_{max,mean} = 0,95 \cdot 194,7 = 185,0 \text{ kN} \quad (12)$$

where  $P_{sustained,IV}$  is the sustained load level that is applied to series IV.

The normal distribution function of the short-term ultimate capacities (S4B1, S4B2 and S4B3) is shown in Fig. 40. The 95% lower and upper confidence limits of series IV are 176,1 kN and 213,3 kN, respectively. With a sustained loading level of 185 kN, the chance of failure the beam is 14,7%.

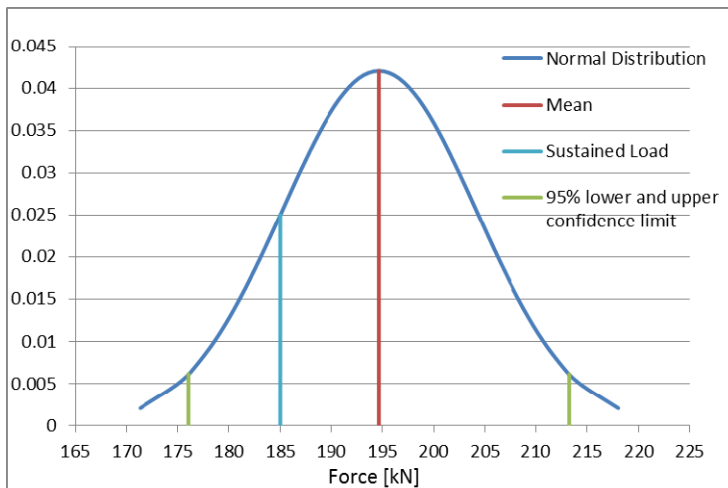


Fig. 40: Normal distribution function of test data, Series IV. The sustained load value (185 kN) is larger than lower confidence limit

Specimen S4B6 failed after  $t = 145$  minutes under sustained loading test, at a load level of 185 kN. The long-term loading of specimens S4B4 and S4B5 under the 95% of the mean value of ultimate capacity performed for 70 days, and then the beams were unloaded for 55 days for the installation of new equipment to increase the capacity, see Table 15.

According to the results of the shear resistance based on Rafla's formula from Table 8, the ratio between the ultimate capacity at the concrete age of 196 days (time of reloading, see Table 15) and the ultimate capacity at the first day of loading (concrete age = 71 days) and is:

$$V_{u,Rafla(196 \text{ days})} / V_{u,Rafla(71 \text{ days})} = 1,032 \quad (13)$$

Likewise, the ratio of ultimate capacities at the time of reloading (concrete age = 423 days) and the first day of loading is:

$$V_{u,Rafla(423 \text{ days})} / V_{u,Rafla(71 \text{ days})} = 1,048 \quad (14)$$

Thus, the actual ultimate capacities can be expressed as:

$$P_{u,actual (196 \text{ days})} = 1,032 P_{max, mean} = 1,032 \cdot 194,7 = 200,9 \text{ kN} \quad (15)$$

$$P_{u,actual (423 \text{ days})} = 1,048 P_{max, mean} = 1,048 \cdot 194,7 = 204,0 \text{ kN} \quad (16)$$

where,  $P_{u,actual}$  is the actual ultimate capacity of the beams.

After 70 days of sustained loading (concrete age = 141 d) and 55 days unloading time, the beams were reloaded to 190,5 kN that was 95% of the actual ultimate capacity (at concrete age = 196 days). The loading steps with the duration of each step are shown in Table 15. Lastly, it was attempted to load the beams to failure, which was at that moment expected to be  $P_{u,actual (423 \text{ days})} = 204,0$  kN, but the beams did not fail until 205,0 kN. At that level of loading, a wide and long shear crack appeared in specimen S3B4, thus the loading stopped at 205,0 kN in both specimens. The specimens then remained under sustained loading with a load level of 205,0 kN (100% of the calculated actual capacity) for 28 days. Afterwards, to obtain the real ultimate capacity of the beams, they were loaded until failure. The ultimate capacities in both specimens were about 13% higher than the expected capacity ( $P_{u,actual (423 \text{ days})}$ ).

**Table 15: Load steps and duration of long-term loading, specimen series IV, concrete age at  $t=0$  was 71 d**

Load step	S4B4	S4B5	S4B6
95% $P_{max,mean}$	185 kN 70 days	185 kN 70 days	185 kN Failed after 145 minutes
Unloaded	– 55 days	– 55 days	–
95% $P_{u,actual (196 \text{ days})}$	190,5 kN 227 days	190,5 kN 227 days	–
100% $P_{u,actual (279 \text{ days})}$	205 kN 28 days	205 kN 28 days	–
Failure	230,4 kN	234,2 kN	–

#### 7.1.4. Series V

The long-term testing of series V started at concrete ages of 510 days (specimens S5B4 and S5B5) and 693 days (specimen S5B6). According to Table 12, The mean value of the failure load under the short term tests was  $P_{max,mean} = 203,2$  kN. The sustained loading ratio of specimen S5B4 was 91% of the ultimate capacity:

$$P_{sustained,S5B4} = 0,91 P_{max,mean} = 0,91 \cdot 203,2 = 185,0 \text{ kN} \quad (17)$$

where  $P_{sustained,S5B4}$  is the sustained load level that is applied to specimens S5B4.

Specimen S5B5 was loaded to 95% of the ultimate capacity (193 kN), but it failed during load application (at 94% = 190,5 ). Thus S5B5 never had chance to be tested under long-term loading. The other specimen in this series, S5B6 was intended to be tested under 95% of ultimate capacity, but when the specimen opposed a long and wide shear crack (crack width > 0.5 mm), the loading stopped at 165,0 kN (= 81% of the ultimate capacity).

The normal distribution function of the short-term ultimate capacities (S5B1, S5B2 and S5B3) is shown in Fig. 41. The 95% lower and upper confidence limits of series IV are 190,9 kN and 215,6 kN, respectively. With a sustained loading level of 185 kN, the chance of failure the beam is 14,7%.

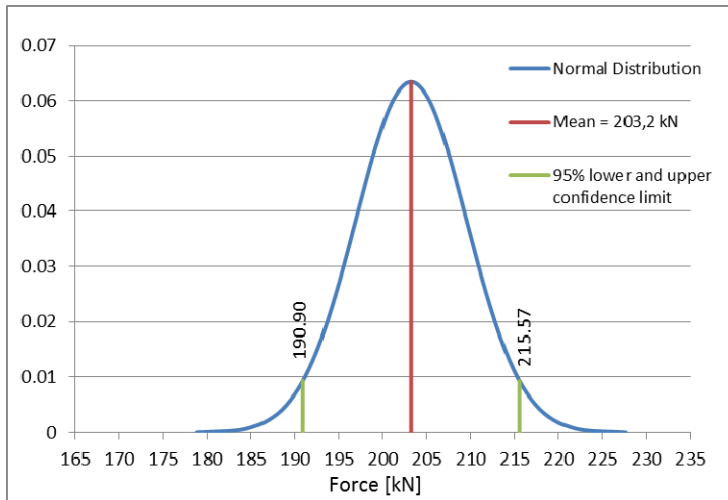


Fig. 41: Normal distribution function of test data, Series V.

### 7.1.5. Series VI

The long-term testing of series VI started at a concrete age of 110 days. Long-term loading on specimens of series VI with high strength concrete is carried out with a load ratio of 90% of the ultimate shear capacity  $P_{max,mean}$ . According to Table 12, the mean value of the failure load under short term loading was  $P_{max,mean} = 250,1$  kN. Thus the sustained load level is;

$$P_{sustained,VI} = 0,9 P_{max,mean} = 0,9 \cdot 250,1 = 225,1 \text{ kN} \quad (18)$$

where  $P_{sustained,VI}$  is the sustained load level that is applied to series VI.

The Normal distribution function of short-term ultimate capacities (S6B1, S6B2 and S6B3) is shown in Fig. 42. The confidence limits of series VI are 236,6 kN and 263,5 kN. With a sustained loading level of 225,1 kN, the chance of failure the beam is lower than 2,5%. However, specimen S6B5 failed during load application at a load level of 221 kN (= 88% load ratio). The long-term loading on beams S6B4 and S6B6 under 225,1 kN (90% of the mean value of ultimate capacity) was performed for a period of more than 2 years (from October 5, 2010 until now).

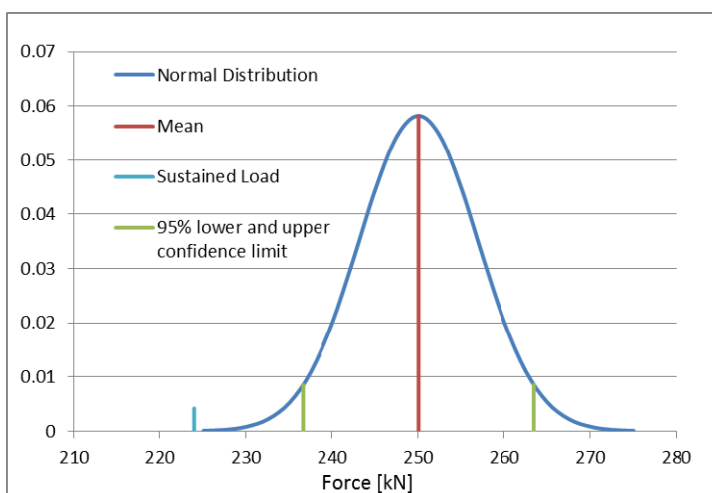


Fig. 42: Normal distribution function of test data, Series VI. The sustained load (224 kN) is lower than lower confidence limit

Table 16. Load steps and duration of long-term loading, specimen series VI

Load step	S6B4	S6B5	S6B6
90% $P_{primary,6}$	224 kN Since 5 Oct 2010	Failed at 221 kN	224 kN Since 5 Oct 2010

7.1.6. Series VII

The long-term testing of series VII started at a concrete age of 212 days with a load ratio of 95% of the ultimate shear capacity  $P_{max,mean}$ . According to Table 12, the mean value of the failure load under short term loading was 229,9 kN. Thus, the sustained load level is;

$$P_{sustained,VII} = 0,95 P_{max,mean} = 0,95 \cdot 229,9 = 218,4 \text{ kN} \tag{19}$$

where  $P_{sustained,VI}$  is the sustained load level that is applied to series VII.

The Normal distribution function of short-term ultimate capacities (S7B1, S7B2 and S7B3) is shown in Fig. 43. The lower and upper confidence limits are 199,5 kN and 260,3 kN, respectively. With a sustained loading level of 218 kN, the chance of losing the beam is 22,4%. Unluckily, specimen S7B4 failed at 218 kN after a few minutes. Specimen S7B5, loaded up to 210,0 kN and the loading stopped at that level after a wide crack appeared on the surface of the beam. Specimen S7B6 experienced a similar accident; a long and wide crack appeared on the surface of the beam that reached the compression zone at 205 kN, then the load decreased to 200 kN to keep the beam. However, the beam failed after 45 hours sustained loading at this level.

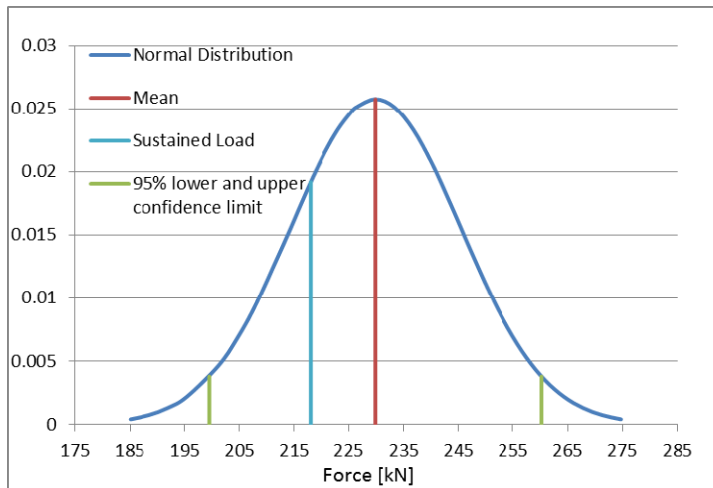


Fig. 43: Normal distribution function of test data, Series VII. The sustained load (218 kN) is larger than lower confidence limit.

Table 17. Load steps and duration of long-term loading, specimen series 7

Load step	S7B4	S7B5	S7B6
90% $P_{primary,7}$	218 kN Failed after few minutes	210 kN	200 kN Failed after 2 days

### 7.2. Observations within a couple of hours after applying the sustained load

Monitoring the concrete beams in the first six hours of the sustained loading, when the midspan and diagonal deflections increase, is very important. The long-term tests results show that there is a limit to the crack width and maximum deflection (will be discussed briefly in section 7.3). However, reaching the maximum deflection due to the creep effect, takes a couple of months, but the maximum diagonal deflection (and so the crack width) could be reached within a few hours/days.

In Fig. 44, the variation of load, midspan vertical deflection and diagonal deflections on right and left side of the beam is presented for each beam in the first 6 hours of loading together with the final values at the end of sustained loading. The irregularities in load-time curve are due to adjustments of the load at a certain level. The values of deflection and crack width for each curve after six hours are shown above the curve and compared with the final value at the end of testing (highlighted value).

As presented in Fig. 51 and Fig. 57, due to the reckless growth of the shear crack, two specimens (S4B6 and S7B6) failed under sustained loading. The beams failed shortly after initial loading, when they were still in the crack initiation stage. Sustained loading time of specimen S4B6 was almost 145 minutes (1/10 day) and specimen S7B6 failed after 45 hrs. As shown in Fig. 51, the crack opening displacements at both sides of the beam are stabilized after 1.5 hour, but suddenly, when the load was still constant, the shear crack on the right side opened and the beam failed (see Fig. 74). Crack propagation and failure stage of S7B6 is shown in Fig. 57.

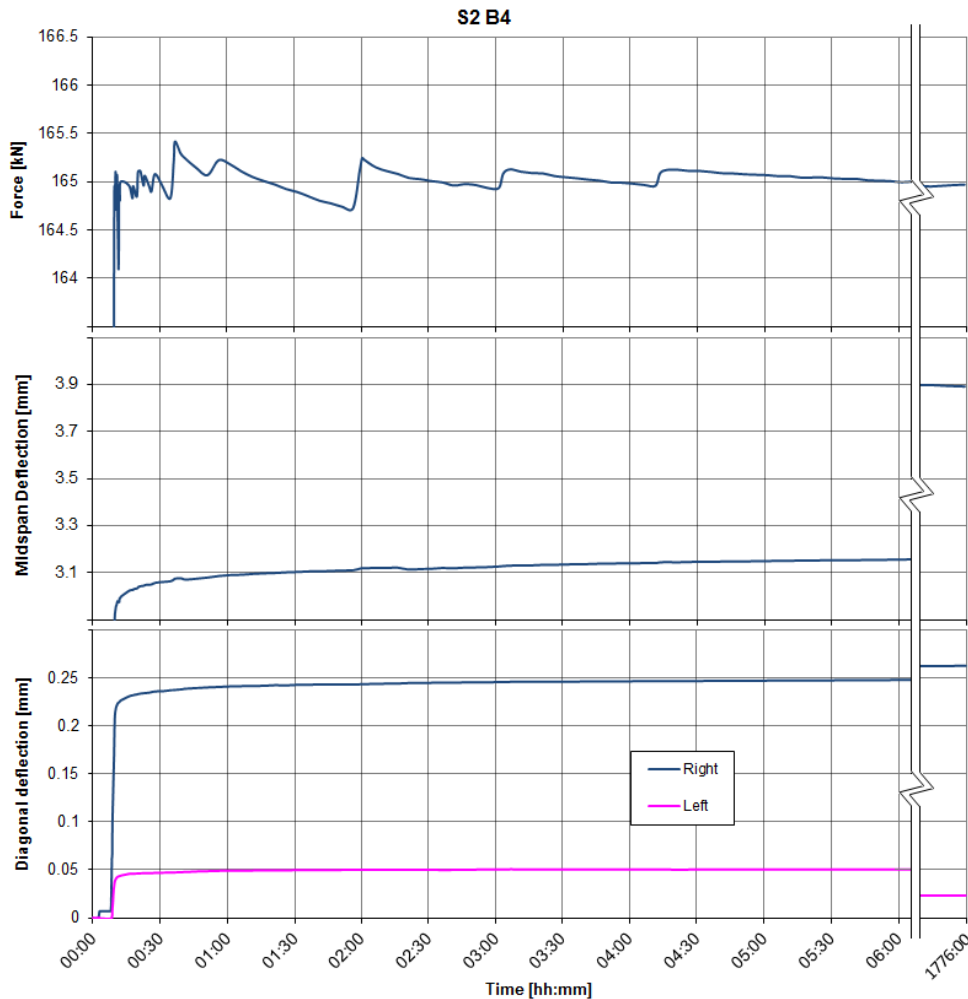


Fig. 44: Variation of load, midspan deflection and diagonal deflection in the first 6 hours and comparison to the end of loading, Specimen S2B4

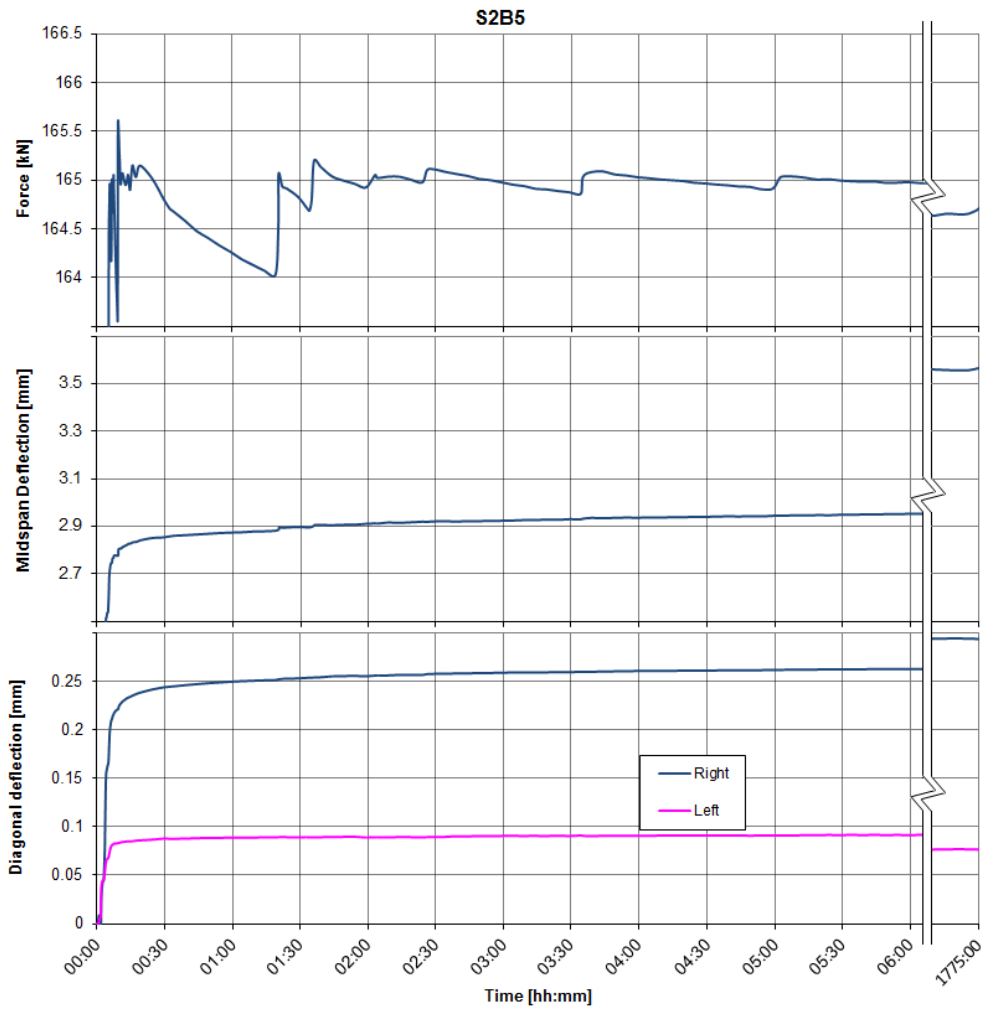
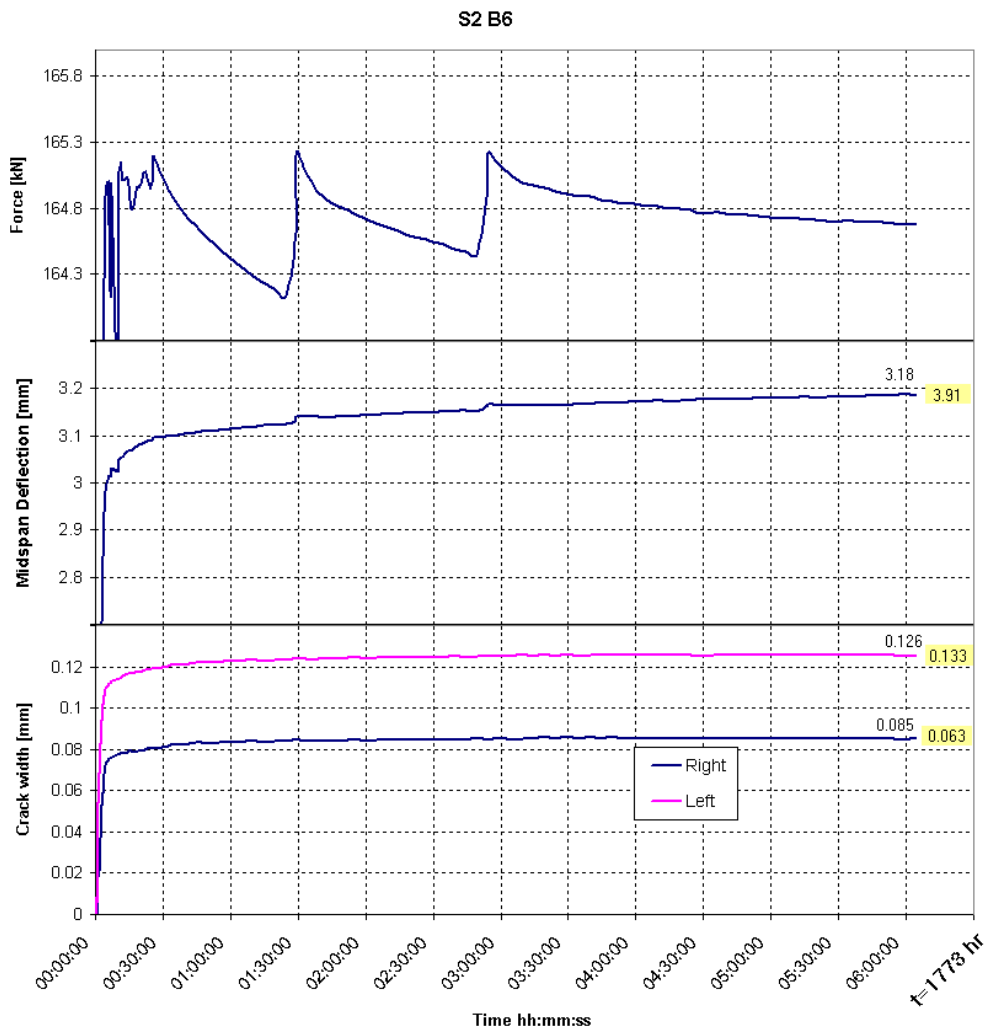
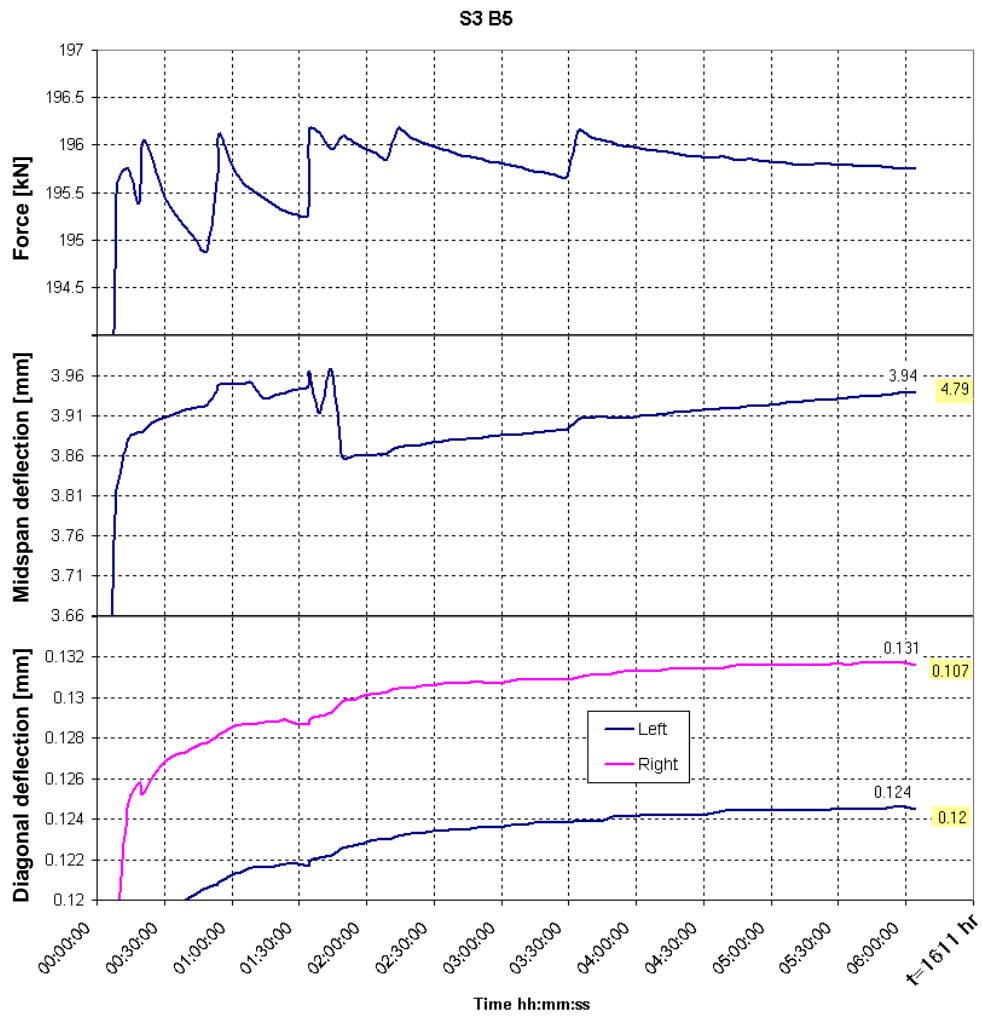


Fig. 45: Variation of load, midspan deflection and diagonal deflection in the first 6 hours and comparison to the end of loading, Specimen S2B5



**Fig. 46: Variation of load, midspan deflection and diagonal deflection in the first 6 hours and comparison to the end of loading, Specimen S2B6**



**Fig. 47: Variation of load, midspan deflection and diagonal deflection in the first 6 hours and comparison to the end of loading, Specimen S3B5**

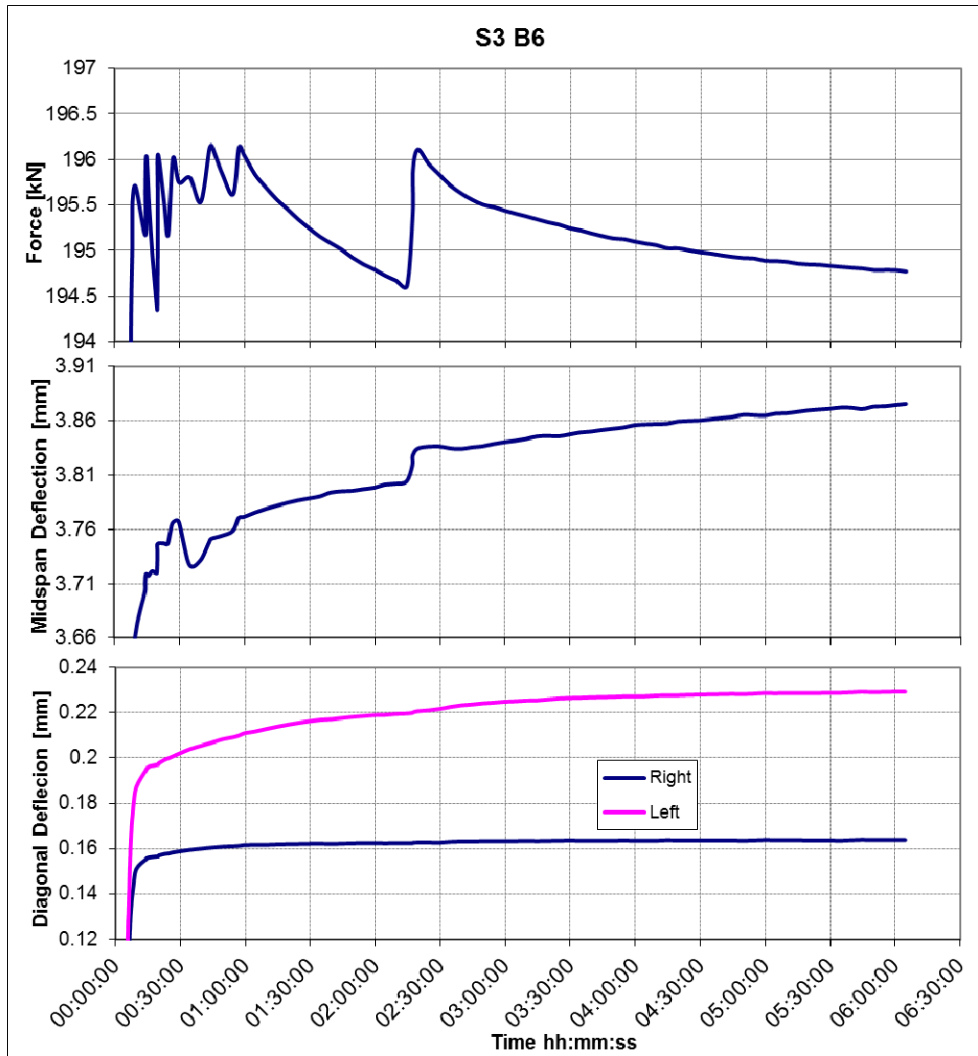


Fig. 48: Variation of load, midspan deflection and diagonal deflection in the first 6 hours and comparison to the end of loading, Specimen S3B6

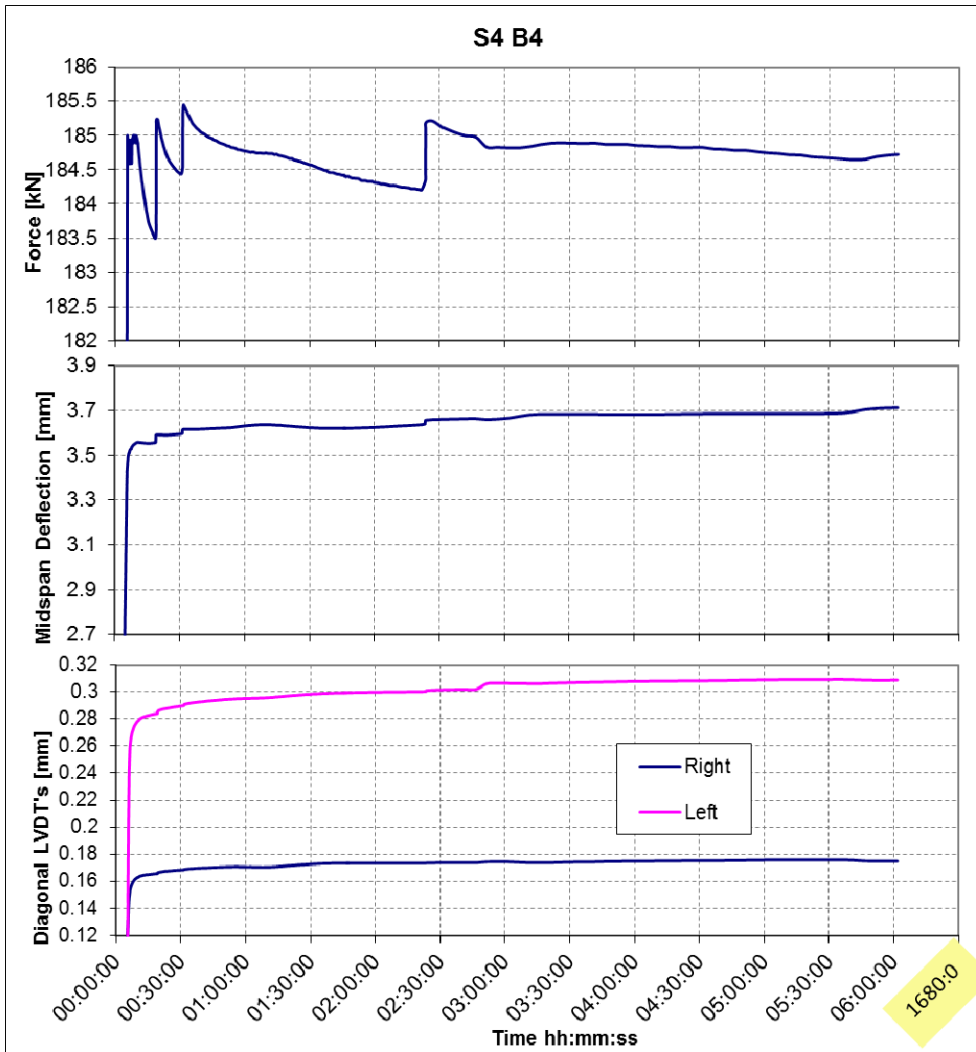


Fig. 49: Variation of load, midspan deflection and diagonal deflection in the first 6 hours and comparison to the end of loading, Specimen S4B4

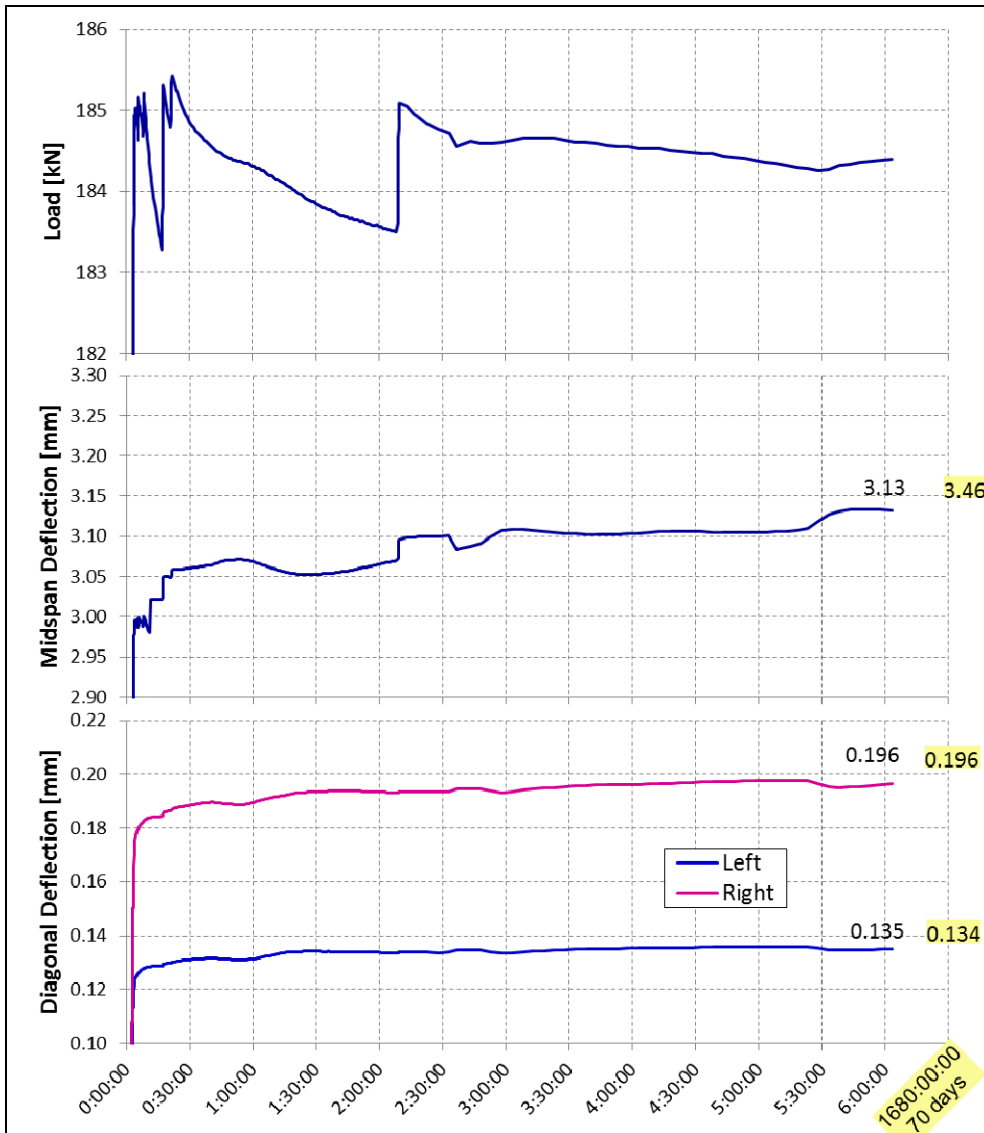


Fig. 50: Variation of load, midspan deflection and diagonal deflection in the first 6 hours and comparison to the end of loading, Specimen S4B5

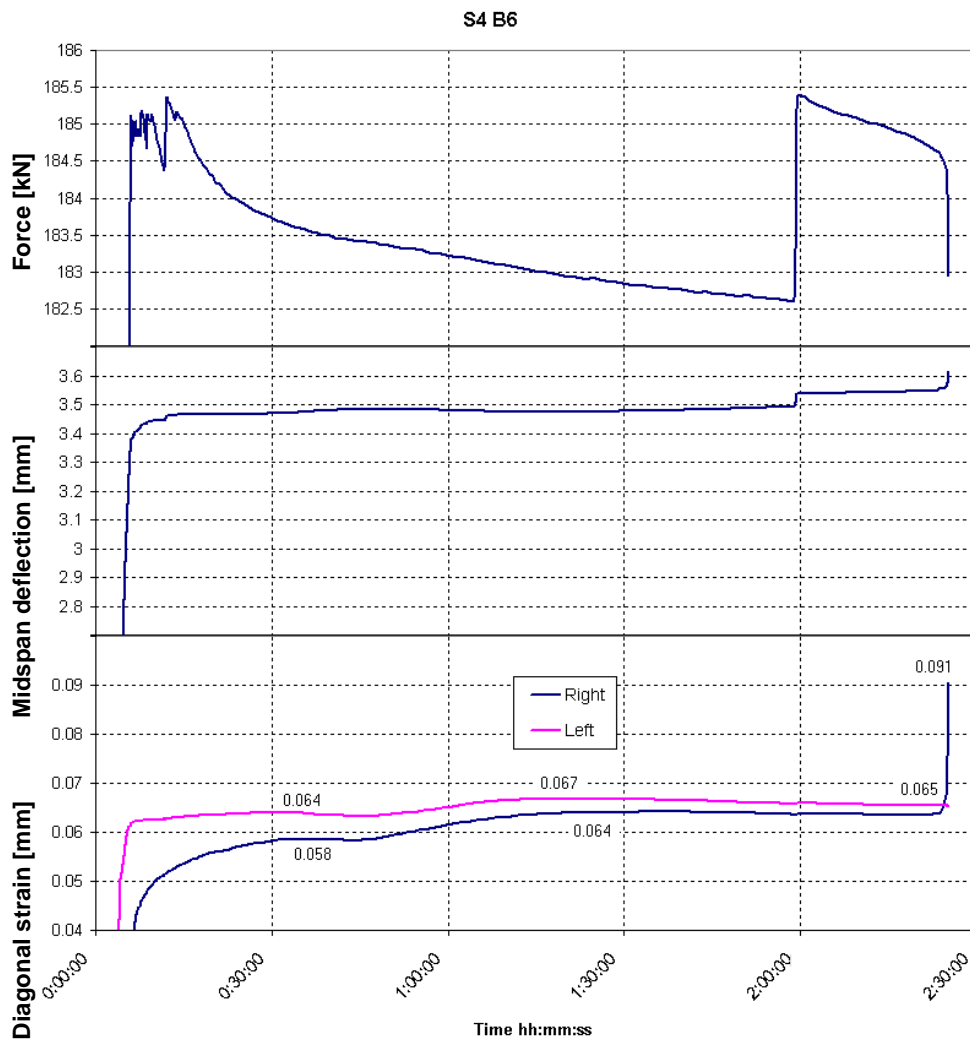


Fig. 51: Variation of load, midspan deflection and diagonal deflection until failure, Specimen S4B6

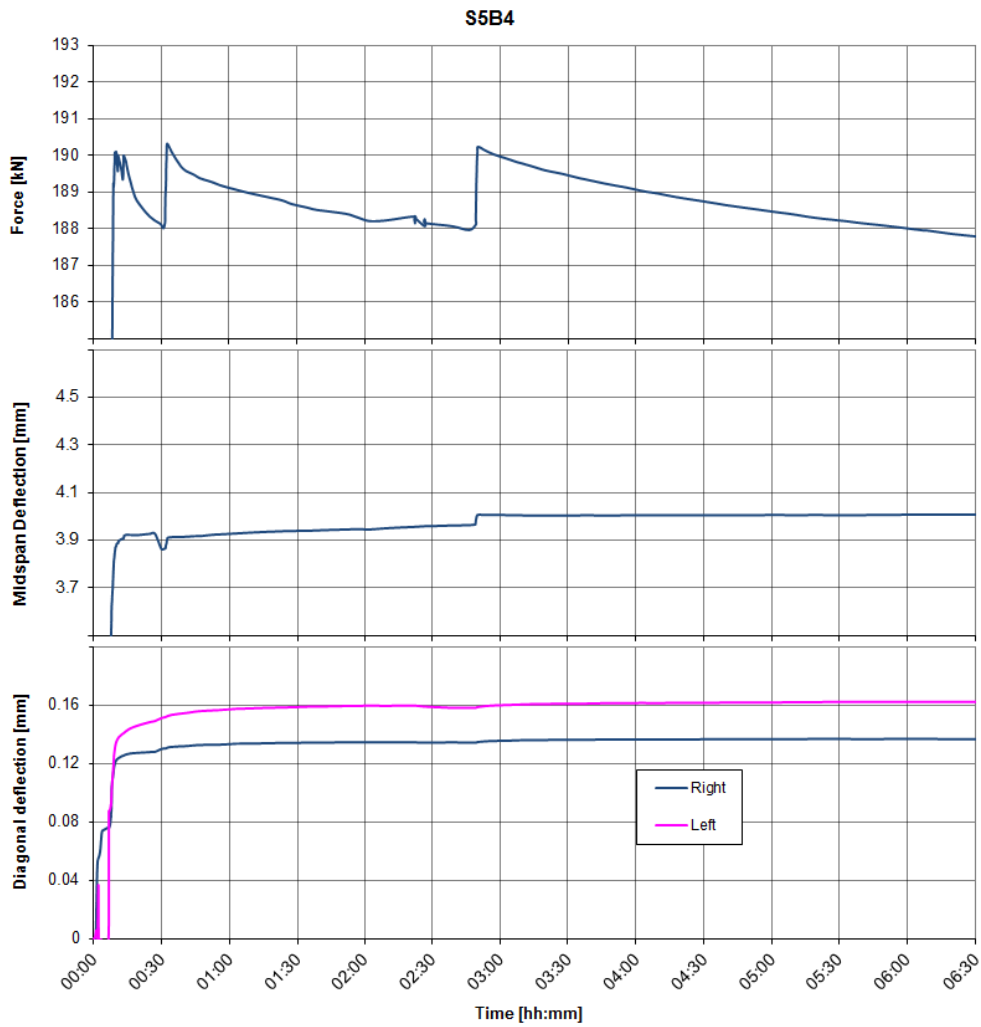


Fig. 52: Variation of load, midspan deflection and diagonal deflection in the first 6 hours, Specimen S5B4

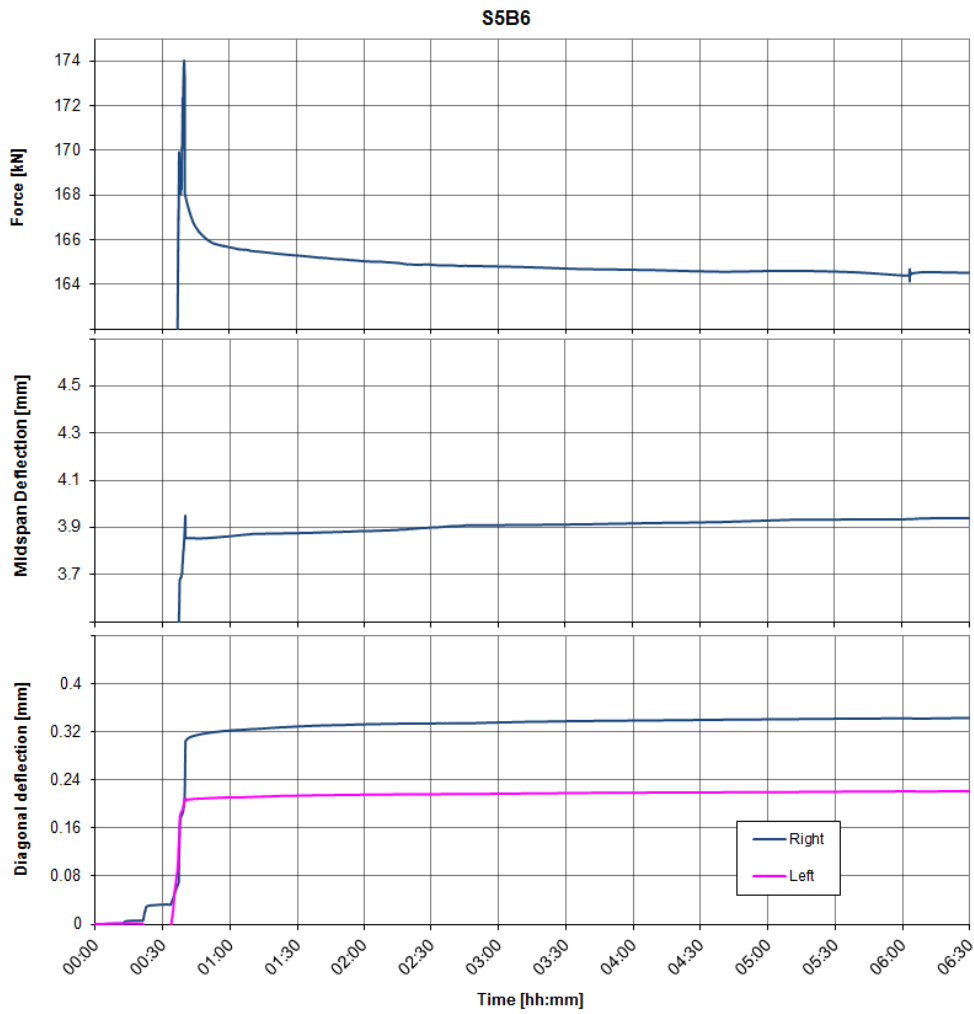


Fig. 53: Variation of load, midspan deflection and diagonal deflection in the first 6 hours, Specimen S5B6

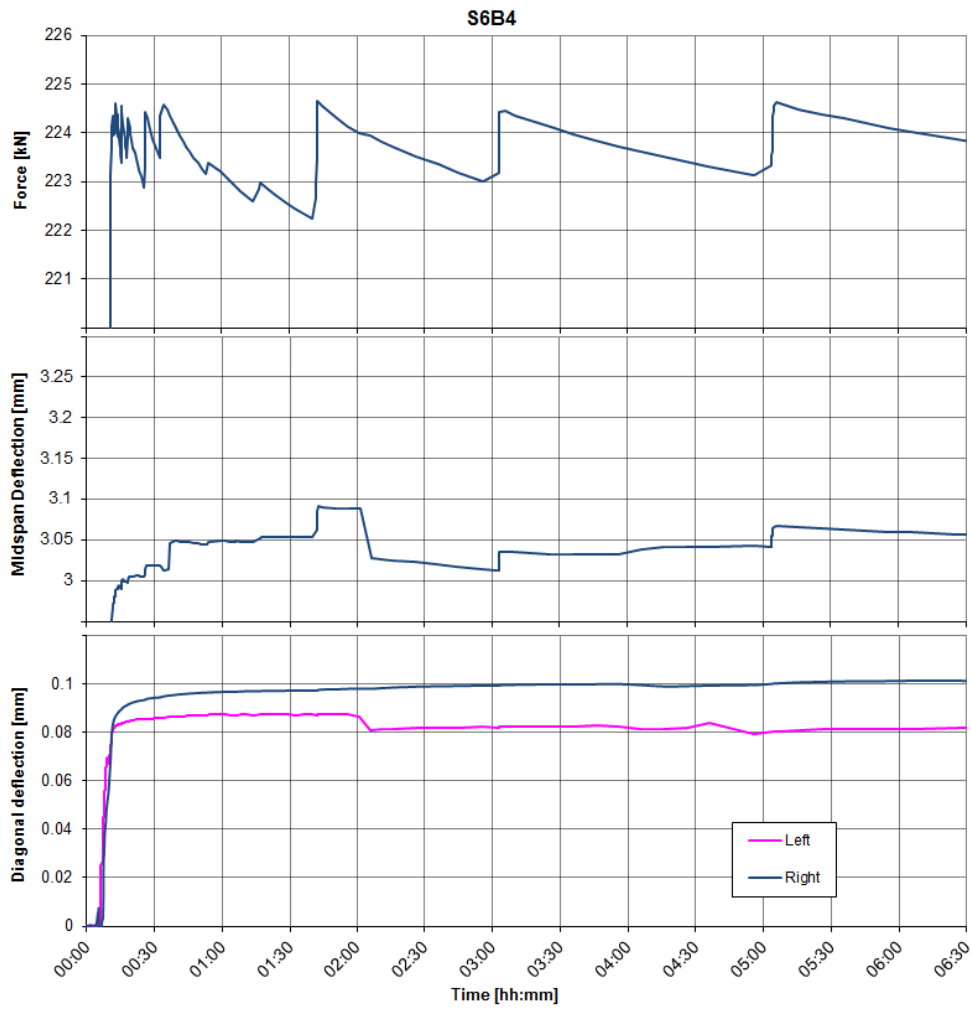


Fig. 54: Variation of load, midspan deflection and diagonal deflection in the first 6 hours, Specimen S6B4

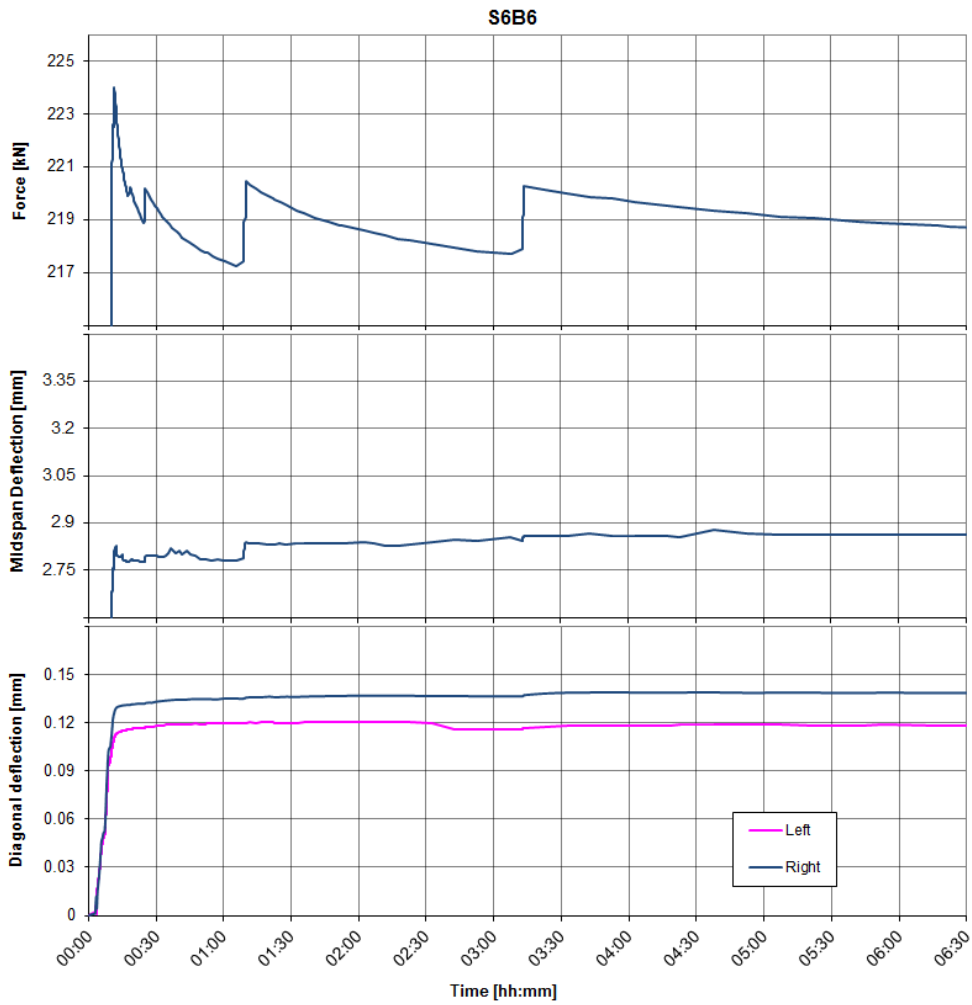


Fig. 55: Variation of load, midspan deflection and diagonal deflection in the first 6 hours, Specimen S6B6

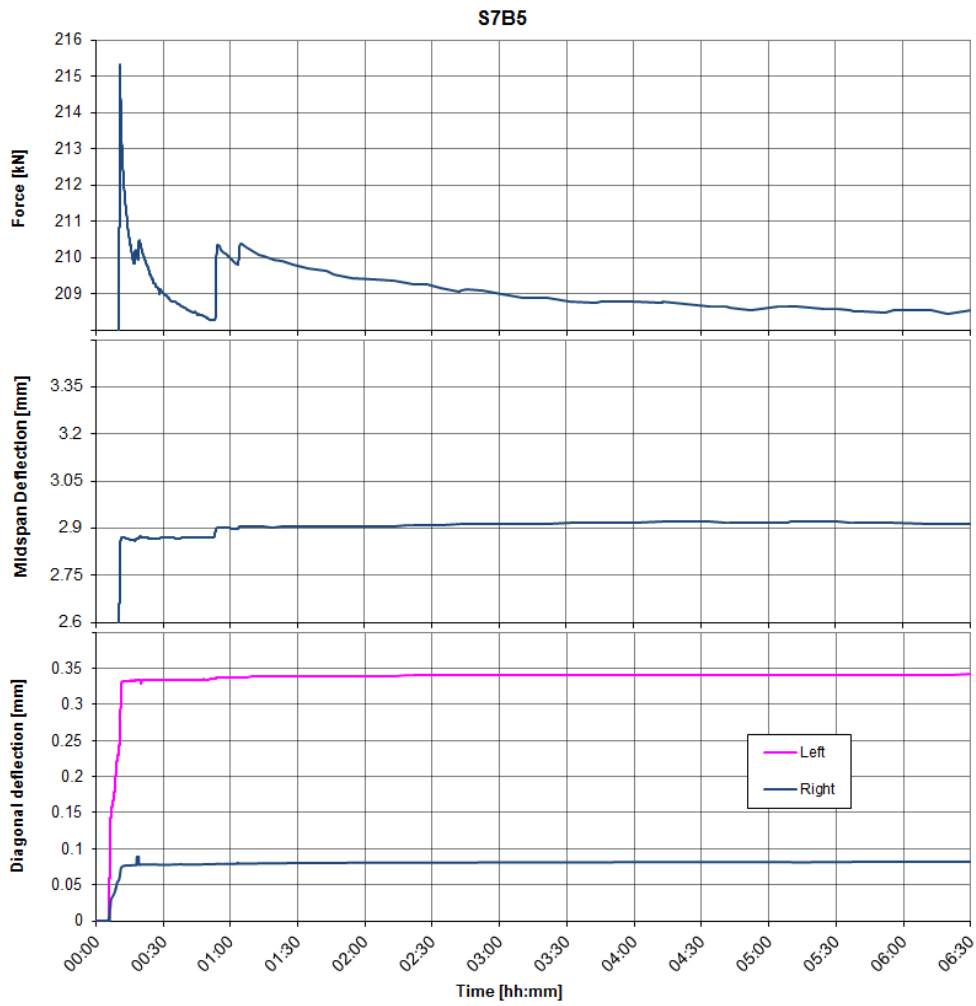


Fig. 56: Variation of load, midspan deflection and diagonal deflection in the first 6 hours, Specimen S7B5

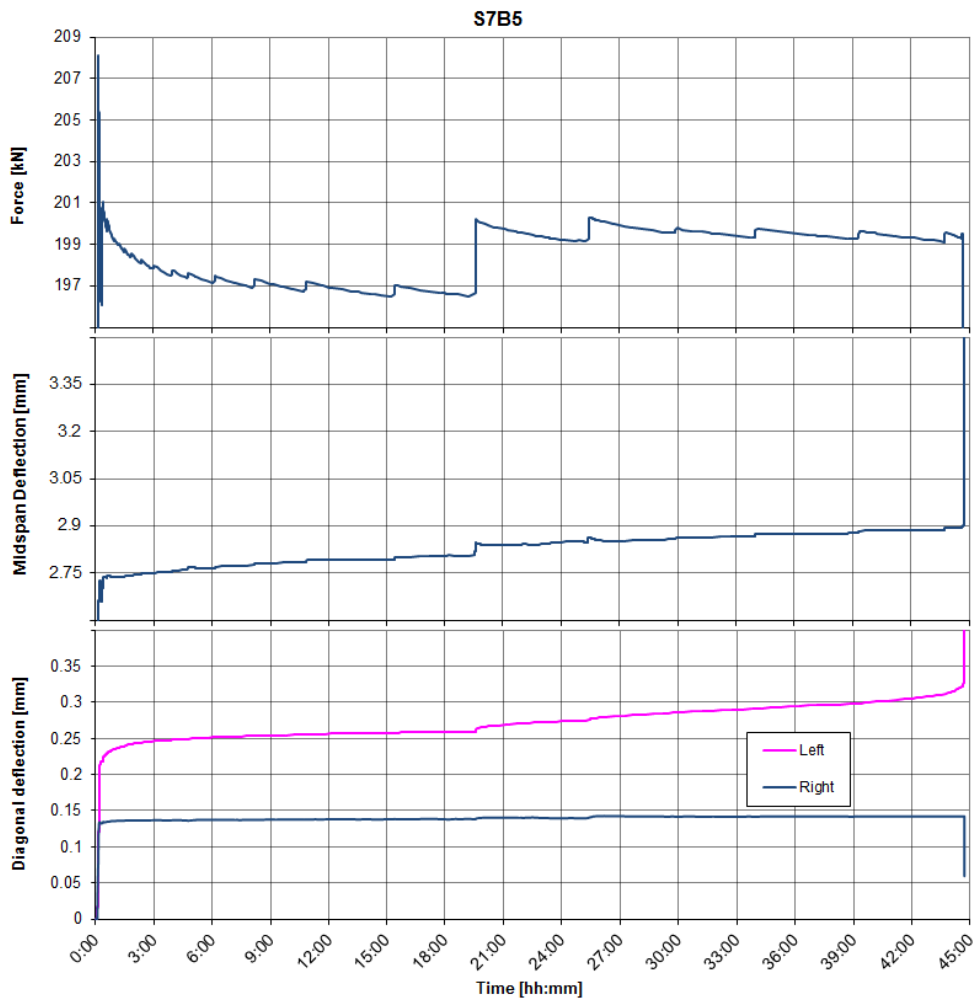


Fig. 57: Variation of load, midspan deflection and diagonal deflection until failure, Specimen S7B6

### 7.3. Long-term test results

In this section, the results of long-term sustained loading are presented. 14 specimens were successfully tested under sustained loading, labelled as:

- S2B4, S2B5, S2B6 (series 2)
- S3B5, S3B6 (series 3)
- S4B4, S4B5, S4B6 (series 4)
- S5B4, S5B6 (series 5)
- S6B5, S6B6 (series 6)
- S7B5, S7B6 (series 7)

Four other specimens failed during load application (S3B4, S5B5, S6B5 and S7B4).

The results consist of the load variation measured by a load cell, midspan deflection measured by a vertical LVDT and the diagonal deflections on right and left shear spans measured by two diagonal LVDT's at 45 and 135 degree angles. The data were recorded automatically by the computer every 15 minutes, and were stored in an

excel file. Extra measurement was applied to specimens in series 5, 6 and 7 by means of a hand-operated LVDT device and pre-installed measuring points on the surface of the beam, see Fig. 13.

Specimens S3B5, S5B4, S5B6, S6B4, S6B6 and S7B5 are still in the setup under long-term sustained loading, and testing of the rest of the concrete beams are completed, see Table 4.

It is mentioned previously that the load was applied by a hand-controlled hydraulic jack and had to be adjusted as well. Any irregularity on the load-time curves is caused by an adjustment of the applied load on the specimen. The results of sustained loading are shown in Fig. 58 to Fig. 65.

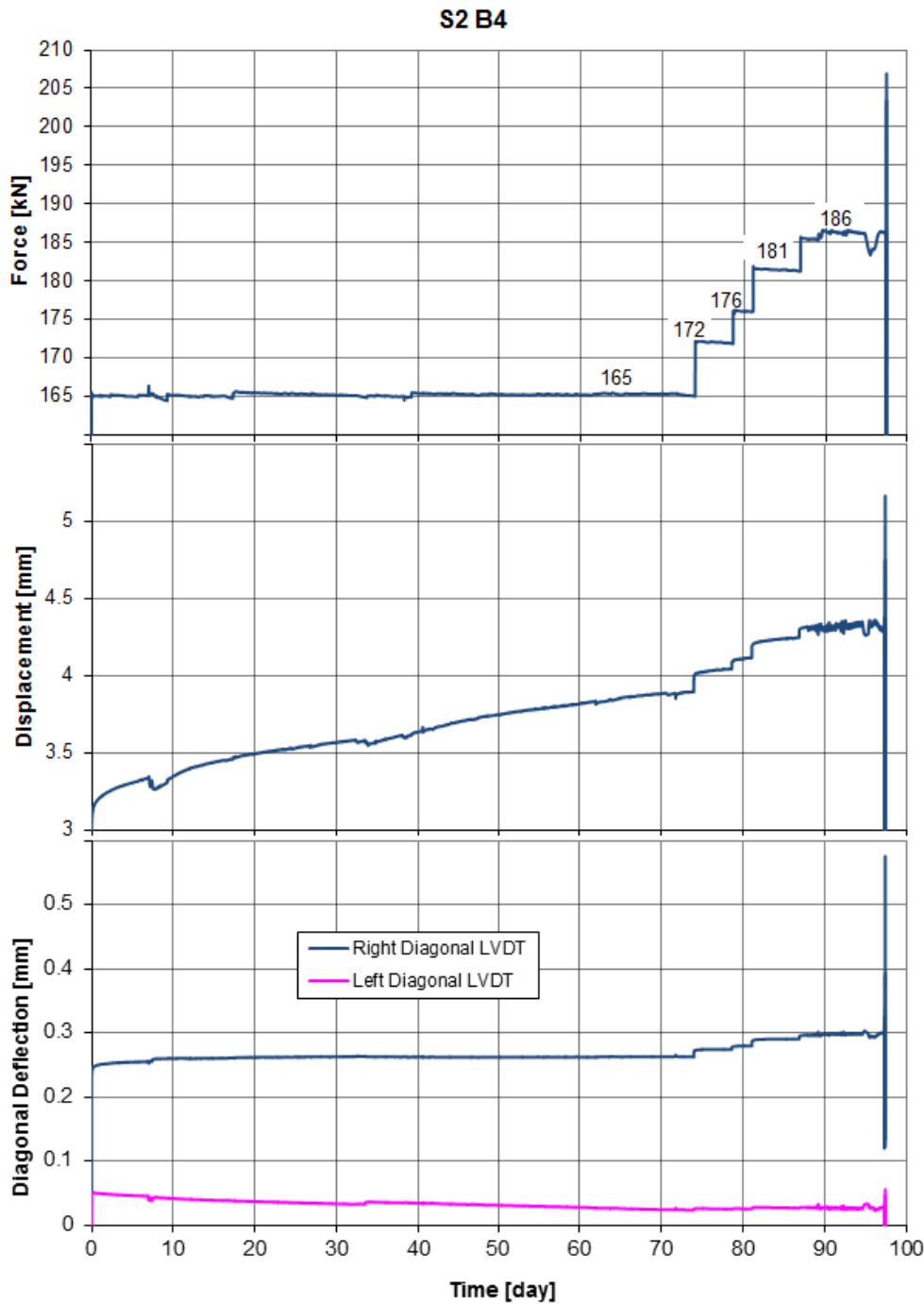


Fig. 58: Variation of load, midspan vertical deflection and diagonal deflection, Specimen S2B4

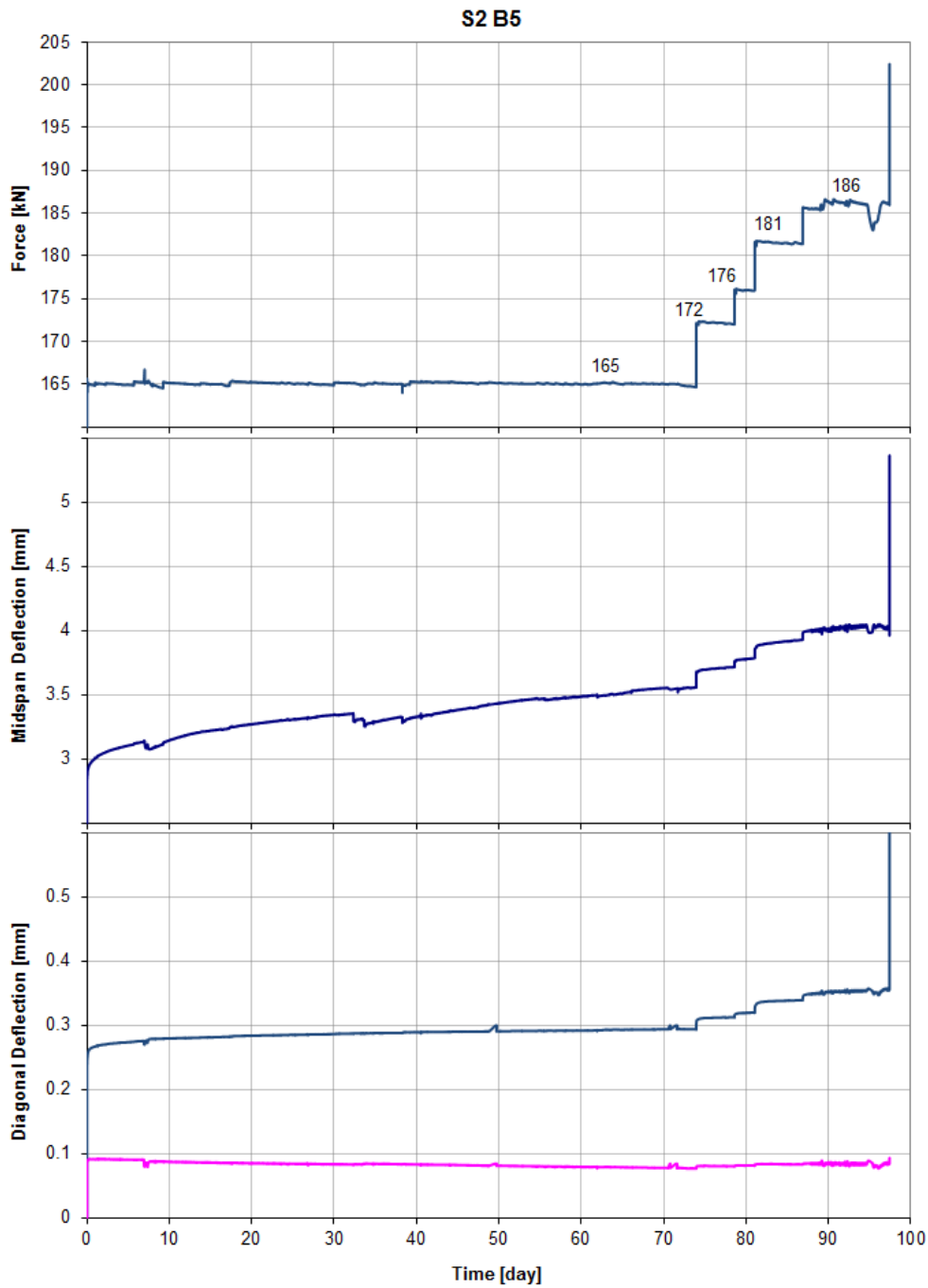


Fig. 59: Variation of load, midspan vertical deflection and diagonal deflection, Specimen S2B5

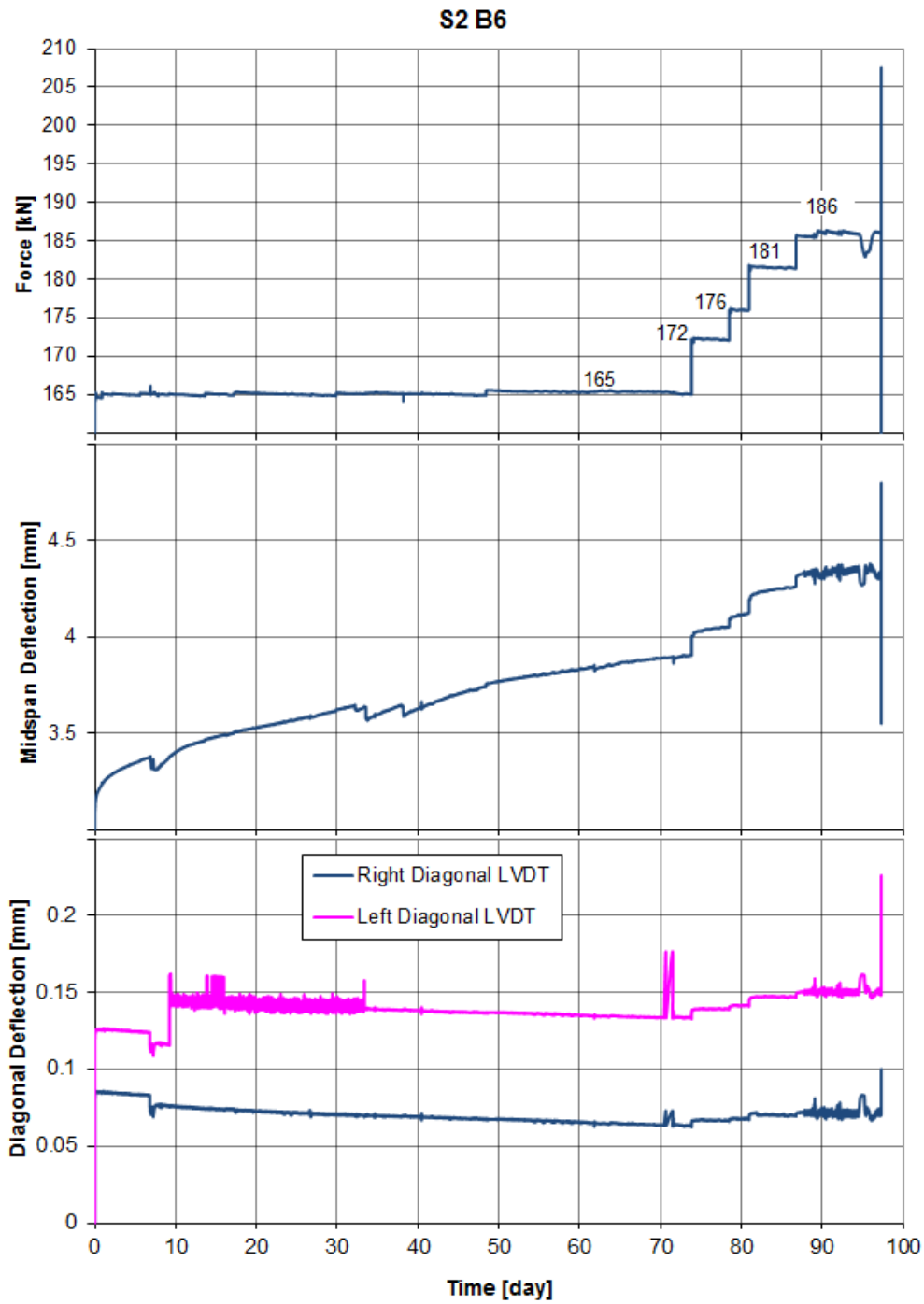


Fig. 60: Variation of load, midspan vertical deflection and diagonal deflection, Specimen S2B6

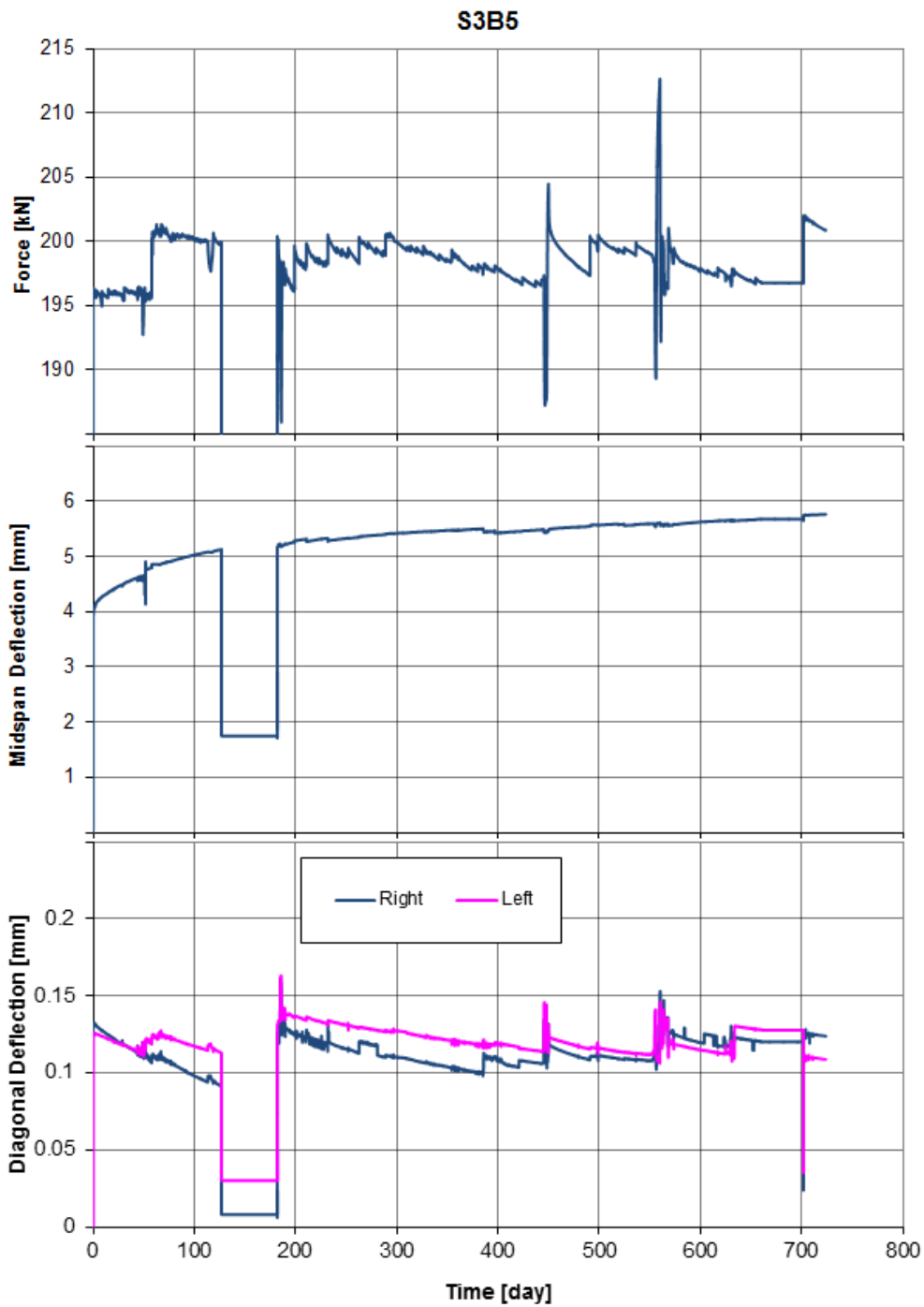


Fig. 61: Variation of load, midspan vertical deflection and diagonal deflection, Specimen S3B5

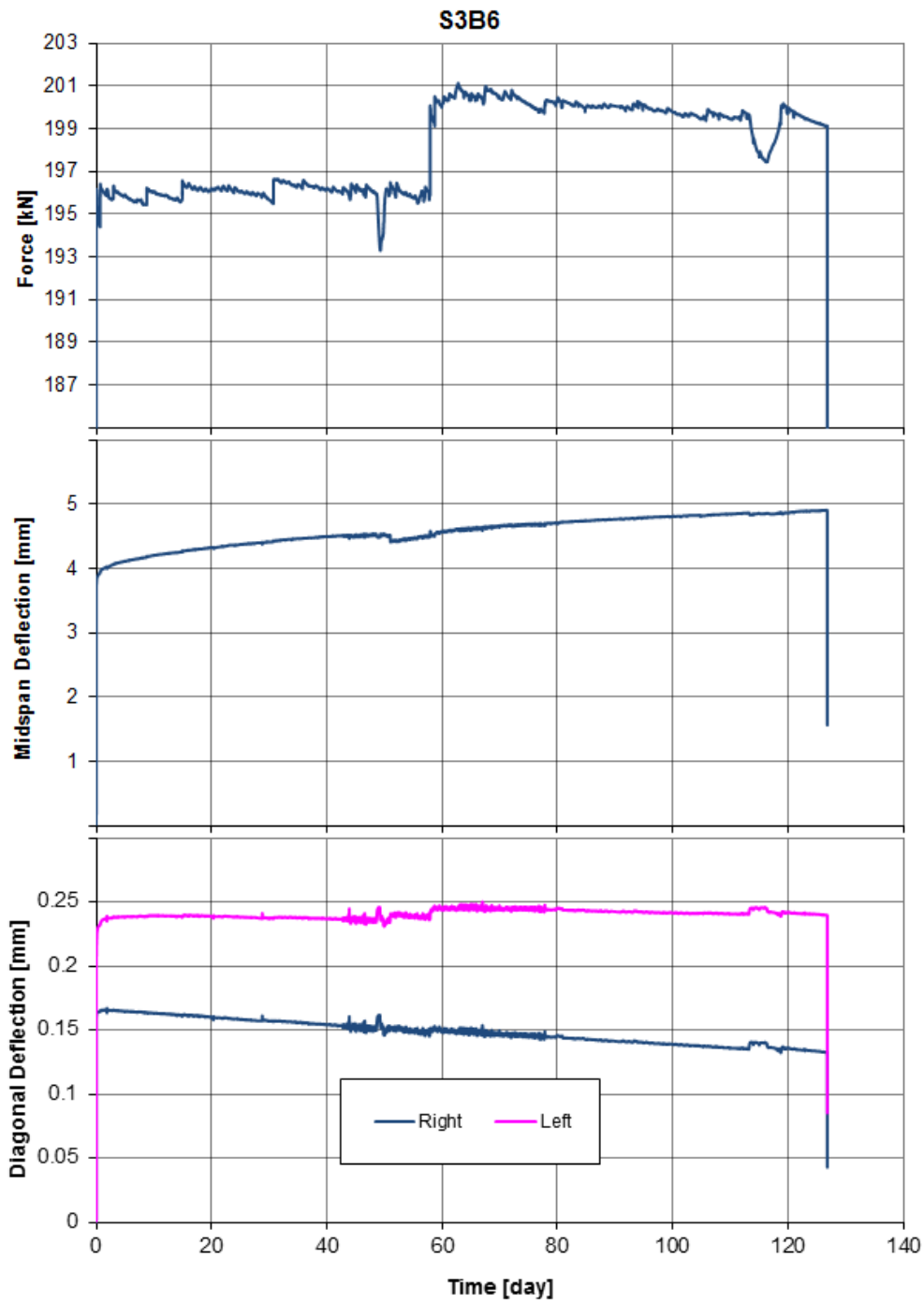


Fig. 62: Variation of load, midspan vertical deflection and diagonal deflection, specimen S3B6. It failed after reloading the beam.

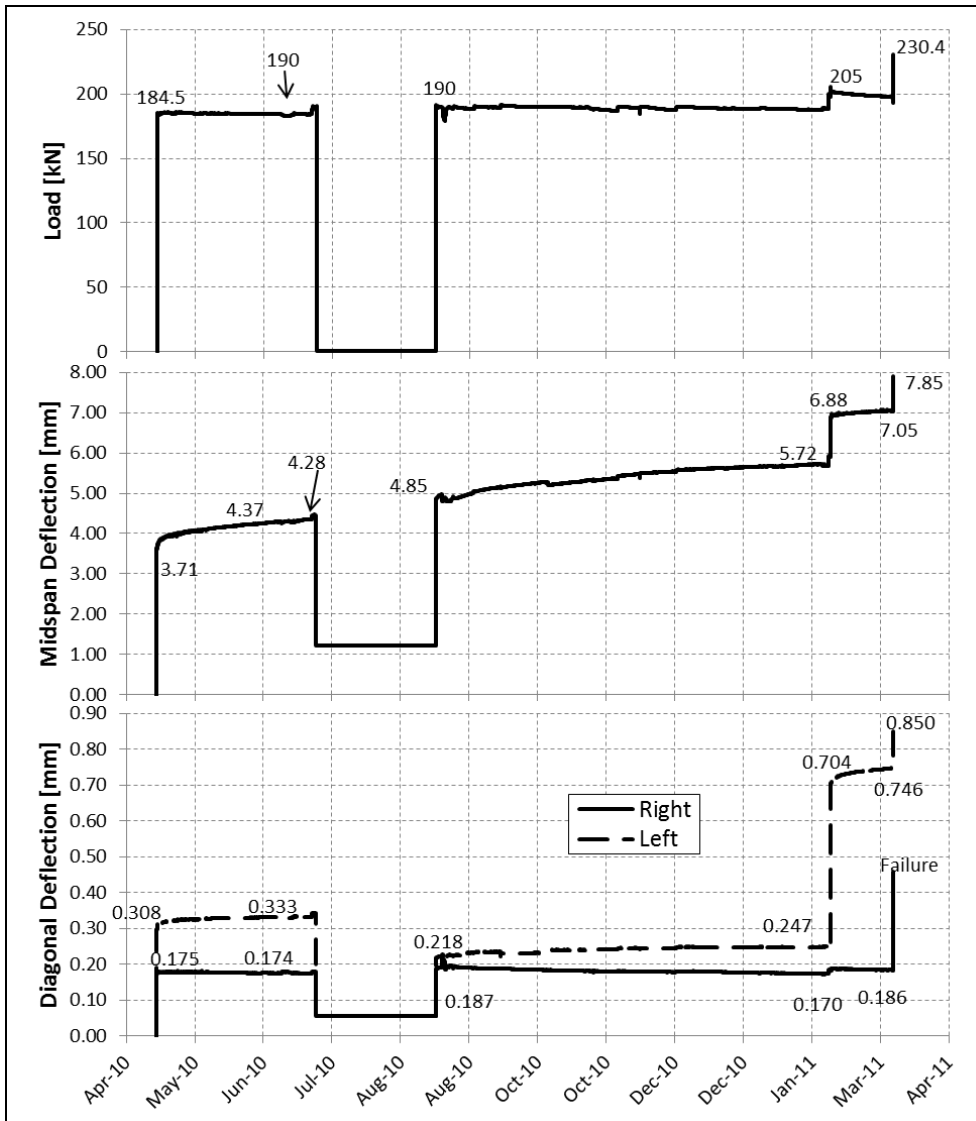


Fig. 63: Variation of load, midspan vertical deflection and diagonal deflection, Specimen S4B4

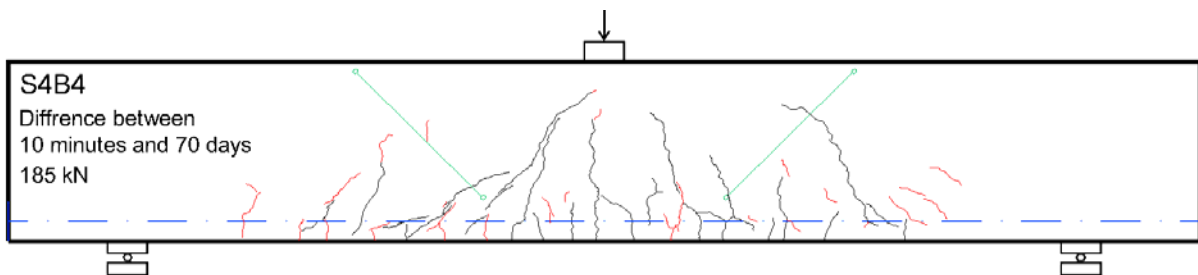


Fig. 64: Crack pattern in specimen S4B4 after 10 minutes loading (dark lines) and 70 days loading (red lines) at load level = 185 kN

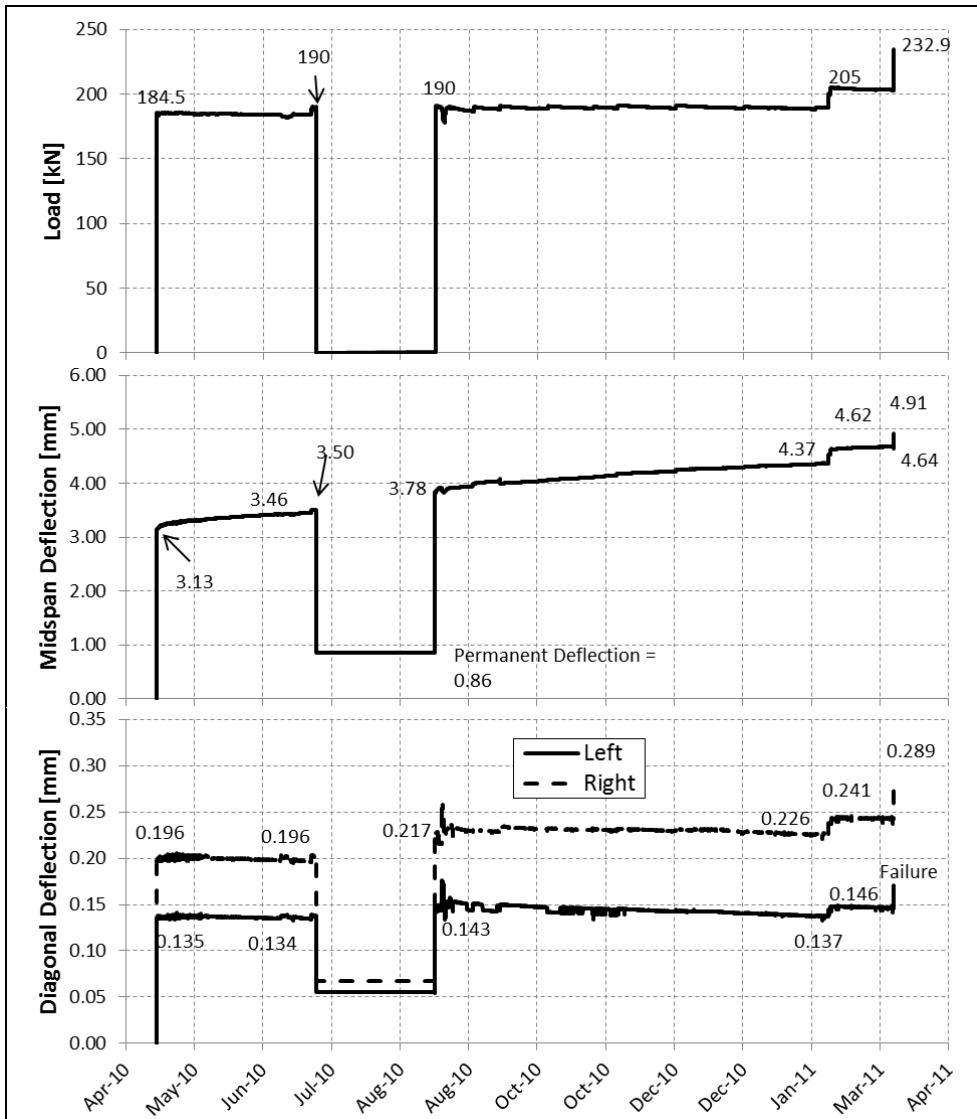


Fig. 65: Variation of load, midspan vertical deflection and diagonal deflection, Specimen S4B5

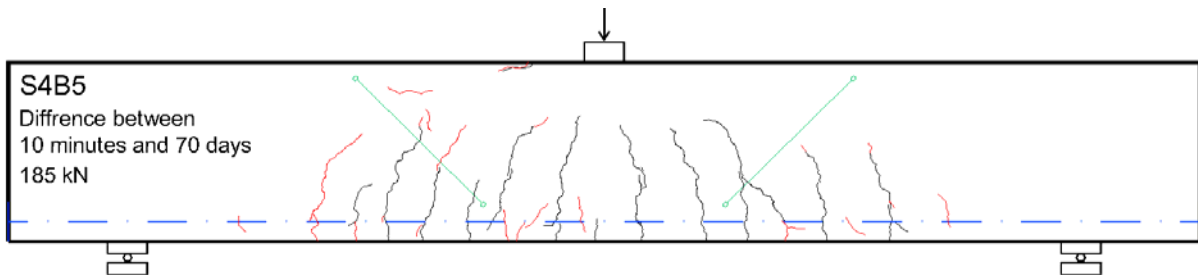


Fig. 66: Crack pattern in specimen S4B5 after 10 minutes loading (dark lines) and 70 days loading (red lines) at load level = 185 kN

#### 7.4. Crack patterns

The crack patterns in the concrete beams are represented in Fig. 67 to Fig. 82. The crack patterns are drawn at different times of loading. The first monitoring of the cracks is performed just after loading at the same day. The most significant development of the crack pattern occurs in the first day of loading. In the figures below, the red cracks are new cracks observed at the indicated time during the sustained loading period.

The last figure is the crack pattern after failure. Hence, some of the bending cracks shown in this figure occur due to large deformation of the beam after failure. In the last figure, the cracks which cause failure are shown in a more pronounced way; the pronounced cracks represent the shear failure cracks, semi-thick crack represents clearly visible wide cracks which could have caused the shear failure, and thin cracks are the cracks which are barely visible. As mentioned in section 6.4, it is tried to mark the shrinkage cracks before the tests. These cracks are not drawn in the crack pattern, but some of the thin cracks appear during the test due to both shrinkage and loading stresses and it is hard to distinguish them from the bending and shear cracks. So, these cracks are shown in the figures. The blue dashed-dot lines and the green lines are representing the position of the longitudinal reinforcement and the position of the diagonal LVDT's, respectively.

One noticeable observation is that the failure crack does not necessarily follow the existing shear cracks. This behaviour can be seen e.g. in Fig. 67 and Fig. 72.

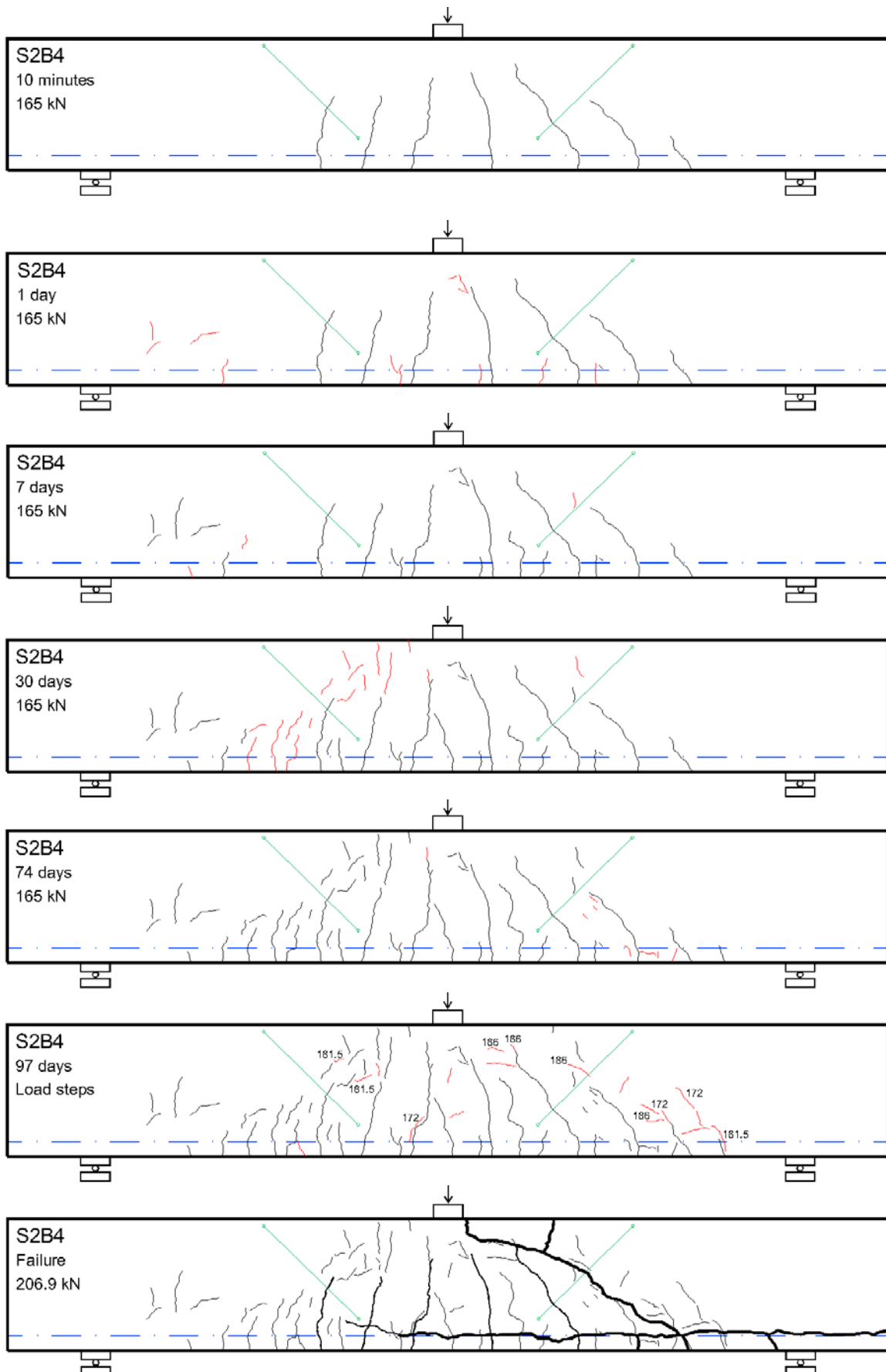


Fig. 67: Crack pattern in beam S2B4 in time

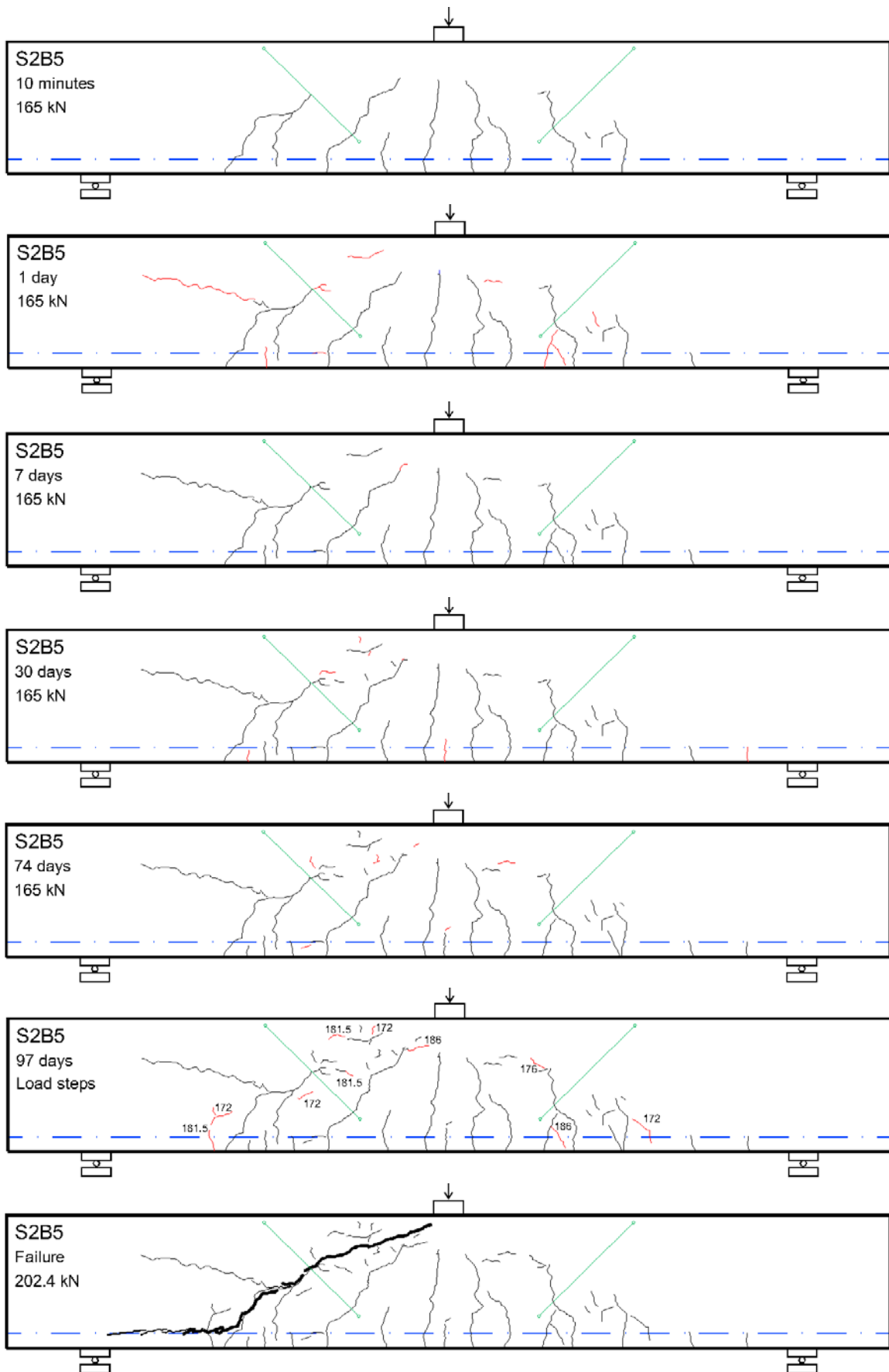


Fig. 68: Crack pattern in beam S2B5 in time

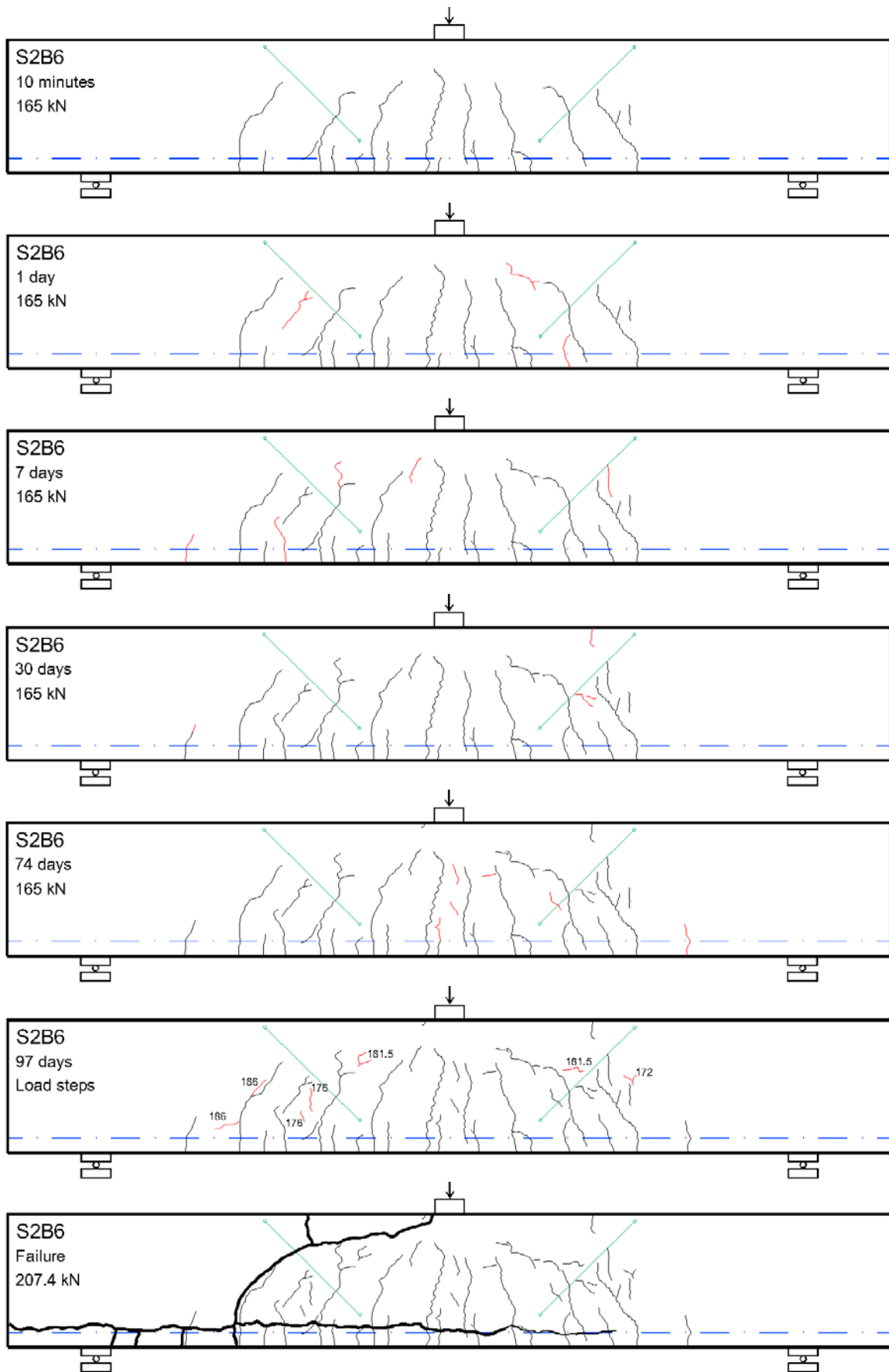


Fig. 69: Crack pattern in beam S2B6 in time

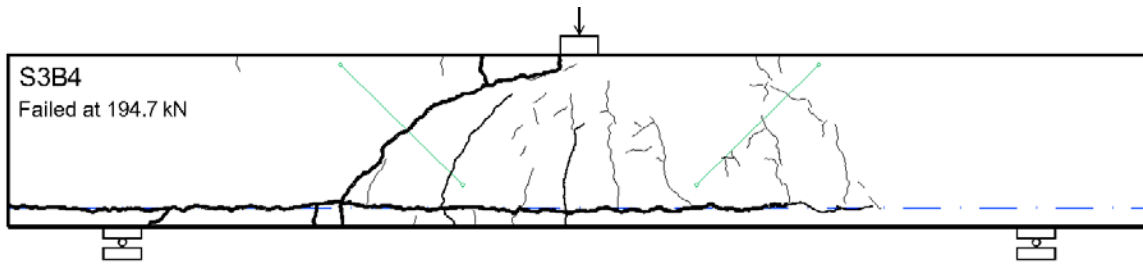
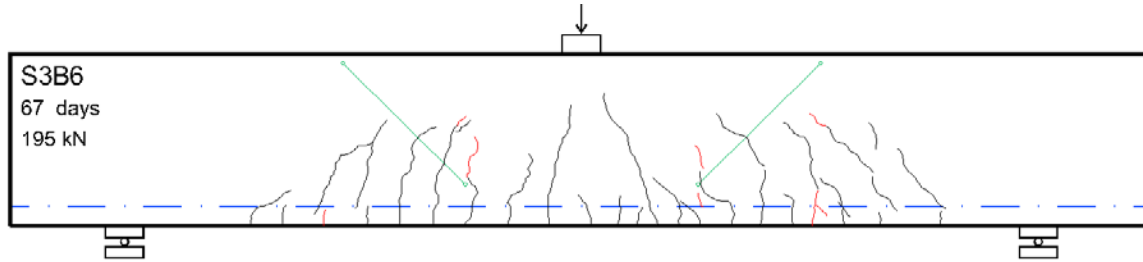
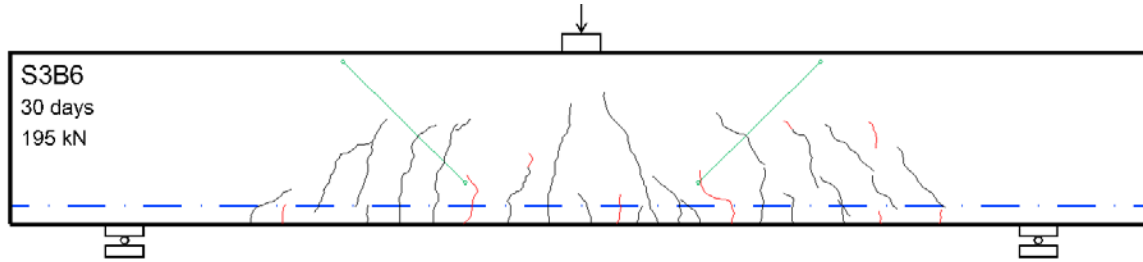
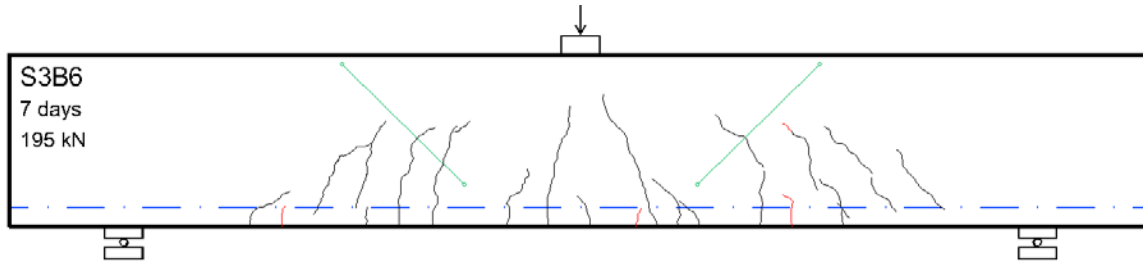
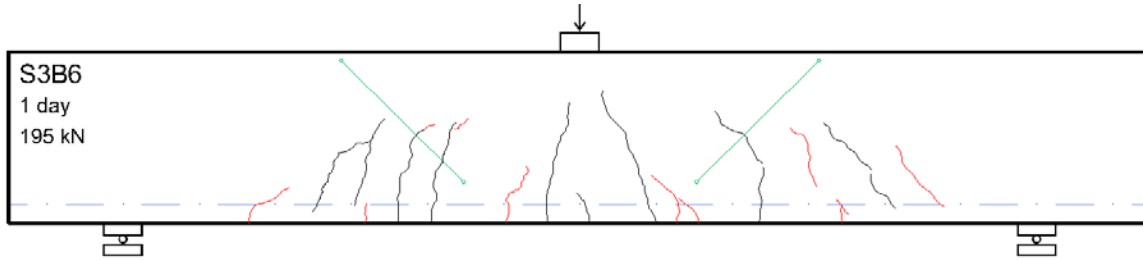
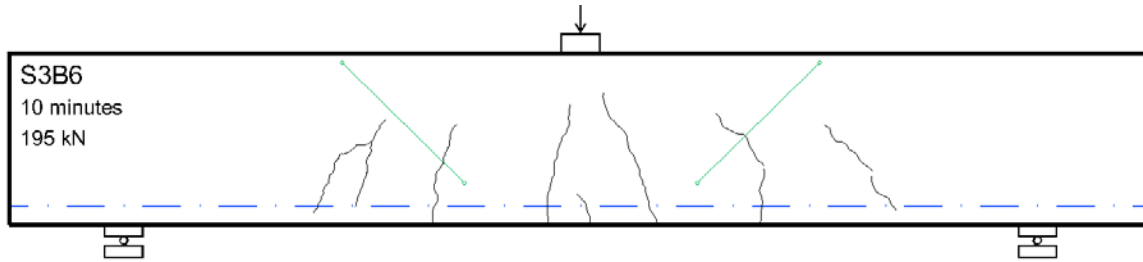


Fig. 70: Crack pattern in specimen S3B4



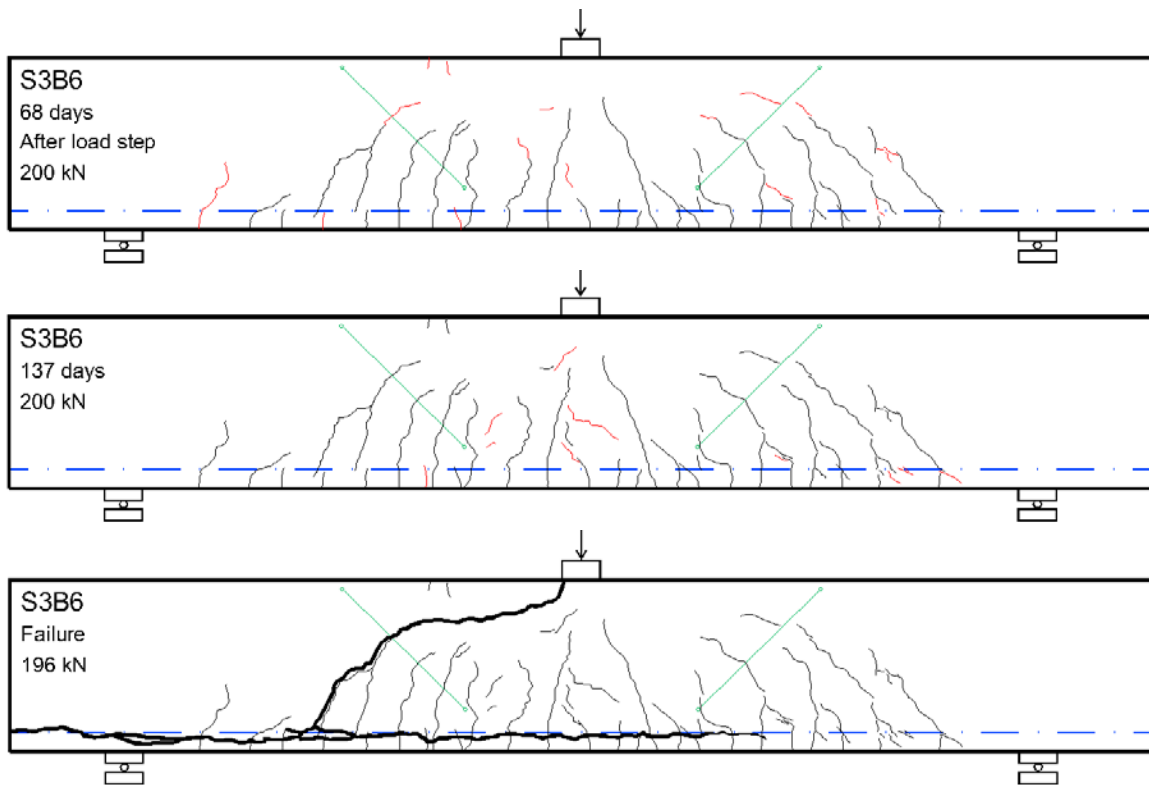
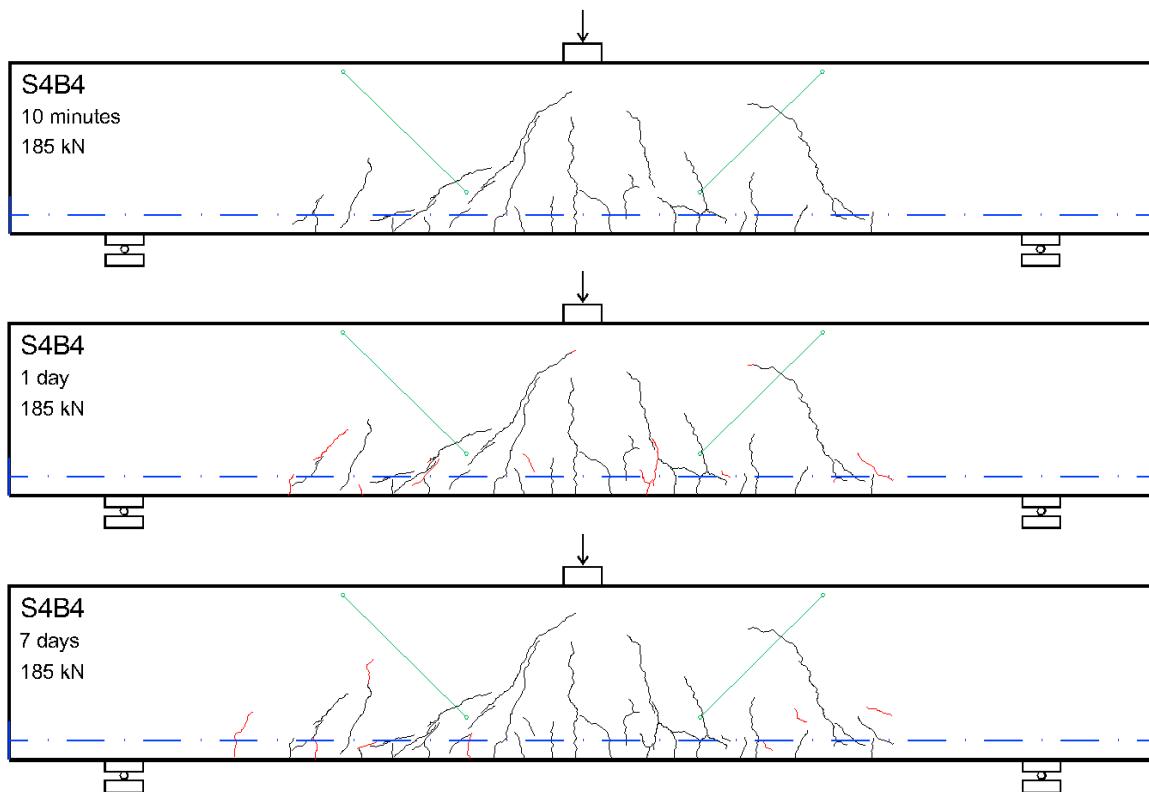
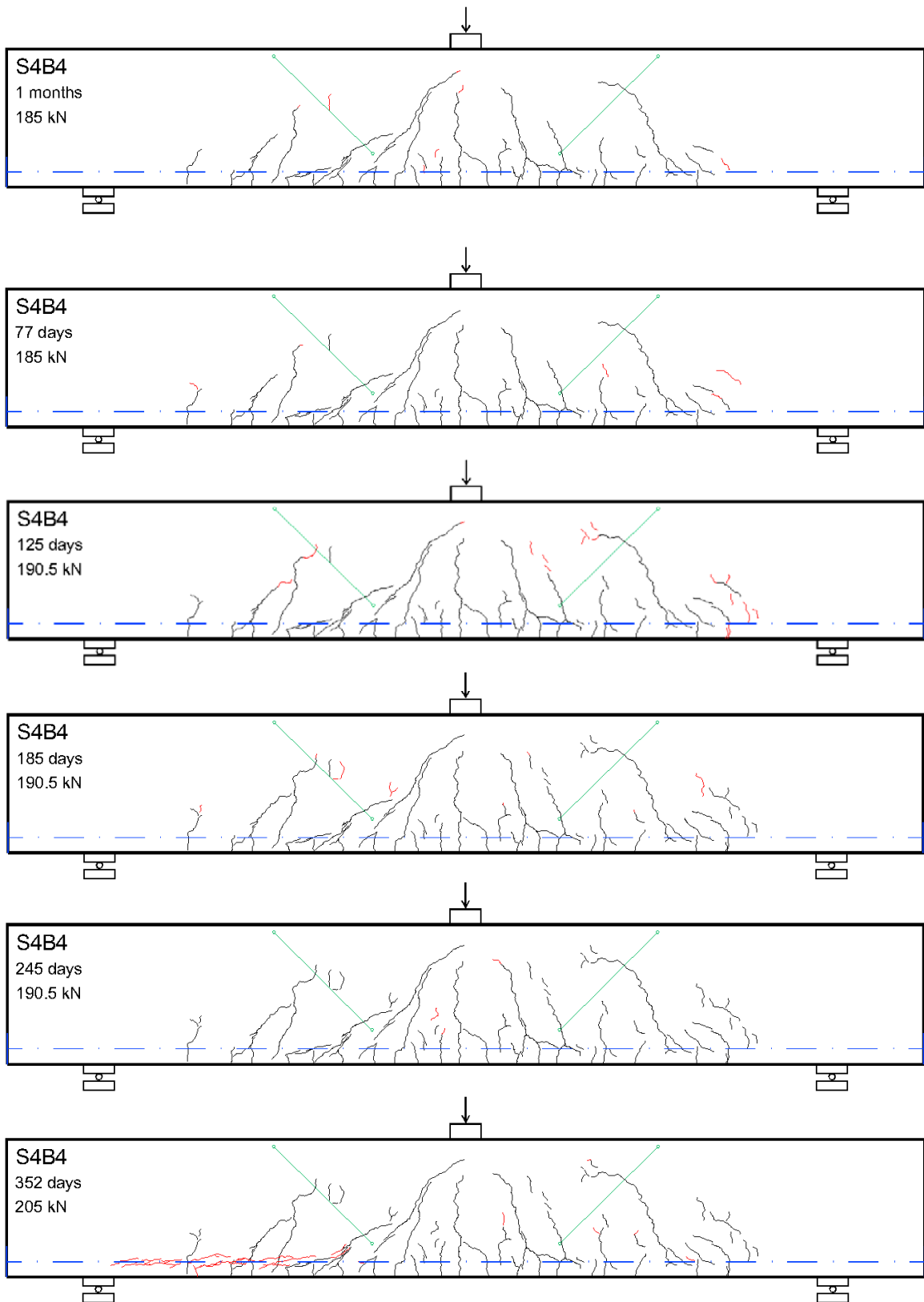


Fig. 71: Crack pattern in beam S3B6 in time





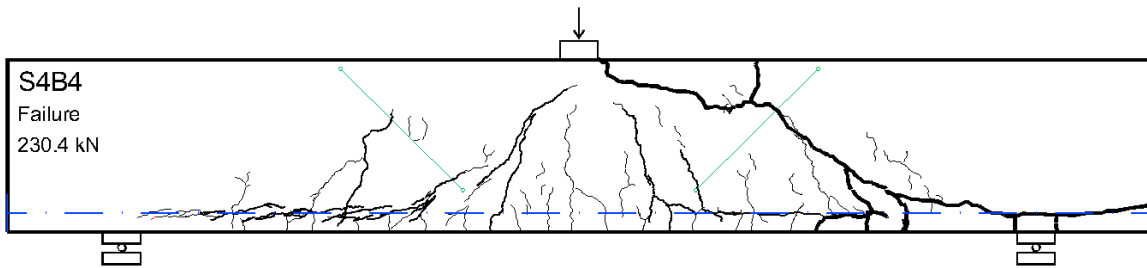
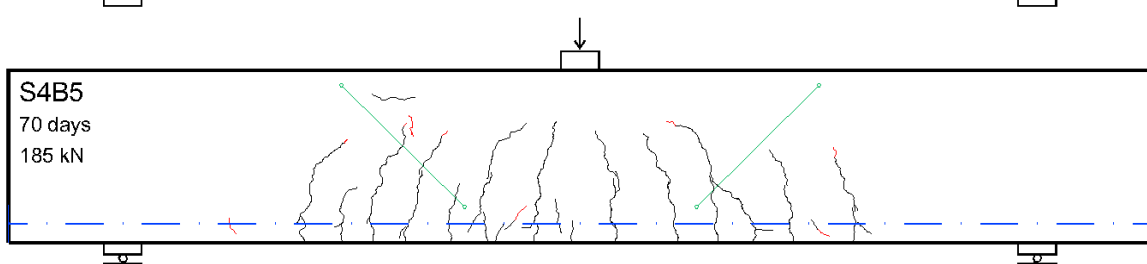
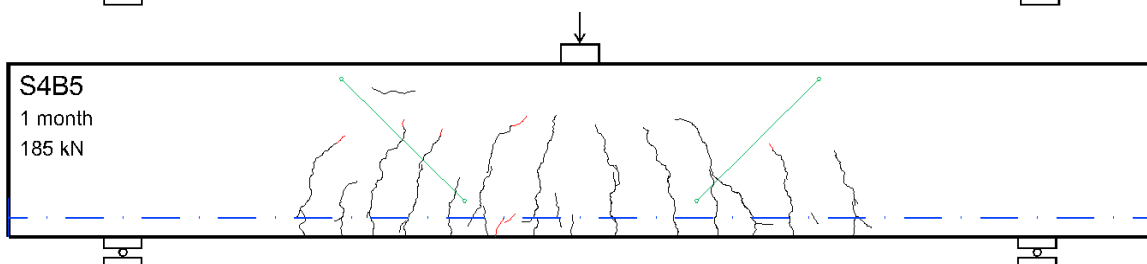
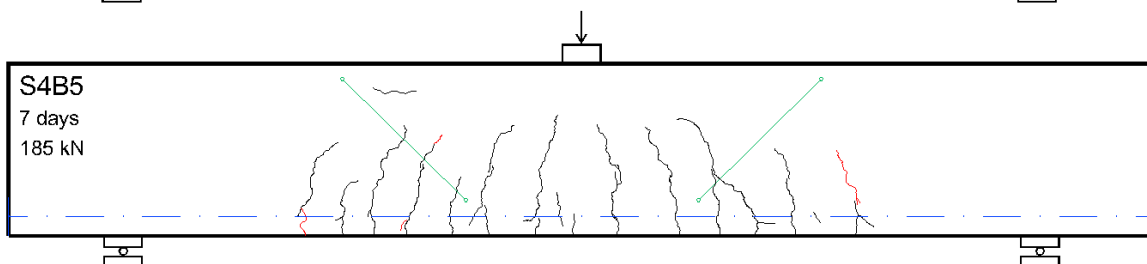
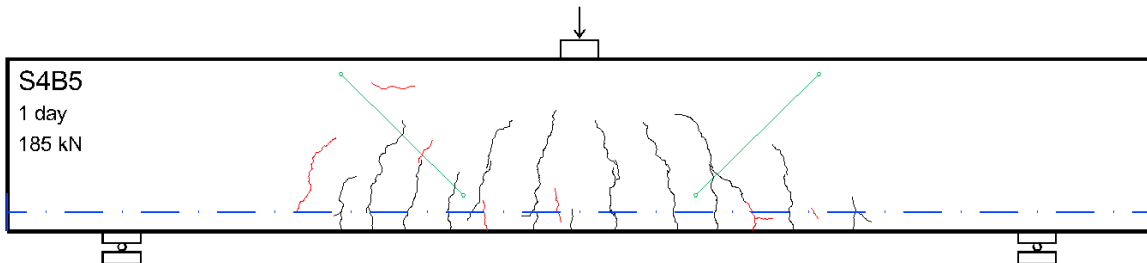
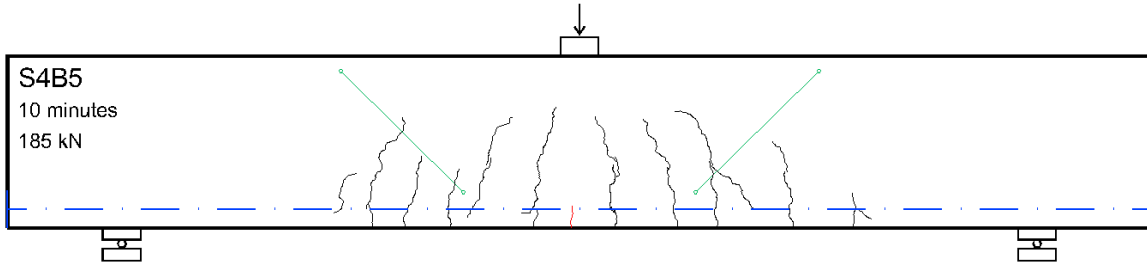


Fig. 72: Crack pattern in beam S4B4 in time



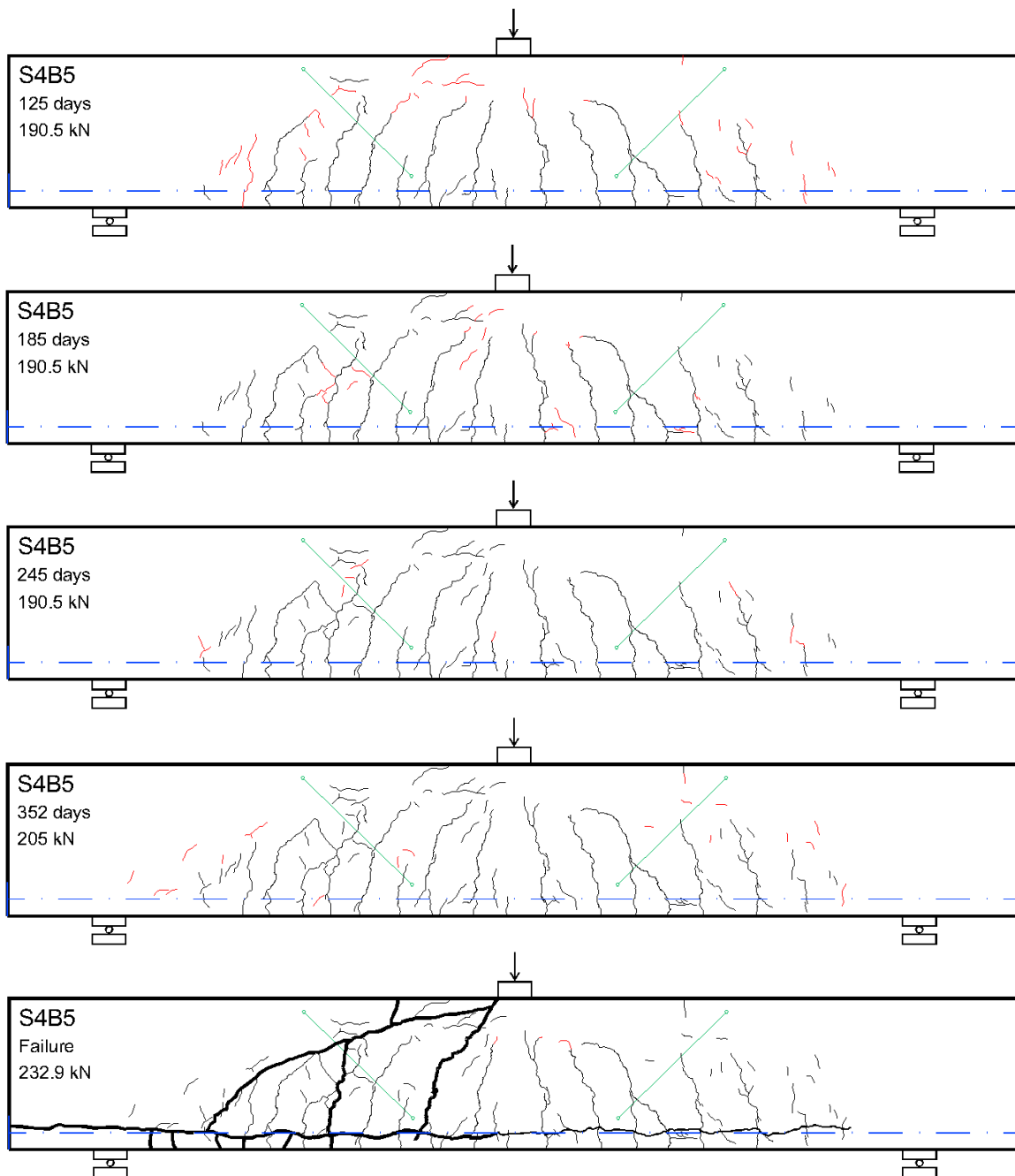


Fig. 73: Crack pattern in beam S4B5 in time

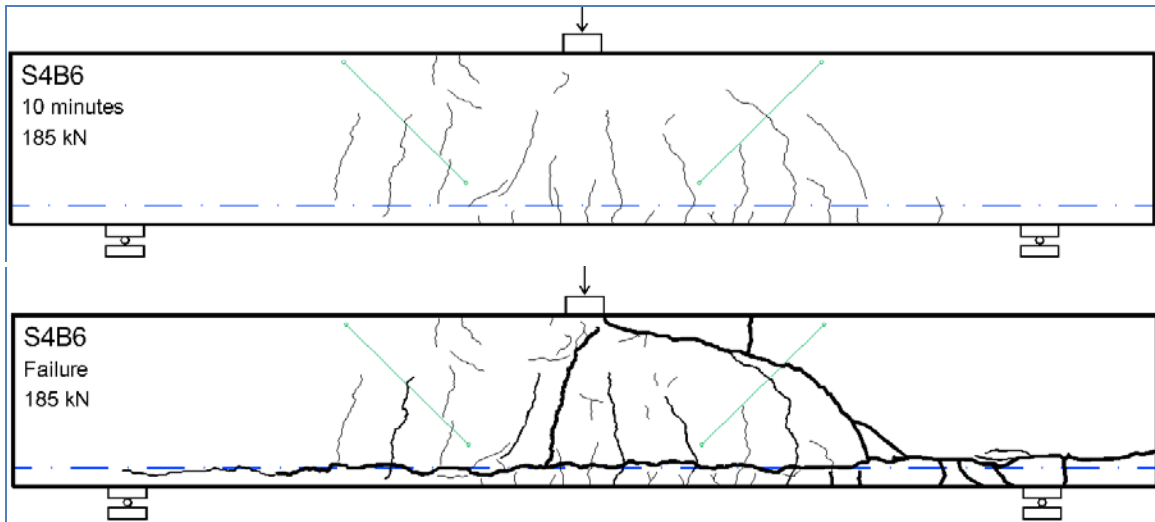
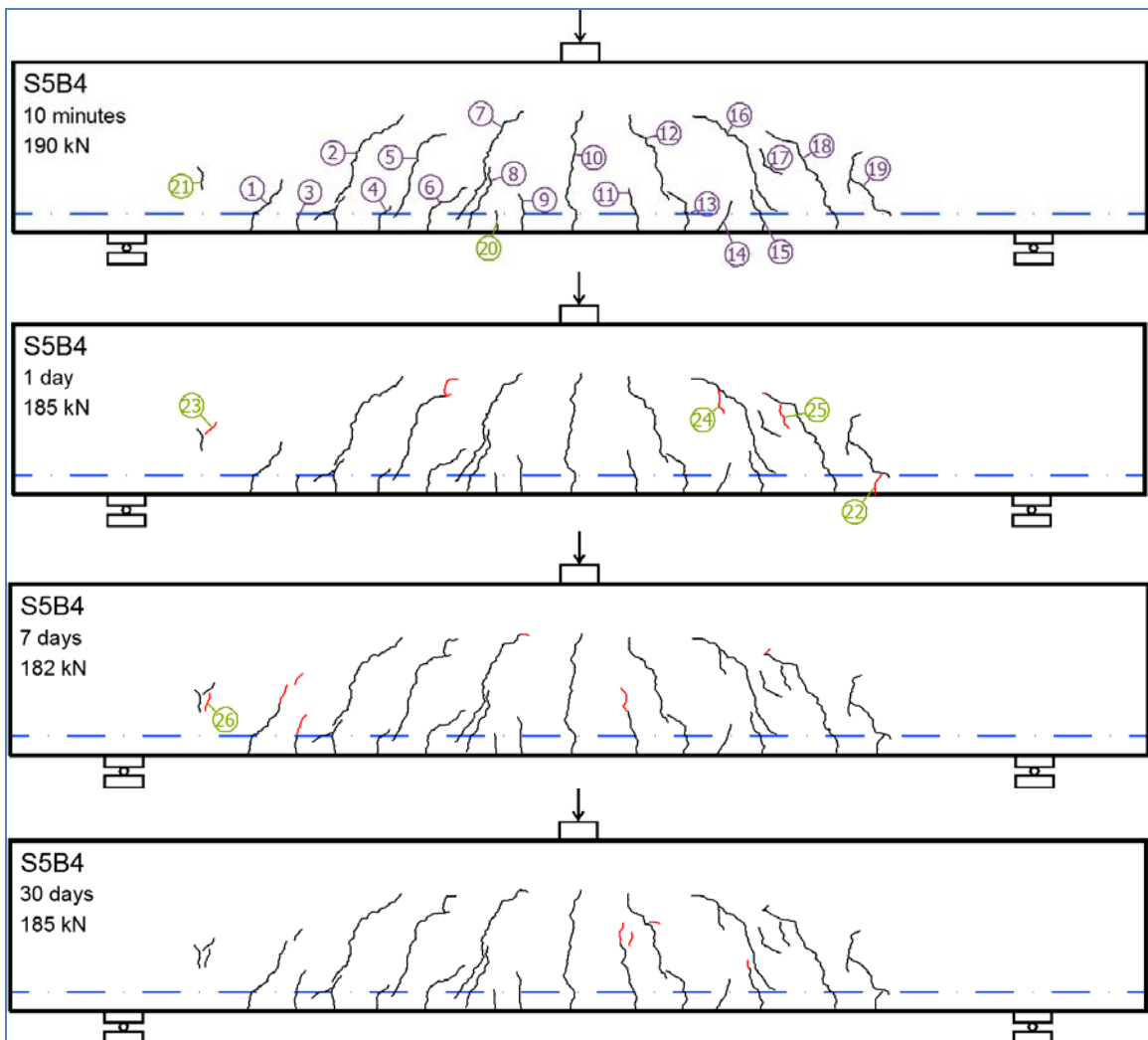


Fig. 74: Crack pattern in beam S4B6 in time



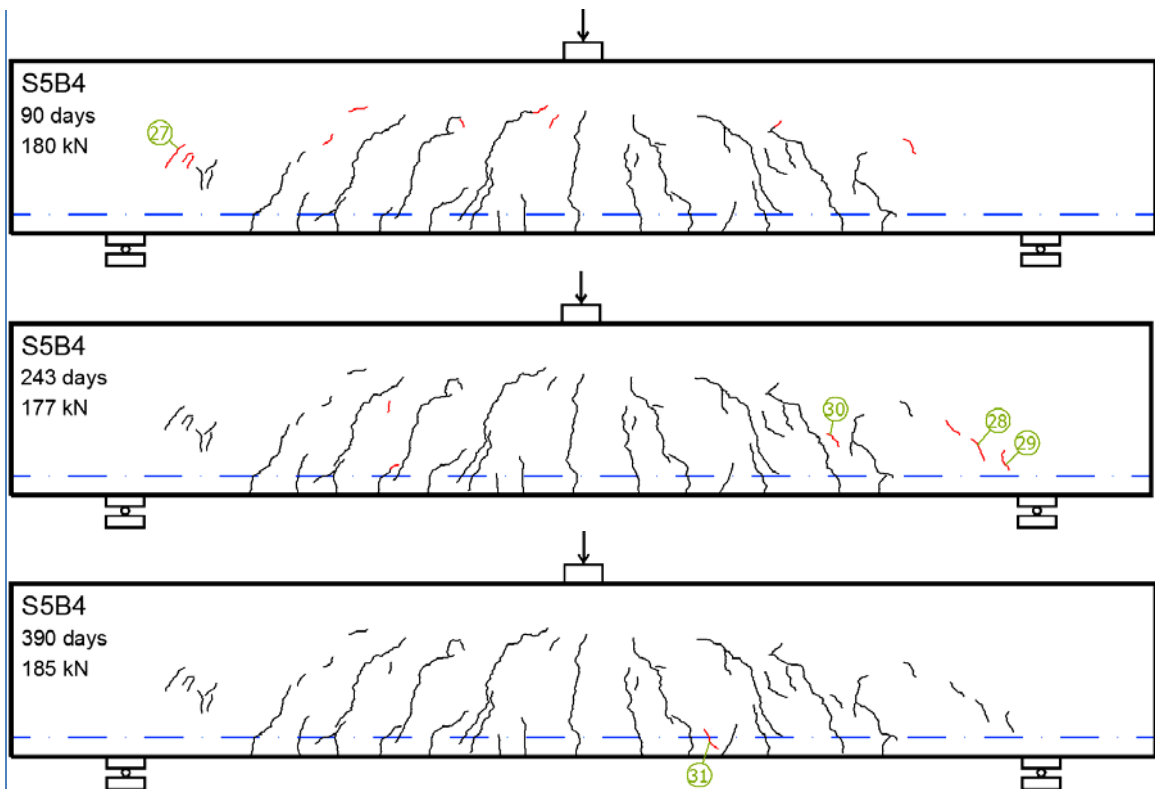
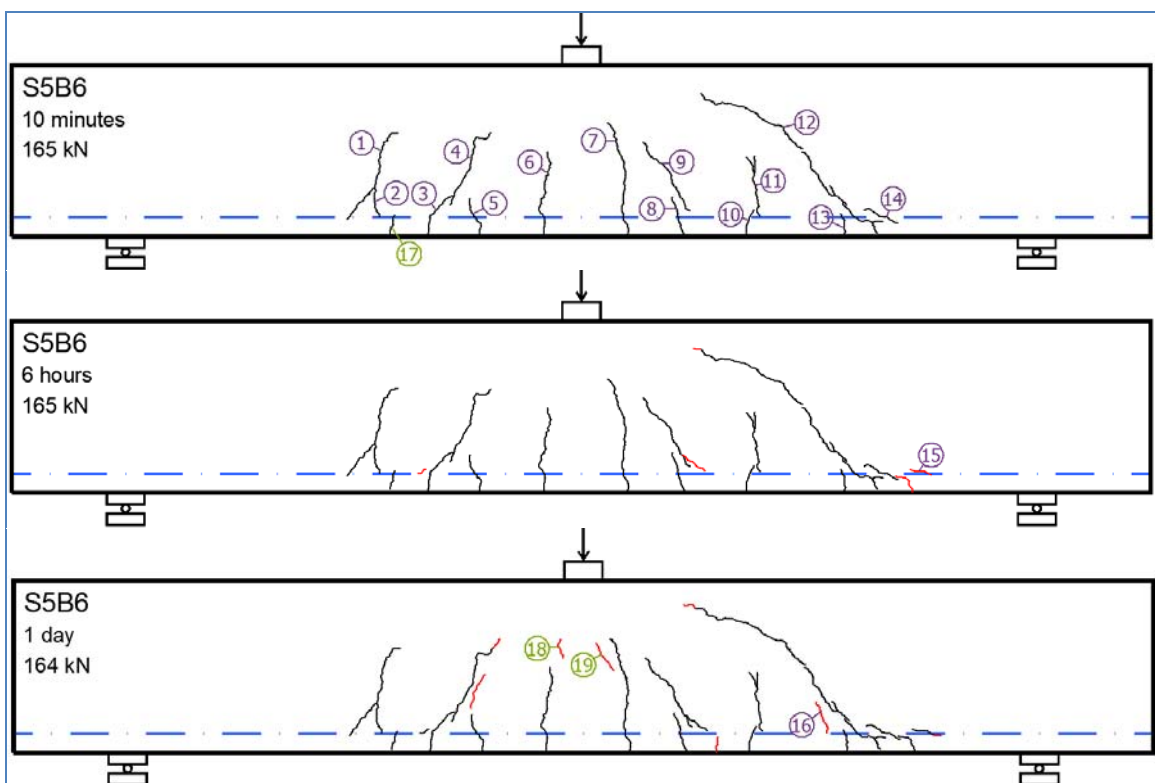


Fig. 75: Crack pattern in specimen S5B4 in time



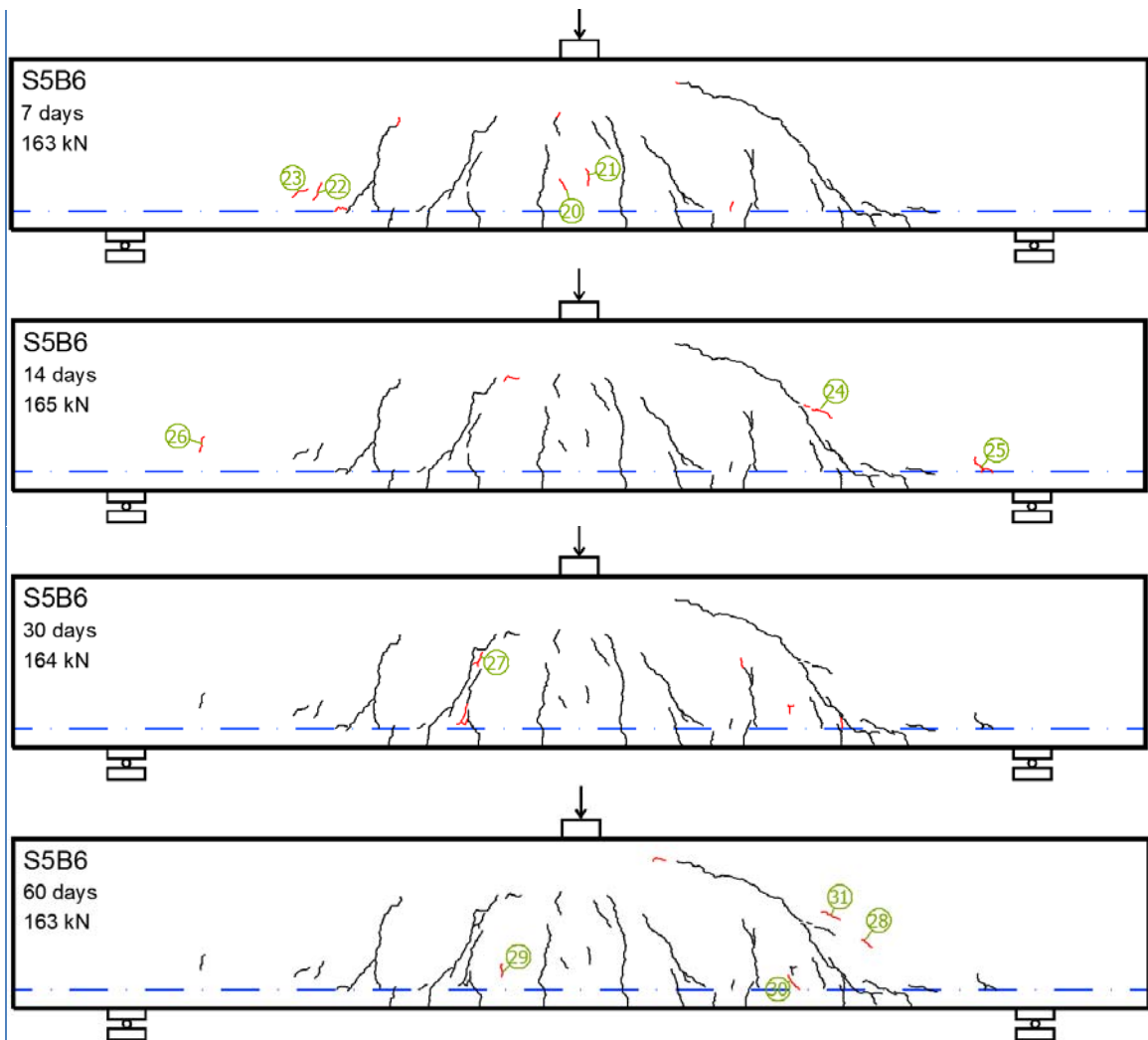
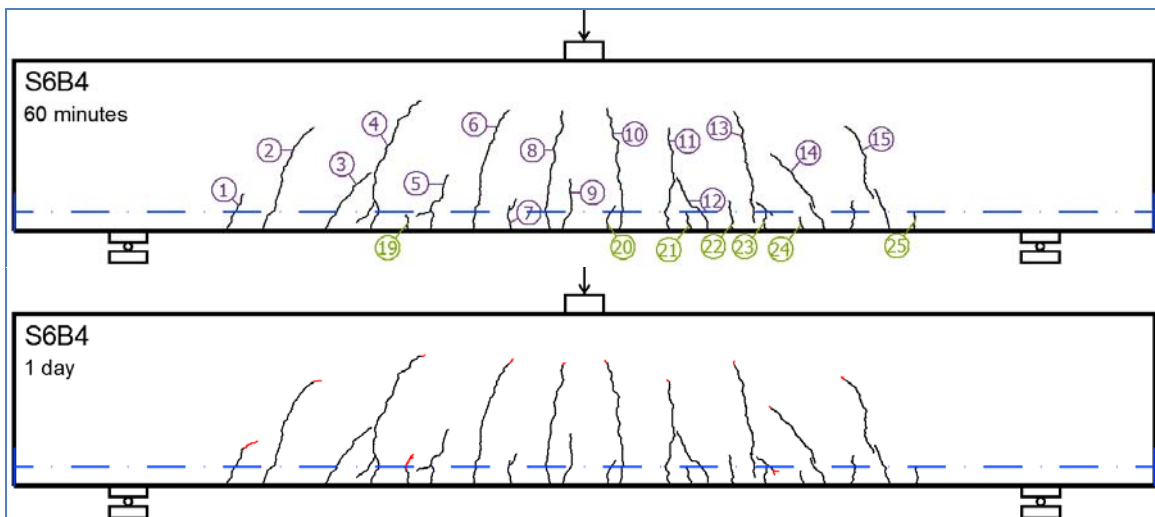


Fig. 76: Crack pattern in specimen S5B6 in time



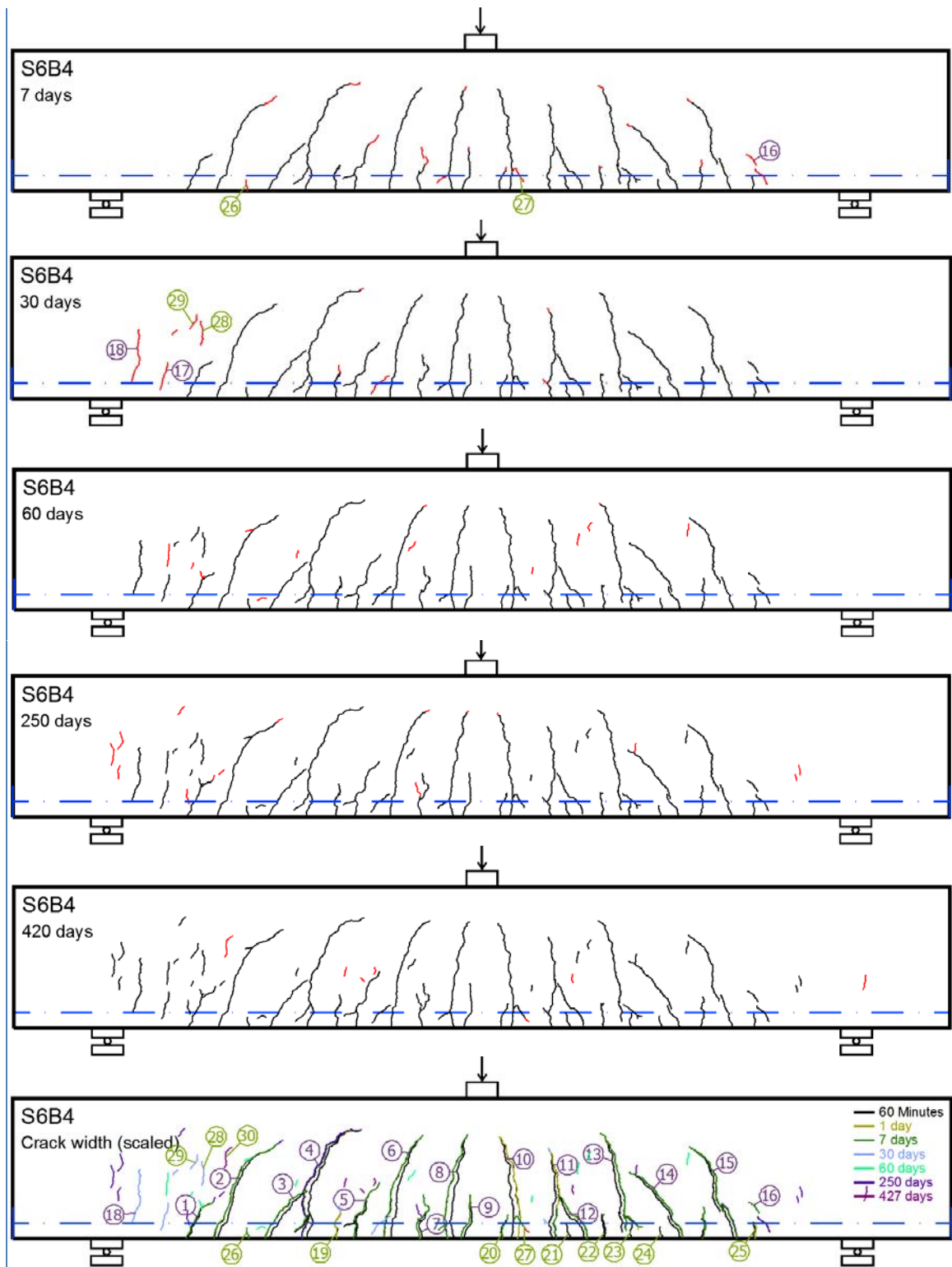


Fig. 77: Crack pattern in specimen S6B4 in time

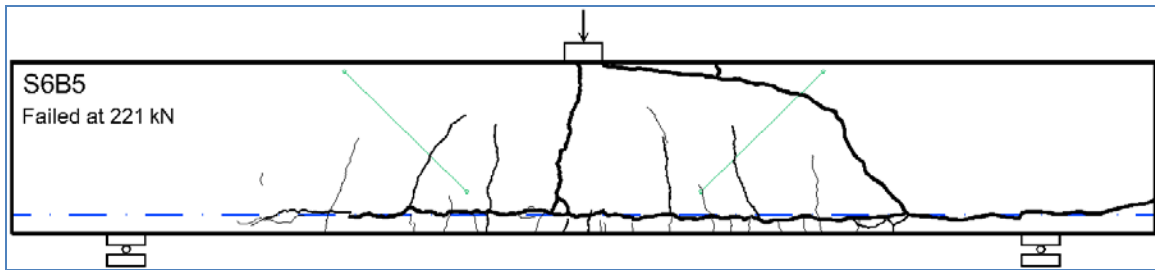
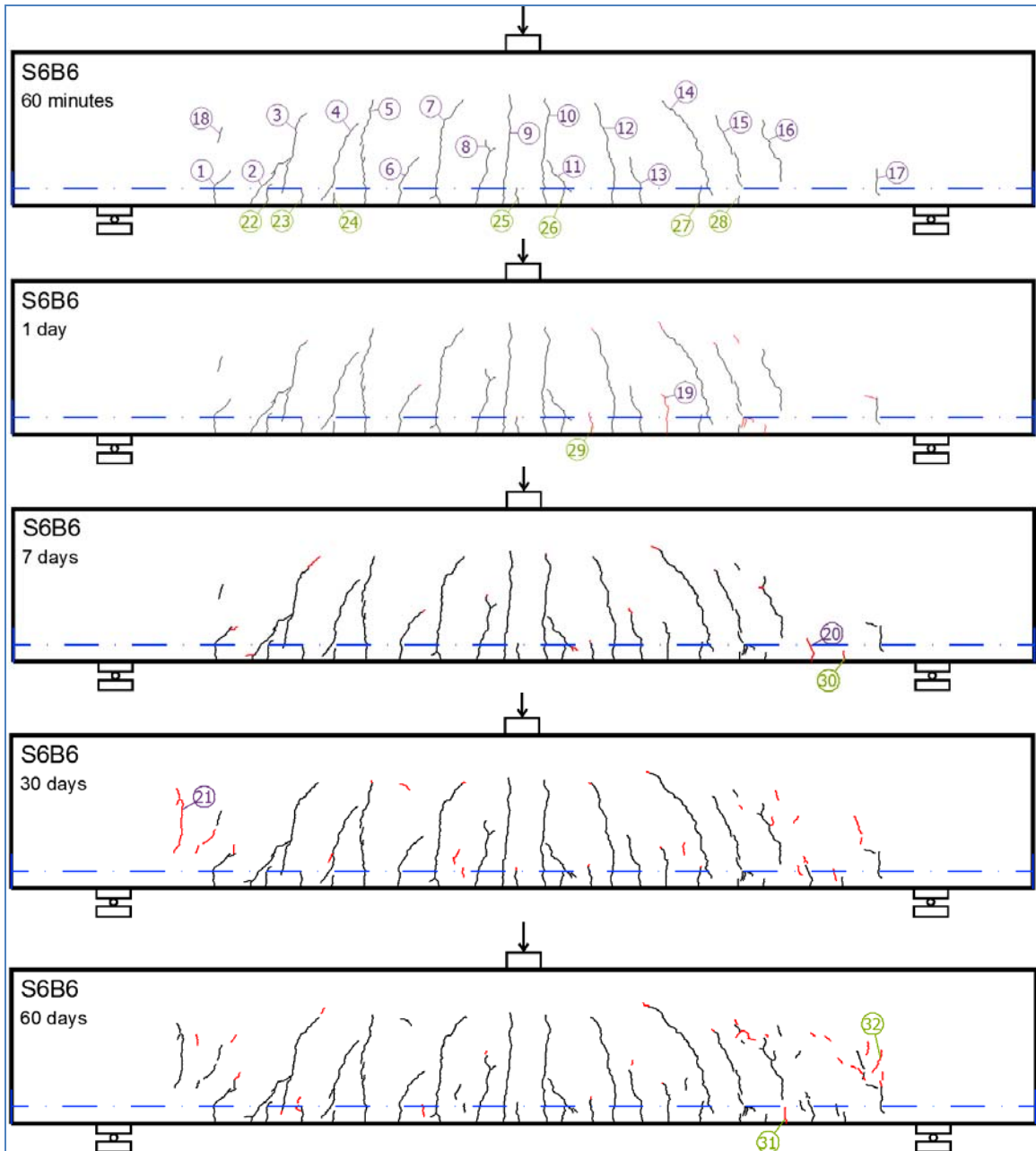


Fig. 78: Crack pattern in beam S6B5



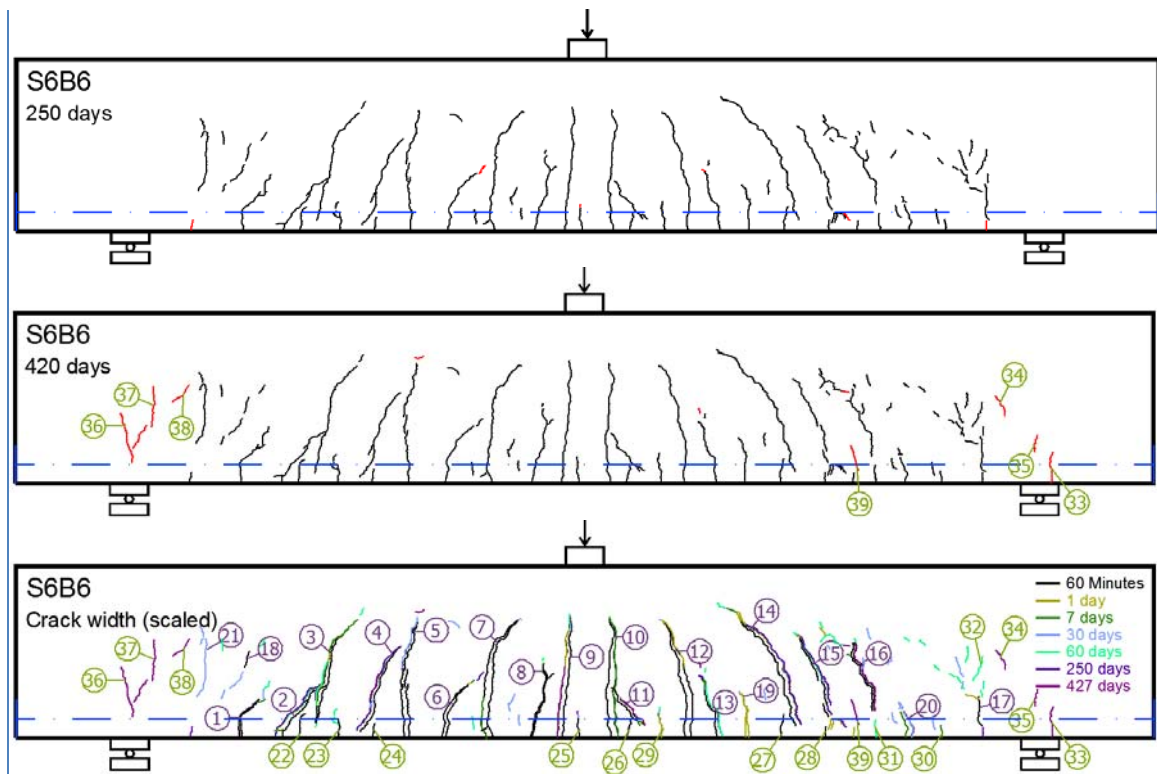


Fig. 79: Crack pattern in beam S6B6

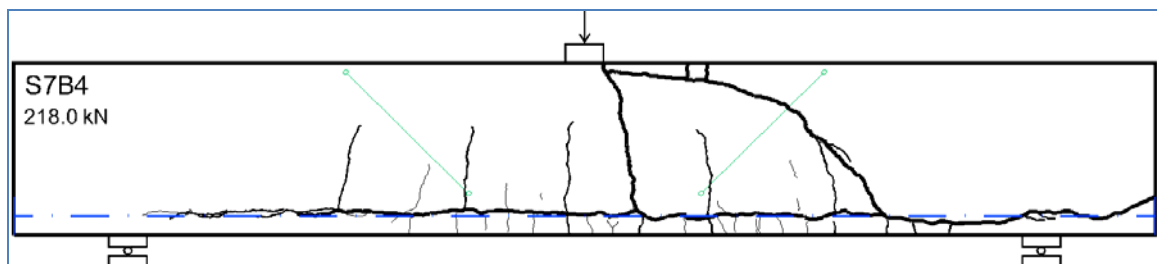


Fig. 80: Crack pattern in beam S7B4

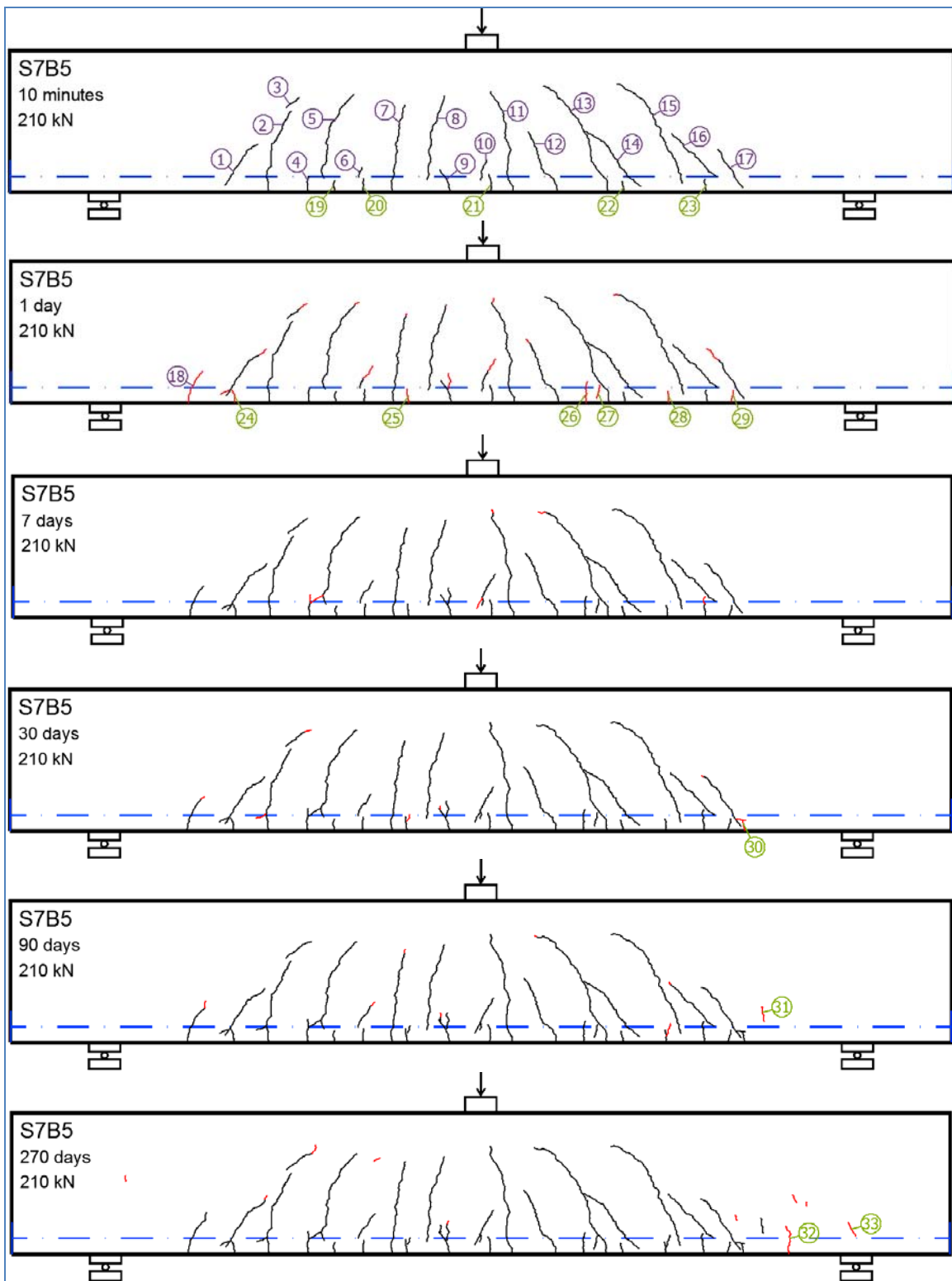


Fig. 81: Crack pattern in beam S7B5

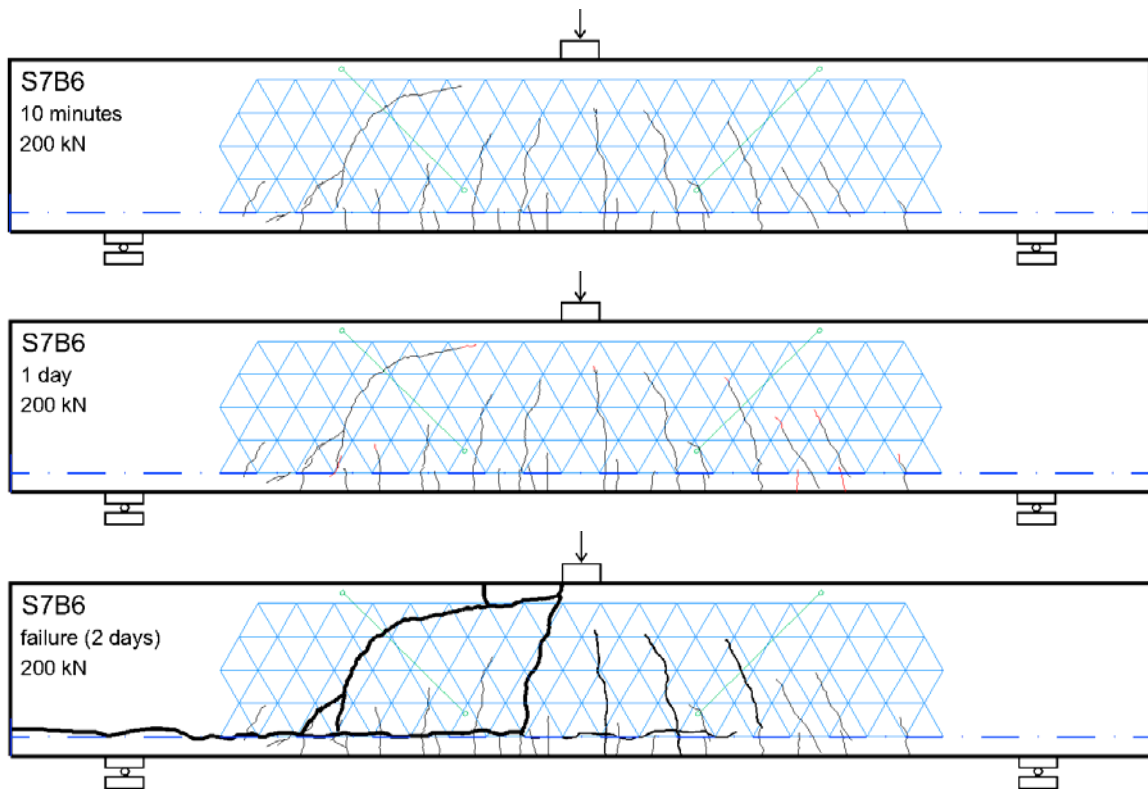


Fig. 82: Crack pattern in beam S7B6 in time and failure of the beam after 2 days

### 7.5. Crack length in time

The progress of every single crack on the surface of the beam is monitored in time. The surface cracks are categorized in two groups; major cracks and minor cracks. Minor cracks are very short cracks (less than 100 mm length) which can never lead to failure or be part of a failure crack, but are large enough (longer than 10 mm) to potentially affect the stress redistribution in the beam. It is attempted to carry out the tests at an age of over 70 days to avoid the development of shrinkage cracks in time. However, the results show that most of the new cracks that develop during the test are shrinkage cracks. This will be explained in detail in section 7.7.

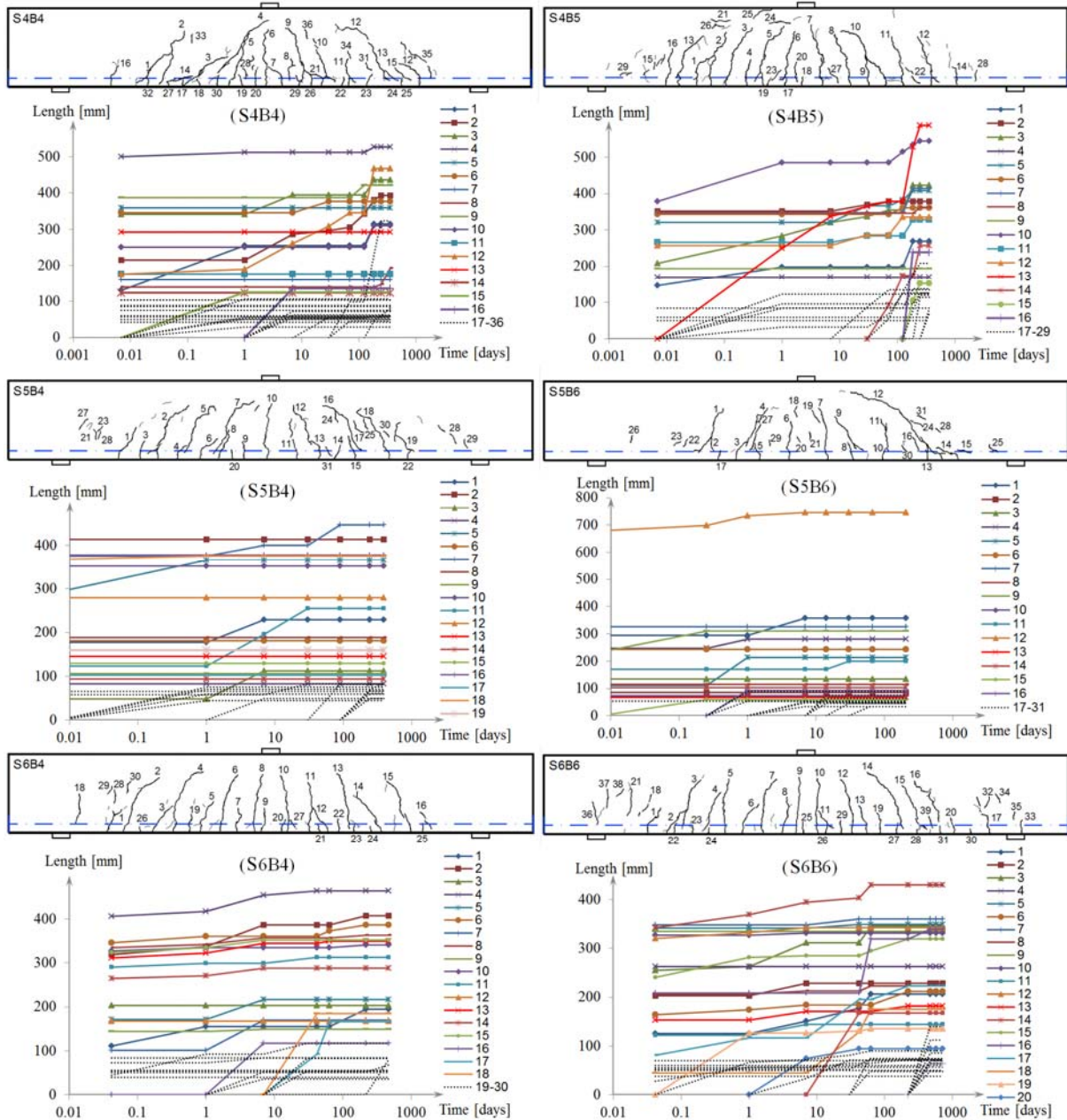


Fig. 83: Development of crack length in time

Fig. 83 shows the development of the crack length in time. Clearly, some of the cracks propagate in time, while some have a constant length. The development of the cracks is not necessarily limited to the large cracks; sometimes, small cracks show considerable progress, while there is no progress in the large cracks. The increasing length of cracks in specimens S4B4 and S4B5 after 145 days are caused by an increase in load ratio, see Fig. 63 and Fig. 65.

A comparison to the crack length development in specimens S5B4 and S5B6 with old concrete (500 days and 710 days old at  $t = 0$ ) and crack length development in specimens with fresh concrete (less than three months old; specimens S4B4, S4B5, S6B4 and S6B6), demonstrates that the crack development in these old beams is less than in fresh beams. Fig. 83 shows that there is a limit to the crack length development. Another observation during the long-term tests is that the cracks do not propagate after 6 months of loading.

### 7.6. Crack opening in time

The width of a single crack on the surface of a beam has its maximum at the mouth of the crack and it reduces along the crack length to zero at the crack tip. In order to find out the maximum crack opening displacement, the crack width is measured perpendicular to the crack face, at several locations along the crack length by means of a hand-operated LVDT and pre-installed measuring points on the surface of the beam.

In Fig. 84, the CMOD of the major cracks is presented during sustained loading. Minor cracks are neglected to be measured, since most of them appear out of the measuring region. Noticeably, in some cracks, CMOD increases in time while in some other cracks it remains constant. The cracks with a considerable increase in length present a significant opening in time (e.g. crack number 3 in specimen S6B6, see Figs. 4 and 5). However, there are always some cracks those propagate in time, but demonstrate a small change in crack width. The same happens with the opening of some cracks in time, but without any visible increase in length.

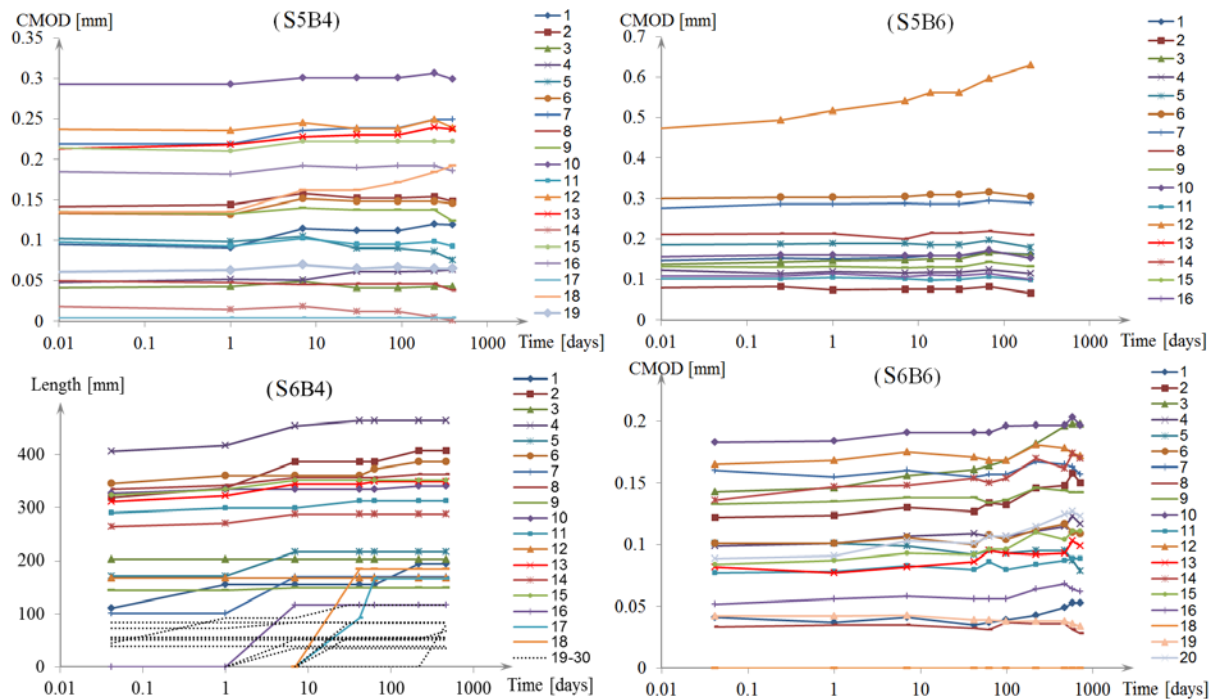


Fig. 84: Development of crack width in time. Crack numbers are related to the beams in Fig. 83.

### 7.7. Appearance of new cracks

A comparison between aged concrete specimens (S5B4 and S5B6) and fresh concrete beams (S4B4, S4B5, S6B4 and S6B6) shows that the development and appearance of new cracks are more visible in fresh concrete beams while in old concrete beams, the new cracks are rare to appear.

It can be concluded that, most of the new cracks that appear in time, are shrinkage cracks. It has also been observed that shortly after loading, the crack pattern is mostly developed in the middle of the beam, while after some time new cracks appear closer to the supports.

## 7.8. Summary of long-term sustained loading tests

A total number of 14 concrete beams were successfully tested in long-term sustained loading. Other four beams those were again supposed to be tested in long-term loading, failed during load application.

Specimen S2B4, S2B5 and S2B6 in series II were tested under long-term sustained loading test with a load ratio of 87% for 74 days. Afterwards, the beams were loaded to failure at the end of sustained loading period in order to find out the effect of sustained loading (any possible reduction in capacity of the beam). Cube compressive strength tests were performed in time together with the beam tests to get insight into the concrete strength development. After 75 days of sustained loading (age of concrete = 145 days), the loading ratio is adjusted to 90% of the actual strength, which is calculated according to the actual cube compressive strength. The load ratio is kept at 90% for 5 days, and then it is increased to 92,5%. This procedure continues until failure of the beam. In Fig. 6 (Right), the results of these tests are presented. Evidently, the ultimate shear capacity of the beams at the end of sustained loading corresponds to the estimated shear capacity (calculated numerically) and no effect of the previous sustained loading is detected. A noticeable result was that during increasing the load level, some new cracks became visible on the beam surface but the main shear cracks did not propagate; only the width of the cracks (according to the diagonal LVDT's) increased.

Two beams in series III were tested in long-term loading at a level of 95% of the mean short-term capacity. Specimen S2B4 failed just before reaching the 95% level. Beam specimen S2B5 and S2B6 were kept at 95% of ultimate short-term capacity, for 67 days. After this period, the load was increased to 97% of the theoretically obtained ultimate capacity at the corresponding time. This load level was kept for 70 days and after that the beams were unloaded for 50 days for changing the test setup. Beam S2B6 failed during reloading up to the previous load level. The other beam is still loaded at 97% of estimated actual ultimate capacity.

The beams of series IV are loaded at 95% of the short-term ultimate capacity. Specimen S4B6 failed after 2,5 hours loading and specimens S2B4 and S2B5 are still in the setup. After 70 days of sustained loading, the strength of the concrete was increased due to further hydration and the ultimate shear capacity is theoretically obtained using Rafia's formula. The load was then adjusted to 92% of the theoretically obtained ultimate capacity. No failure occurred in S2B4 and S2B5 after 11 months of sustained loading. Finally the load was increased to failure. But before reaching the failure mode, at 205 kN, a wide crack (0,7 mm) appeared in specimen S4B4. Both beams were then kept at 205 kN for one month. Due to relaxation, the load decreased meanwhile, but no failure occurred. The reason could be the wide crack in S4B4, which went under the loading plate, so the applied load reduced the stresses at crack tip and prevented the crack to open at the crack tip. Consequently, the beam could resist more loads. Specimen S4B4 and S4B5 had an ultimate capacity of 230,4 kN and 232,9 kN, respectively.

The beams of series VI from high strength concrete ( $f_{cm} = 73,4$  MPa) are loaded at 90% of ultimate shear capacity obtained in short-term tests. One of the beams failed during loading (S2B5) at 88,4% of the mean short-term capacity and beams S2B4 and S2B6 are still under the sustained load.

In series 7 with HSC ( $f_{cm} = 77,8$  MPa), the beams were supposed to be loaded at 218 kN (95% of ultimate capacity), but unfortunately none of the beams reached that load level; S7B4 failed after 2 minutes at 218 kN, S7B5 stopped at 210 kN when a wide crack appeared on the beam and S7B6 stopped at 200 kN when a long crack passing through the compression zone appeared on the beam. S7B6 failed after 2 days of sustained loading and S7B5 is still under loading at 210 kN.

Based on the results obtained from the sustained loading tests and the short-term loading tests, reaching the maximum deflection possibly takes a couple of months due to creep effects in the concrete beam. The maximum crack width was reached within a couple of hours and if the beam resists the load in this period, it would probably resist "forever". As it is shown by the development of the crack patterns of the beams in time (Fig. 67 to Fig. 82), only a few of the current cracks grow during long-term loading and growth is not permanent. It means that the propagation of the crack could stop after a few months or just a few days. This phenomenon can be seen also in the diagonal deflection of beams (Fig. 58 to Fig. 65) where the crack width stays constant during long-term loading even though the midspan deflection increases due to creep. Another phenomenon is the appearance of new cracks which leads to stress relaxation in old cracks. Certainly some additional shrinkage

cracks appear on the surface of the beam particularly in Normal Strength Concrete but it is tried to neglect these cracks in crack patterns.

Specimen S4B6 is one of the samples which failed under sustained loading, even though the duration of the loading was not too long and probably the load was too close to the ultimate capacity of the beam. However, this sample shows that when the load level is close enough to the ultimate capacity, the beam fails and this failure may happen within a few hours after loading.

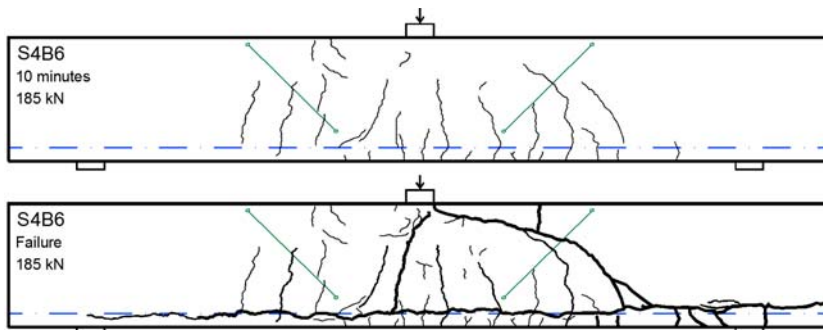


Fig. 85: Failure of S4B6 after 145 minutes.

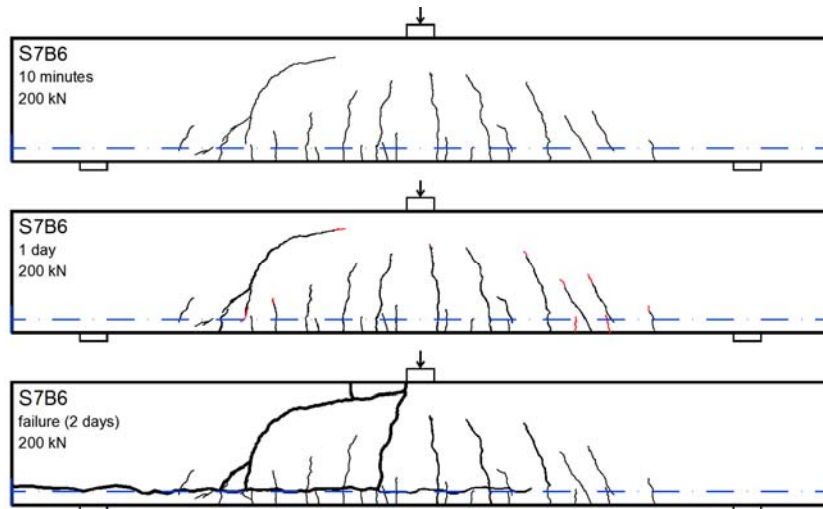


Fig. 86: Failure of S7B6 after 145 minutes.

## Conclusions

---

Based on the results of 24 short-term tests and 18 long-term tests the following provisional conclusions can be drawn:

- Shear tests are carried out on concrete beams without shear reinforcement, subject to high levels of loading. The level of the sustained loading corresponds to 87% – 95% of the average short-term shear capacity, which is determined in separate tests. The long-term tests up to 3 years, do not show a significant sustained loading effect.
- During sustained loading slight propagation of shear cracks is observed. This crack propagation is more pronounced in the first six months of loading. Furthermore, the results of monitoring the crack opening displacement in time show that the crack widths increase in the first week of loading, but afterwards the cracks stabilize and become dormant. Only one crack (crack nr. 12) in specimen S5B6 is still opening in time (Fig. 84), but after 220 days of sustained loading, no signs of failure are detected. It should be noticed that this crack had nearly 0,5 mm width at  $t = 0$ .
- As drawn in Fig. 83, the development of the crack lengths dormant after a few months of sustained loading (in these tests between 3 and 6 months) and the cracks do not propagate anymore, indicating that there is limit to the crack length under sustained loading with constant load ratio. A similar conclusion can be drawn for the width of the cracks, which become dormant after 1 week, indicating that there is also a limit to the crack width opening under sustained loading. Another conclusion can be drawn for the appearance of new cracks, which seems to be shrinkage cracks, as explained in 7.7.
- In two cases shear failure occurred under sustained load: in one case 2,4 hours after loading and in the other case 44 hours after loading. In those cases, however, the sustained load was in the 95% confidence interval of the short-term shear capacity. The specimens in Table 1 marked with an asterisk (\*) next to the label, are still under sustained loading. For further extensions of the sustained loading results described in this work, numerical investigation is required.
- The failure crack does not necessarily originate from the existing visible shear cracks
- During long-term loading, due to creep effect, the deflection of the beam increases but it does not lead to failure.
- There are certainly some invisible cracks in the concrete beam subjected to high-sustained load. These cracks are not just appeared on the beam surface in the beginning of loading or some are so small to see, so-called micro-cracks. Due to stress distribution in the beam, invisible cracks and/or micro-cracks become visible on the beam surface during long-term loading. Contrary to this behaviour, some main shear cracks do not propagate anymore.

## References

---

- [1] Eurocode 2 commentary, European Concrete Platform ASBL, June 2008
- [2] Portland Cement Association (PCA), (1994), "Design and Control of Concrete Mixtures", Old Orchard Road, Skokie.
- [3] Rüsç, H. (1960), "Researches toward general flexural theory of structural concrete", Journal of American Concrete Institute, Vol. 57.
- [4] Zhang, B., Phillips, D. V. and Green, D. R. (1998), Sustained loading effect on the fatigue life of plain concrete, Magazine of Concrete Research, Volume 50, Issue 3, pp. 263 –278
- [5] Zhou, F.P. (1992), Time-dependent crack growth and fracture in concrete. PhD thesis, Report TVBM-1011, Lund University of Technology, Sweden.
- [6] Zhou, F.P., Hillerborg, A. (1992), Time-dependent fracture of concrete: testing and modelling. In: Ba zant, Z.P. (Ed.), Fracture Mechanics of Concrete Structures. Elsevier Applied Science, The Netherlands, pp. 906–911.

## Appendix I: Sieve analysis and concrete mix

**Table 18. Sieve analysis of concrete, cast 1**

Sieve	Sand 0-2	Sand 0-4	Gravel 4-16	Mixture Percentage
16 mm	0,0%	0,0%	3,7%	2,0%
8 mm	0,0%	0,0%	61,0%	32,7%
4 mm	0,0%	2,8%	94,7%	52,0%
2 mm	0,0%	16,9%	98,5%	60,6%
1 mm	0,0%	31,6%	99,5%	68,0%
500 µm	0,6%	30,7%	100%	81,7%
250 µm	22,1%	89,8%	100%	95,3%
125 µm	91,9%	99,1%	100%	99,6%
63 µm	100%	100%	100%	100%
Fineness modulus	1,15%	3,01	6,57	4,92
Moisture	3,0%	4,0%	2,0%	
Fraction	0,0%	46,4%	53,6%	

**Table 19. Mix proportions of the concrete per m<sup>3</sup>, cast 1**

Component	Wet	Dry
CEM III/B 42,5 N LH/HS NA	330 kg	330 kg
Sand 0-2 mm	0 kg	0 kg
Sand 0-4 mm	868 kg	835 kg
Gravel 4-16 mm	982 kg	963 kg
PL BV-1M	0,495 kg	0,495 kg
Super plasticizer SPL VC 1550	0,660 kg	0,660 kg
Water	141 kg	194 kg
Air	15 L	15 L
Total	2322 kg	

**Table 20. Sieve analysis of concrete, cast 2**

Sieve	Sand 0-4	Sand 0-2	Gravel 4-16	Mixture Percentage
16 mm	0,0%	0,0%	58,8%	1,2%
8 mm	0,0%	0,0%	91,5%	30,1%
4 mm	4,2%	0,0%	99,0%	48,9%
2 mm	18,6%	0,0%	99,8%	59,8%
1 mm	34,6%	0,0%	100%	68,0%
500 µm	61,3%	0,6%	100%	81,1%
250 µm	89,8%	22,1%	100%	95,0%
125 µm	99,4%	91,9%	100%	99,7%
63 µm	100%	100%	100%	100%
Fineness modulus	3,08	1,15	6,51	4,84
Moisture	4,0%	3,0%	2,0%	
Fraction	48,8%	0,0%	51,2%	

**Table 21. Mix proportions of the concrete per m<sup>3</sup>, cast 2**

Component	Wet	Dry
CEM III/B 42,5 N LH/HS NA	330 kg	330 kg
Sand 0-4 mm	915 kg	880 kg
Sand 0-2 mm	0 kg	0 kg
Gravel 4-16 mm	942 kg	924 kg
Water	135	189
Air	15 L	15 L
Total	2323 kg	

**Table 22. Sieve analysis of concrete, cast 3**

Sieve	Sand 0-4	Sand 0-2	Gravel 4-16	Mixture Percentage
16 mm	0,0%	0,0%	1,9%	1,0%
8 mm	0,0%	0,0%	56,5%	30,5%
4 mm	4,2%	0,0%	91,1%	51,1%
2 mm	16,8%	0,0%	98,9%	61,1%
1 mm	30,9%	0,0%	99,7%	68,0%
500 µm	64,2%	0,6%	100%	83,5%
250 µm	90,2%	22,1%	100%	95,5%
125 µm	99,7%	91,9%	100%	99,9%
63 µm	100%	100%	100%	100%
Fineness modulus	3,06	1,15	6,48	4,90
Moisture	4,0%	3,0%	2,0%	
Fraction	46,1%	0,00%	53,9%	

**Table 23. Mix proportions of the concrete per m<sup>3</sup>, cast 3**

Component	Wet	Dry
CEM III/B 42,5 N LH/HS NA	330 kg	330 kg
Sand 0-4 mm	865 kg	831 kg
Sand 0-4 mm	0 kg	0 kg
Gravel 4-16 mm	992 kg	972 kg
Super plasticizer SPL VC 1550	0,594 kg	0,594 kg
Water	136 kg	189 kg
Air	15 L	15 L
Total	2323 kg	

**Table 24. Sieve analysis of concrete, cast 4**

Sieve	Sand 0-4	Sand 0-2	Gravel 4-16	Mixture Percentage
16 mm	0,0%	0,0%	2,3%	1,2%
8 mm	0,0%	0,0%	57,5%	31,0%
4 mm	7,0%	0,0%	95,8%	54,9%
2 mm	12,1%	0,0%	99,0%	59,0%
1 mm	30,9%	0,0%	99,7%	68,0%
500 $\mu$ m	53,3%	0,6%	100%	78,5%
250 $\mu$ m	90,5%	22,1%	100%	95,6%
125 $\mu$ m	99,0%	91,9%	100%	99,5%
63 $\mu$ m	100%	100%	100%	100%
Fineness modulus	2,93	1,15	6,54	4,88
Moisture	4,0%	3,0%	2,0%	
Fraction	46,1%	0,0%	53,9%	

**Table 25. Mix proportions of the concrete per m<sup>3</sup>, cast 4**

Component	Wet	Dry
CEM III/B 42,5 N LH/HS NA	330 kg	330 kg
Sand 0-4 mm	864 kg	831 kg
Sand 0-4 mm	0 kg	0 kg
Gravel 4-16 mm	993 kg	973 kg
Super plasticizer SPL VC 1550	0,596 kg	0,594 kg
Water	136 kg	189 kg
Air	15 L	15 L
Total	2323 kg	

**Table 26. Sieve analysis of concrete, cast 5**

Sieve	Sand 0-4 Type I (Grensmaas)	Sand 0-4 Type II	Sand 0-2	Gravel 4-16	Mixture Percentage
16 mm	0,0%	0,0%	0,0%	0,6%	0,3%
8 mm	0,0%	0,0%	0,0%	51,5%	27,8%
4 mm	1,7%	2,0%	0,0%	86,5%	47,4%
2 mm	14,1%	13,6%	0,0%	98,9%	59,5%
1 mm	35,7%	28,4%	0,0%	99,9%	68,0%
500 µm	60,8%	56,9%	0,6%	100%	80,7%
250 µm	89,8%	92,5%	22,1%	100%	96,1%
125 µm	99,3%	99,8%	91,9%	100%	99,8%
63 µm	100%	100%	100%	100%	100%
Fineness modulus	3,01	2,93	1,15	6,38	4,80
Moisture	4,0%	4,0%	3,0%	2,0%	
Fraction	16,2%	30,1%	0,0%	53,7%	

**Table 27. Mix proportions of the concrete per m<sup>3</sup>, cast 5**

Component	Wet	Dry
CEM III/B 42,5 N LH/HS NA	320 kg	320 kg
Sand 0-4 mm Type I	304 kg	292 kg
Sand 0-4 mm Type II	565 kg	543 kg
Sand 0-2 mm	0 kg	0 kg
Gravel 4-16 mm	990 kg	970 kg
Water	142 kg	195 kg
Air	15 L	15 L
Total	2321 kg	

**Table 28. Sieve analysis of concrete, cast 6**

Sieve	Sand 0-4 Type I (Grensmaas)	Sand 0-4 Type II	Gravel 4-16	Mixture Percentage
16 mm	0,0%	0,0%	5,5%	3,0%
8 mm	0,0%	0,0%	51,8%	27,9%
4 mm	1,8%	5,1%	92,1%	51,4%
2 mm	13,0%	15,7%	99,0%	59,8%
1 mm	34,6%	19,1%	99,7%	68,0%
500 $\mu$ m	60,9%	54,9%	100%	81,0%
250 $\mu$ m	88,5%	91,3%	100%	95,5%
125 $\mu$ m	99,3%	99,2%	100%	99,6%
63 $\mu$ m	100%	100%	100%	100%
Fineness modulus	2,98	2,97	6,48	
Moisture	4,0%	4,0%	2,0%	
Fraction	16,2%	30,0%	53,8%	

**Table 29. Mix proportions of the concrete per m<sup>3</sup>, cast 6**

Component	Wet	Dry
CEM I 52,5 R Deuna	280 kg	280 kg
CEM III/B 42,5 N LH/HS NA	145 kg	145 kg
Sand 0-4 mm Type I	282 kg	271 kg
Sand 0-4 mm Type II	523 kg	503 kg
Gravel 4-16 mm	920 kg	902 kg
Fly ash	60 kg	60 kg
Super Plasticizer SPL VC 1550	3,686 kg	3,686 kg
Delayer VTR VZ 1	0,97 kg	0,97 kg
Water	122 kg	171 kg
Air	15 L	15 L
Total	2336 kg	

**Table 30. Sieve analysis of concrete, cast 7**

Sieve	Mixture Percentage
16 mm	2,9%
8 mm	27,6%
4 mm	52,4%
2 mm	60,8%
1 mm	79,8%
500 $\mu\text{m}$	95,8%
250 $\mu\text{m}$	99,7%
125 $\mu\text{m}$	100%
63 $\mu\text{m}$	100%

**Table 31. Mix proportions of the concrete per m<sup>3</sup>, cast 7**

Component	Wet	Dry
CEM I 52,5 R Deuna	280 kg	280 kg
CEM III/B 42,5 N LH/HS NA	145 kg	145 kg
Sand 0-4 mm Type I	288 kg	277 kg
Sand 0-4 mm Type II	535 kg	515 kg
Gravel 4-16 mm	919 kg	901 kg
Fly ash	60 kg	60 kg
Super Plasticizer SPL VC 1550	2,91 kg	2,91 kg
Delayer VTR VZ 1	0,97 kg	0,97 kg
Water	115 kg	165 kg
Air	15 L	15 L
Total	2347 kg	

## Appendix II: Compressive and tensile tests

**Table 32. Compressive and tensile strength of cubes, series I**

No.	Dimensions [mm]	Age [days]	Store room* Fog/Climate	Loading rate [kN/s]	$f_{cc}$ [MPa]		$f_{csp}$ [MPa]	
					Cubes	Mean	Samples	Mean
1	150×150×150	4	F	13,5	15,27			
2	150×150×150	4	F	13,5	16,34	16,01		
3	150×150×150	4	F	13,5	16,41			
4	150×150×150	4	F	1,1			5,01	
5	150×150×150	4	F	1,1			2,97	4,01
6	150×150×150	4	F	1,1			4,06	
7	150×150×150	7	F	13,5	23,61			
8	150×150×150	7	F	13,5	24,13	23,66		
9	150×150×150	7	F	13,5	23,24			
10	150×150×150	7	F	1,1			3,44	
11	150×150×150	7	F	1,1			6,16	4,51
12	150×150×150	7	F	1,1			3,93	
13	150×150×150	14	F	13,5	28,70			
14	150×150×150	14	F	13,5	33,40	30,98		
15	150×150×150	14	F	13,5	30,81			
16	150×150×150	14	F	1,1			3,03	
17	150×150×150	14	F	1,1			3,19	3,09
18	150×150×150	14	F	1,1			3,04	
19	150×150×150	28	F	13,5	37,06			
20	150×150×150	28	F	13,5	38,95	38,18		
21	150×150×150	28	F	13,5	38,52			
22	150×150×150	28	F	1,1			3,50	
23	150×150×150	28	F	1,1			3,46	3,54
24	150×150×150	28	F	1,1			3,65	
25	150×150×150	57	C	13,5	32,72			
26	150×150×150	57	C	13,5	32,53	33,16		
27	150×150×150	57	C	13,5	34,22			
28	150×150×150	57	C	1,1			2,93	
29	150×150×150	57	C	1,1			2,67	2,76
30	150×150×150	57	C	1,1			2,67	
31	150×150×150	70	C	13,5	35,51			
32	150×150×150	70	C	13,5	30,70	35,50		
33	150×150×150	70	C	13,5	35,79			
34	150×150×150	70	C	1,1			2,90	
35	150×150×150	70	C	1,1			3,07	3,00
36	150×150×150	70	C	1,1			3,02	
37	150×150×150	103	C	13,5	40,59			
38	150×150×150	103	C	13,5	33,58	37,78		
39	150×150×150	103	C	13,5	39,16			
40	150×150×150	120	C	13,5	43,14			
41	150×150×150	120	C	13,5	35,71	37,67		
42	150×150×150	120	C	13,5	34,16			

\* Cubes moved from the fog room (F) to the climate room (C) after 28 days

**Table 33. Compressive and tensile strength of cubes and cores, series II**

No.	Dimensions [mm]	Age [days]	Store room* Fog/Climate	Loading rate [kN/s]	$f_{cc}$ [MPa]		$f_{cspl}$ [MPa]	
					Cubes	Mean	Cubes	Mean
1	150×150×150	14	F	13,5	27,72			
2	150×150×150	14	F	13,5	27,17	27,65		
3	150×150×150	14	F	13,5	28,12			
4	150×150×150	28	F	13,5	34,21			
5	150×150×150	28	F	13,5	34,33	34,62		
6	150×150×150	28	F	13,5	35,32			
7	150×150×150	46	F	13,5	35,41			
8	150×150×150	46	F	13,5	36,10	36,82		
9	150×150×150	46	F	13,5	38,95			
10	150×150×150	63	F	13,5	38,85			
11	150×150×150	63	F	13,5	38,72	38,81		
12	150×150×150	63	F	13,5	38,87			
13	150×150×150	70	F	13,5	37,19			
14	150×150×150	70	F	13,5	38,03	38,38		
15	150×150×150	70	F	13,5	39,92			
16	150×150×150	77	F	13,5	42,33			
17	150×150×150	77	F	13,5	41,24	41,12		
18	150×150×150	77	F	13,5	39,79			
19**	100×100	109	C	13,5	37,80			
20**	100×100	109	C	13,5	32,12			
21**	100×100	109	C	13,5	38,02	35,87		
22**	100×100	109	C	13,5	40,04			
23**	100×100	109	C	13,5	39,54			
24**	100×100	109	C	13,5	27,69			
25	150×150×150	120	F	13,5	41,72			
26	150×150×150	120	F	13,5	42,78	41,54		
27	150×150×150	120	F	13,5	40,12			

\* All of the cubes stored in the fog room

\*\* Drilled cores out of beams

**Table 34. Compressive and tensile strength of cubes and cores, series III**

No.	Dimensions [mm]	Age [days]	Store room* Fog/Climate	Loading rate [kN/s]	$f_{cc}$ [MPa]		$f_{csp1}$ [MPa]	
					Cubes	Mean	Cubes	Mean
1	150×150×150	7	F	13,5	29,04		2,95	
2	150×150×150	7	F	13,5	25,97	28,37	2,87	2,93
3	150×150×150	7	F	13,5	30,09		2,96	
4	150×150×150	14	F	13,5	38,14		3,27	
5	150×150×150	14	F	13,5	37,33	38,80	3,29	3,30
6	150×150×150	14	F	13,5	40,92		3,35	
7	150×150×150	21	C	13,5	44,45		3,89	
8	150×150×150	21	C	13,5	45,84	45,93	3,80	3,85
9	150×150×150	21	C	13,5	47,50		3,85	
10	150×150×150	28	C	13,5	49,84		3,93	
11	150×150×150	28	C	13,5	42,57		3,72	
12	150×150×150	28	C	13,5	48,65		3,88	
13	150×150×150	28	F	13,5	51,64	48,43	-	3,83
14	150×150×150	28	F	13,5	47,00		-	
15	150×150×150	28	F	13,5	50,89		-	
16	150×150×150	49	F	13,5	48,22		4,19	
17	150×150×150	49	F	13,5	53,69	51,29	4,03	4,04
18	150×150×150	49	F	13,5	51,96		3,90	
19	150×150×150	63	C	13,5	51,04		4,30	
20	150×150×150	63	C	13,5	51,00	52,01	4,17	4,22
21	150×150×150	63	C	13,5	53,98		4,20	
22	150×150×150	70	C	13,5	48,03		-	
23	150×150×150	70	C	13,5	51,76	50,82	-	-
24	150×150×150	70	C	13,5	52,68		-	
25	150×150×150	84	C	13,5	49,01		4,03	
26	150×150×150	84	C	13,5	51,37	50,09	4,18	4,11
27	150×150×150	84	C	13,5	49,89		4,11	
28**	100×100	91	C	13,5	45,06		-	
29**	100×100	91	C	13,5	29,74		-	
30**	100×100	91	C	13,5	40,71		-	
31**	100×100	91	C	13,5	31,14	38,11	-	-
32**	100×100	91	C	13,5	35,66		-	
33**	100×100	91	C	13,5	46,32		-	
34	150×150×150	98	C	13,5	52,98		4,37	
35	150×150×150	98	C	13,5	54,79	53,45	4,68	4,50
36	150×150×150	98	C	13,5	52,57		4,45	
37	150×150×150	112	C	13,5	54,95		4,1	
36	150×150×150	112	C	13,5	48,34	52,24	4,5	4,28
39	150×150×150	112	C	13,5	53,42		4,23	

\*\* Drilled cores out of beams

## Appendix III: Analysis of specimens series I-V

### Cover

<BS EN 1992-1-2: Tables 5.8, 5.9, 5.10, 5.11>

Nominal cover,  $c_{nom}$

$$c_{nom} = c_{min} + \Delta c_{dev}$$

where

$$c_{min} = \max[c_{min,b}; c_{min,dur}]$$

where

$c_{min,b}$  = minimum cover due to bond  
= diameter of bar.

Assume 20 mm main bars

$c_{min,dur}$  = minimum cover due to environmental conditions.

Assuming XC3 (moderate humidity or cyclic wet and dry) and secondarily XF1 (moderate water saturation without de-icing salt) using C30/37 concrete

$$c_{min,dur} = 25 \text{ mm}$$

$\Delta c_{dev}$  = allowance in design for deviation. Assuming no measurement of cover  $\Delta c_{dev} = 5 \text{ mm}$

$$\therefore c_{nom} = 25 + 5 = 30 \text{ mm}$$

### Fire:

<BS EN 1992-1-2, 5.6.3(1), Table 5.6>

Check adequacy of section for 90 minutes fire resistance (i.e.  $R = 90$ )

For  $b_{min} = 200 \text{ mm}$ , minimum axis distance,  $a = 45 \text{ mm} \therefore \text{OK}$

$$c_{nom} = 30 \text{ mm}$$

### Effective Depth

$$d = 450 - 30 - 20 / 2 = 410 \text{ mm}$$

### Shear Capacity

<Rafla's formula>

$$\tau_c = 0,29 \alpha_u \alpha_h (f_{cm})^{1/2} (\rho)^{1/3}$$

where,

$$\alpha_u = 0,795 + 0,293 (3,5 - a/d)^{2,5} \quad \text{for } 2,0 \leq a/d \leq 3,5$$

$$a/d = 1200/410 = 2,92$$

$$\therefore \alpha_u = 0,795 + 0,293 (3,5 - 2,92)^{2,5} = 0,87$$

$$\alpha_h = 1/(d/100)^{1/4} = 1/(410/100)^{1/4} = 0,7027$$

$$f_{cm} = 35 \text{ MPa (Cube test)}$$

$$\rho = 1,047$$

$$\therefore \tau_c = 0,29 \alpha_u \alpha_h (f_{cm})^{1/2} (\rho)^{1/3} = 0,29 (0,87) (0,7027) (35)^{1/2} (1,047)^{1/3}$$

$$\tau_c = 1,07 \text{ N/mm}^2$$

### Shear Resistance,

$$V_{Rd} = \tau_c b d$$

where,

$$\tau_c = \text{shear capacity} = 1,07 \text{ N/mm}^2$$

$$b = \text{width of the beam} = 200 \text{ mm}$$

$$d = \text{effective depth} = 410 \text{ mm}$$

$$\therefore V_{Rd} = 87,7 \times 10^3 \text{ N}$$

Upper Confidence Limit (UCL) of Shear Resistance

$$V_{Rd,0,95} = V_{RD} (1 + \lambda \cdot SD)$$

where,

$$\lambda = 1,64$$

$$SD = 0,12$$

$$\therefore V_{Rd,0,95} = 87740 (1 + 1,64 \times 0,12) = 105 \times 10^3 \text{ N}$$

### Ultimate bond stress

$$f_{bd} = 2,25 \eta_1 \eta_2 f_{ctd}$$

where,

$$\eta_1 = 1,0 \text{ when the 'good' condition is obtained}$$

$$\eta_2 = 1,0 \text{ for } \emptyset < 32$$

$$f_{ctd} = \text{the design value of the tensile strength}$$

$$= \alpha_{ct} f_{ctk,0,05} / \gamma_c$$

$$f_{ctk,0,05} = 2,0 \text{ MPa (for } f_{ck} = 35 \text{ MPa)}$$

$$\gamma_c = 1,5$$

$$\alpha_{ct} = 1$$

$$\therefore f_{ctd} = (1)(2,0) / (1,5) = 1,33 \text{ MPa}$$

$$\therefore f_{bd} = 2,25 (1) (1) (1,33) = 3,0 \text{ MPa}$$

### Anchorage

The basic required anchorage length  $l_{b,rqd}$ , for anchorage the force  $A_s \cdot \sigma_{sd}$  in a straight bar assuming constant bond stress equal to  $f_{bd}$  follows from:

$$l_{b,rqd} = (\emptyset/4)(\sigma_{sd}/f_{bd}) = (20/4)(\sigma_{sd}/3,0)$$

where,

$$f_{bd} = 3,0 \text{ MPa}$$

$\sigma_{sd}$  is the design stress of the bar at the position from where the anchorage is measured from.

$$\sigma_{sd} = N_s / A_s$$

where,

$$N_s = R_{Ed} (450) / 410$$

where,

$$R_{Ed} = 1,5 V_{Rd,0,95} = 157,5 \times 10^3 \text{ N}$$

$$\therefore N_s = 172,8 \times 10^3 \text{ N}$$

$$\therefore \sigma_{sd} = 172,8 \times 10^3 / 942 = 183,5 \text{ N/mm}^2$$

$$\therefore l_{b,rqd} = (20/4)(183,5/3) = 306 \text{ mm}$$

### Analysis

Design moments

$$M_{Ed} = V_{Rd,0,95} L / 2 + w L^2 / 8$$

where,

$$V_{Rd,0,95} = 105 \times 10^3 \text{ kN}$$

$$L = 2,4 \text{ m}$$

$w$  = self-weight of the beam per meter = 2,25 kN/m

$$M_{Ed} = 127 \text{ kNm}$$

*Effective depth*

$$d = 450 - 30 - 20 / 2 = 410 \text{ mm}$$

*Flexure in span*

$$K = M_{Ed} / b d^2 f_{ck} = 127 \times 10^6 / (200 \times 410^2 \times 35) = 0,1079$$

$$z / d = 0,9$$

$$z = 0,9 \times 410 = 369$$

Stress in steel

$$\begin{aligned} \sigma_s &= f_{ck} b d [0,633 - (0,4 - 1,46 K)^{1/2}] / A_s \\ &= (35)(200)(410)[0,633 - (0,4 - 1,46 \times 0,1079)^{1/2}] / 942 = 425 \text{ N/mm}^2 \end{aligned}$$

**Concrete Volume**

$$\text{Total volume} = 30 \times 0,2 \times 0,45 \times 3 = 7,29 \text{ m}^3$$

**Reinforcement**

$$\text{Total length} = 30 \times 3 \times 3 = 270 \text{ m}$$

$$\text{Steel weight} = 270 \times 78 \pi 0,01^2 = 6,62 \text{ kN}$$

## Appendix IV: FE Modelling in ATENA

Finite Element Modelling is performed in ATENA 2D version 4,1.1. The element type chosen for concrete is "3D Nonlinear Cementitious 2". This element type very appositely characterises the behaviour of concrete in terms of tension (the origination and propagation of tension cracks) and compression. It is based on the non-linear fracture mechanics and incorporates the reduction in the strength of the material after the origination of cracks. The main parameters of the 3D Nonlinear Cementitious 2 material are tensile strength and energy to fracture. A maximum element size of 37,5 mm is chosen for this element type. Meshes are refined around the loading plate and reinforcing bar, see Fig. 87. The material properties e.g. elastic modulus and fracture energy is calculated automatically by the software based on the cube compressive strength. Only the tensile strength is adjusted by the values obtained from test results.

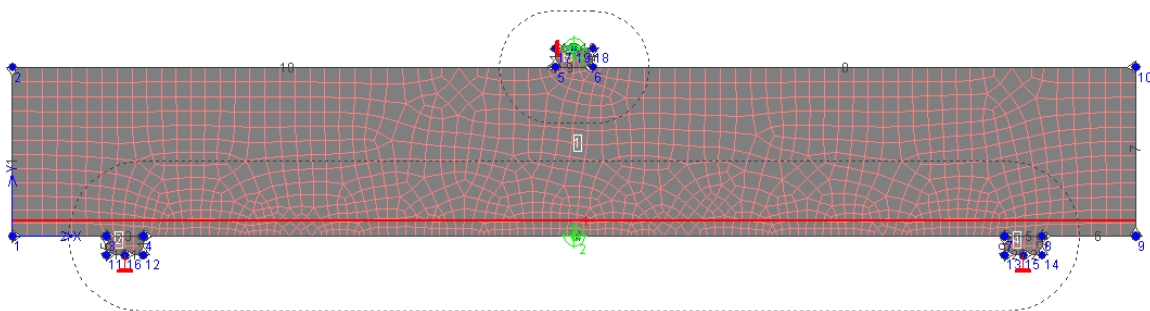


Fig. 87: FE Modelling of the beam in ATENA

"Reinforcement" and "Bond for Reinforcement" elements are used to model the reinforcing bars and the bond between bars and concrete, respectively. The material properties for reinforcement is; elastic modulus  $E=2,1E+05$  MPa, yield strength  $\sigma_y=555,0$  MPa for 20 mm diameter bars and 572,0 MPa for 25 diameter bars. For bond properties CEB-FIP Model Code 1990 is used with ribbed reinforcement, good bond quality and confined concrete is

To model the loading plate and supports, "Plane Stress Elastic Isotropic" element is chosen.

Newton – Raphson method was used for the solution in ATENA 2D.

### ATENA input data

The material properties, which are given in this file is according to series I, 28 days concrete age.

#### General data

```
Desc.      :
Note      :
Num. of smeared reinf. layers : 0
Analysis Type: 2D
```

#### Materials

##### Material n. 1

```
Name : 3D Non Linear Cementitious 2
Type : CC3DNonLinCementitious2
Elastic modulus E = 3.210E+04 [MPa]
Poisson's ratio  $\nu_m$  = 0.200 [-]
Tensile strength  $F_t$  = 2.543E+00 [MPa]
Compressive strength  $F_c$  = -2.933E+01 [MPa]
Specific fracture energy  $G_f$  = 6.359E-05 [MJ/m2]
Critical compressive displacement  $W_d$  = -5.0000E-04 [m]
Eccentricity, defining the shape of the failure surface  $Exc$  = 0.520 [-]
Multiplier for the direction of the plastic flow  $Beta$  = 0.000 [-]
Specific material weight  $Rho$  = 2.300E-02 [MN/m3]
Coefficient of thermal expansion  $Alpha$  = 1.200E-05 [1/K]
Fixed smeared crack model will be used  $Fixed$  = 1.000 [-]
```

Plastic strain at compressive strength EPS\_CP = -9.135E-04 [-]  
Reduction of comp. strength due to cracks RC\_LIM = 0.6 [-]  
Crack Shear Stiff. factor S\_F = 20.0 [-]  
Aggregate Size = 0.0200 [m]

**Material n. 2**

Name : Plane Stress Elastic Isotropic  
Type: CCPlaneStressElastIsotropic  
Elastic modulus E = 2.100E+05 [MPa]  
Poisson's ratio sm = 0.300 [-]  
Specific material weight Rho = 2.300E-02 [MN/m3]  
Coefficient of thermal expansion Alpha = 1.200E-05 [1/K]

**Material n. 3**

Name : Reinforcement  
Type: CCReinforcement  
Typ: BiLinear  
Elastic modulus E = 2.100E+05 [MPa]  
Sigma Y = 555.000 [MPa]  
Specific material weight RHO = 7.850E-02 [MN/m3]  
Coefficient of thermal expansion ALPHA = 1.200E-05 [1/K]  
Active in compression

**Material n. 4**

Name : Bond for Reinforcement  
Type: CCReinforcementBondMaterial  
Function: (0.0000; 5.099E+00) (0.0003; 6.695E+00) (0.0005; 9.663E+00)  
(0.0010; 1.275E+01) (0.0030; 1.275E+01) (0.0150; 5.099E+00) (1.0000; 5.099E+00)

**Joints**

**Joint topology**

Number	Coordinates	
	X [m]	Y [m]
1	0.0000	0.0000
2	0.0000	0.4500
3	0.2500	0.0000
4	0.3500	0.0000
5	1.4500	0.4500
6	1.5500	0.4500
7	2.6500	0.0000
8	2.7500	0.0000
9	3.0000	0.0000
10	3.0000	0.4500
11	0.2500	-0.0500
12	0.3500	-0.0500
13	2.6500	-0.0500
14	2.7500	-0.0500
15	2.7000	-0.0500
16	0.3000	-0.0500
17	1.4500	0.5000
18	1.5500	0.5000
19	1.5000	0.5000

**Mesh refinement at joints**

No joint mesh refinement is specified

**Joint springs**

No joint springs are specified

**Line**

**Line topology**

Number	Segment	Joints		Center		Radius	Orient.	Fictiv
		Beg.	End	X [m]	Y [m]			
1	Line	2	1					
2	Line	1	3					
3	Line	3	4					
4	Line	4	7					
5	Line	7	8					
6	Line	8	9					
7	Line	9	10					

8 Line	10	6
9 Line	6	5
10 Line	5	2
11 Line	5	17
12 Line	17	19
13 Line	19	18
14 Line	18	6
15 Line	3	11
16 Line	11	16
17 Line	16	12
18 Line	12	4
19 Line	7	13
20 Line	13	15
21 Line	15	14
22 Line	14	8

**Mesh refinement. at lines**

Number line	Input method	Ext. R [m]	and length D [m]	Number div.
4	by length and ext.	0.2000	0.0200	
9	by length and ext.	0.1500	0.0200	

**Line contacts**

Number line	Connection type	Material	Thickness [m]	Method analysis
3	fixed			
5	fixed			
9	fixed			

**Line springs**

No line springs are defined

**Macro-elements**

**Macro-element topology**

Number	Material	Thickness [m]	Line list
1	3D Non Linear C	0.2000	1, 2, 3, 4, 5, 6, 7, 8, 9, 10
2	Plane Stress El	0.2000	3, 15, 16, 17, 18
3	Plane Stress El	0.2000	9, 11, 12, 13, 14
4	Plane Stress El	0.2000	5, 19, 20, 21, 22

**Mesh generation parameters**

Number	Mesh type	Elem. size [m]	Smoothing Mesh	Quad type elem.	Method analysis
1	quadrilaterals	0.0400	yes	CCIsoQuad	nonlinear
2	quadrilaterals	0.0400	yes	CCIsoQuad	nonlinear
3	quadrilaterals	0.0400	yes	CCIsoQuad	nonlinear
4	quadrilaterals	0.0400	yes	CCIsoQuad	nonlinear

**Bar reinforcement**

**Reinforcement top.**

Number	Topology - segments [m]
1	Beg. (0.0000, 0.0400), Lin.to(3.0000, 0.0400)

**Reinforcement properties**

Number	Segment	Material	Area [m <sup>2</sup> ]	Act. anch	Coeff. [-]	External cable C [MN/m]	Meth. R [m] anl.
1	norm.	Reinforceme	9.425E-04				nln.

**Reinforcement bond**

Number	Perimetr [m <sup>2</sup> ]	Bond material	Slip prevented begin.	end

-----  
 1 1.8850E-01 Bond for Reinforcement yes      yes

**Load case 1**

**Properties**

Name:            Load case number 1  
 Coefficient :    1.0000 [-]  
 Code :           Supports

**Joint support**

-----  

Join. numbe	Support X	Support Y	Direction	Axis X rotation X [m]	Axis X rotation Y [m]
15	free	fixed	Global		
19	fixed	free	Global		
16	free	fixed	Global		

 -----

**Line support**

No line supports are prescribed

**Load case 2**

**Properties**

Name:            Load case number 2  
 Coefficient :    1.0000 [-]  
 Code :           Prescribed deformation

**Joint deformation**

-----  

Join. numbe	Support and deformation [m]	Direction	Axis X rotation X [m]	Axis X rotation Y [m]
19	free      fixed	-1.000E-04	Global	

 -----

**Line deformation**

No line deformations are prescribed

**Monitoring points**

-----  

Number	Title	Location	Coordinate		Value	Specification Item	Coeff. [-]
			X [m]	Y [m]			
1	external l	Node	1.5000	0.5000	Reactions	Component 2	1000.000
2	Bottom mid	Node	1.5000	0.0000	Displacements	Component 2	-1000.000

 -----